

D-CYSTEINE ETHYL ESTER NOT NALOXONE REVERSES FENTANYL
MEDIATED INHIBITION OF INTRINSIC CALCIUM ACTIVITY IN CELLS
ISOLATED FROM SUPERIOR CERVICAL GANGLION

A dissertation submitted
to Kent State University in partial
fulfillment of the requirements for the
degree of Doctor of Philosophy

by

Tej R. Nakashe

December 2024

Copyright

All rights reserved

Except for previously published materials

Dissertation written by

Tej R. Nakashe

Ph.D., Kent State University, 2024

Approved by

Colleen Novak, Ph.D. ,

Chair, Doctoral Dissertation Committee

Gary Koski, Ph.D.,

Members, Doctoral Dissertation Committee

Jennifer McDonough, Ph.D.

Stephen J. Lewis, Ph.D.

Lee Gilman , Ph.D.

Accepted by

John D. Johnson, Ph.D.,

Director, School of Biomedical Sciences

Mandy Munro-Stasiuk, Ph.D.,

Dean, College of Arts and Science

Table Of Contents

<i>List of Figures</i>	v
CHAPTER I—INTRODUCTION	1
<i>What are opioids?</i>	1
<i>Opioid use and addiction</i>	3
<i>Opioid pathophysiology</i>	5
<i>Fentanyl</i>	6
<i>Opioid induced respiratory depression</i>	7
<i>Ca²⁺ as a second messenger</i>	10
<i>Calcium channels and their importance in neurons</i>	11
<i>Calcium channels in superior cervical ganglion</i>	13
<i>Calcium signaling in mu-opioid receptor signaling</i>	14
<i>Involvement of calcium in fentanyl mediated signaling</i>	16
<i>Potential solution to fentanyl-induced respiratory depression?</i>	18
CHAPTER II—METHODS	22
PART I: DRIVERS OF INTRINSIC CA²⁺ ACTIVITY	22
<i>Rationale: Importance of Ca²⁺ in neurons</i>	22
<i>Rat model</i>	24
<i>Surgical isolation of superior cervical ganglion tissue</i>	25
<i>Isolation of cells from superior cervical ganglion</i>	27
<i>Real-time Ca²⁺ imaging</i>	29
PART II: FENTANYL AND NALOXONE: DOES NALOXONE ALONE ALTER SCG CALCIUM ACTIVITY?	32
<i>Surgical isolation of superior cervical ganglion tissue</i>	32
<i>Real-time Ca²⁺ imaging and analysis</i>	33
CHAPTER III – RESULTS	34
PART I: CHARACTERIZATION OF INTRINSIC CA²⁺ ACTIVITY	34
<i>Real-time Ca²⁺ imaging</i>	34
<i>Cultured SCG cells showed intrinsic calcium activity</i>	34

<i>Extracellular calcium is crucial for the activity</i>	41
<i>N-type calcium channel is partly involved in regulating the activity</i>	47
<i>Sodium channels are implicated in neurotransmitter release</i>	58
PART II: FENTANYL D-CYSEE AND NALOXONE	65
<i>Fentanyl inhibits intrinsic calcium activity</i>	65
<i>Naloxone inhibits intrinsic calcium activity</i>	72
<i>D-CYSee successfully reversed fentanyl-mediated effects on intrinsic calcium activity</i>	85
<i>Naloxone did not have any effect on the fentanyl mediated inhibition of intrinsic Ca²⁺ activity</i>	92
CHAPTER IV — DISCUSSION	97
<i>Role of superior cervical ganglion in breathing</i>	98
<i>Calcium and calcium channels in superior cervical ganglion</i>	100
<i>Sodium and sodium channels in superior cervical ganglion</i>	103
<i>Role of mu opioid receptor in calcium modulation in superior cervical ganglion</i>	106

List of Figures

Figure 1. : National drug-involved overdose deaths by specific category—number among all ages, 1999-20202

Figure 2. National drug-involved overdose deaths4

Figure 3. Role of superior cervical ganglion in modulation of respiratory dynamics 10

Figure 4. Changes in tidal volume (left panel) elicited by IV injections of vehicle (VEH, saline, IV), D-CYSee (500 $\mu\text{mol/kg}$), or D-cysteine (500 $\mu\text{mol/kg}$) in morphine (10 mg/kg, IV)-treated rats 19

Figure 5. Withdrawal behaviors elicited by naloxone HCl (1.5 mg/kg, IP) in rats treated for 24h with a subcutaneous depot of morphine (150 mg/kg) with or without continuous infusion of D-CYSee (20 $\mu\text{mol/kg/h}$, IV)20

Figure 6. Schematic representation of superior cervical ganglia (SCG) cell isolation rat pups....28

Figure 7. Schematic representation of real time Ca^{2+} imaging; superior cervical ganglia (SCG).....30

Figure 8. Real time Ca^{2+} imaging timeline.....33

Figure 9. Typical traces depicting the effects of control drug free intervention in NeuO-labeled neurons (A) and SR101 labeled astrocytes (B) show consistent activity throughout all 5 phases 35

Figure 10. Detailed analyses revealing the major activity phenotypes detected in neurons (A) and glia (B) under drug free control, conditions38-39

Figure 11. Summary graphs of superior cervical ganglia (SCG) neurons and glia under control conditions	40
Figure 12. Typical traces depicting the effects of Ca ²⁺ -free medium in NeuO-labeled neurons (A) and SR101 labeled astrocytes (B) show inhibition of activity in Ca ²⁺ -free Phases (2 and 3) with return to control levels in washout Phases (4 and 5).....	41
Figure 13. Detailed analyses revealing the major activity phenotypes detected in neurons (A) and glia (B) under drug-free, control conditions.....	44-45
Figure 14. Summary graphs of superior cervical ganglion (SCG) neurons and glia after removal of extracellular Ca ²⁺	46
Figure 15. Typical traces depicting the effects of conotoxin (50nM) in NeuO-labeled neurons (A) and SR101 labeled astrocytes (B).....	47
Figure 16. Detailed analyses revealing the major activity phenotypes detected in neurons (A) and glia (B) under 50nM conotoxin conditions.	50-51
Figure 17. Summary graphs of superior cervical ganglion (SCG) neurons and glia after application of N-type calcium channel blocker conotoxin.....	52
Figure 18. Typical traces depicting the effects of verapamil (50uM) in NeuO-labeled neurons (A) and SR101-labeled astrocytes (B).....	53
Figure 19. Detailed analyses revealing the major activity phenotypes detected in neurons (A) and glia (B) under 50uM verapamil conditions.	56-57

Figure 20. Summary graphs of superior cervical ganglion (SCG) neurons and glia after application of L-type calcium channel blocker verapamil	58
Figure 21. Typical traces depicting the effects of tetrodotoxin (50nM) in NeuO-labeled neurons (A) and SR10- labeled astrocytes (B)	59
Figure 22. Detailed analyses revealing the major activity phenotypes detected in neurons (22A) and glia (22B) under 50nM tetrodotoxin	62-63
Figure 23: Summary graphs of superior cervical ganglion (SCG) neurons and glia after application of sodium channel blocker tetrodotoxin.....	64
Figure 24. Typical traces depicting the effects of fentanyl (100nM) in NeuO-labeled neurons and SR101 labeled astrocytes.....	65
Figure 25. Detailed analyses revealing the major activity phenotypes detected in neurons (A) and glia (B) under 100nM fentanyl conditions	69-70
Figure 26. Summary graphs of superior cervical ganglion (SCG) neurons and glia after application of 100nM fentanyl.....	71
Figure 27. Typical traces depicting the effects of single dose naloxone (100uM) in NeuO-labeled neurons (A) and SR101 labeled astrocytes (B).....	72
Figure 28. Detailed analyses revealing the major activity phenotypes detected in neurons (A) and glia (B) under 100uM naloxone control conditions.....	76-77

Figure 29. Summary graphs of superior cervical ganglion (SCG) neurons and glia after application of 100uM naloxone78

Figure 30. Typical traces depicting the effects of D-CYSee (100uM) in NeuO-labeled neurons (A) and SR101-labeled astrocytes (B)79

Figure 31. Detailed analyses revealing the major activity phenotypes detected in neurons (A) and glia (B) under 100uM D-CYSee conditions 82-83

Figure 32. Summary graphs of SCG neurons and glia after application of 100uM D-CYSee84

Figure 33. Typical traces depicting the effects of D-CYSee (100uM) in presence of fentanyl (100nM) in NeuO-labeled neurons and SR101 labeled astrocytes.....85

Figure 34. Detailed analyses revealing the major activity phenotypes detected in neurons (A) and glia (B) after application of D-CYSee in presence of fentanyl 89-90

Figure 35. Summary graphs of SCG neurons and glia after application of 100uM D-CYSee. In presence of 100nM fentanyl91

Figure 36. Typical traces depicting the effects of naloxone (100uM) in presence of fentanyl (100nM) in NeuO-labeled neurons and SR101 labeled astrocytes.....92

Figure 37. Detailed analyses revealing the major activity phenotypes detected in neurons (A) and glia (B) after application of naloxone in presence of fentanyl. 94-95

Figure 38. Summary graphs of superior cervical ganglion (SCG) neurons and glia after application of 100uM naloxone n presence of 100nM fentanyl96

Acknowledgements

I have a lot of people to thank for their love, support, encouragement and guidance during this journey. Firstly, I would like to start off by thanking God for giving me the opportunity to pursue this dream of mine and giving me the strength throughout this journey. I want to express my deepest thank you to my advisors Dr. Derek Damron and Dr. Colleen Novak for their guidance and constant feedback throughout my time here. Special thank you to Dr. Novak who stepped in to take over as my advisor at a very difficult time. She has guided me and been there with me through completion in the most patient and amazing way. I would like to thank each of my committee members, starting with Dr. Charles Thodeti for guiding me whenever I needed his help and for providing consumables and materials whenever I needed, Dr. Gary Koski for providing timely guidance and support, and Dr. Jennifer McDonough for agreeing to be a part of my committee at the last moment and providing guidance and looking after me after my advisor passed away. An extremely special thank you to Dr. Stephen J. Lewis for agreeing to fund my studies and having faith in me completing my work. Dr. Lewis provided unparalleled support and whatever I asked for to complete my studies. This would not have been possible without any of you. I would also like to thank Dr. Devin Mueller for providing important resources to complete my studies.

I would like to give my deepest thank you to my family and friends who have supported me throughout this journey. I would like to give a very big thank you to my grandparents for encouraging me to pursue my dream and inspiring me to keep aiming higher. This dissertation is for you. The most special thank you to my wife, Ms. Neha Bhavnani, who has stuck by me throughout graduate school. You have really supported me in the best way possible. You always inspire me to keep working hard and you are truly an inspiration for me. You are the most hard-

working person I know, and I strive to be more like you. I could not thank God enough for putting you by my side. I am grateful to my parents Mrs. Suparna Nakashe and Mr. Rajesh Nakashe for their constant words of encouragement and support. I would never ask for any other 2 people to be my parents. Your journey has truly inspired me to do better. I also thank my younger sister Ms. Esha Nakashe who, in spite of being younger to me, shows me what it is to work hard and stay focused. She often drops the odd pearls as well. My life is literally a better place with you all in it.

I would like to express my appreciation for my Dearest friends Mr. Prasad Gogate and Dr. Sid Gaikwad for keeping me sane during this process and for being the best friends a person could ask for. I would also like to give a special thanks to the very recent Dr. Zackery Knauss who is not only a good friend but an amazing lab mate and person. He has guided and helped me a lot through this journey as well. Thank you for developing this model when we were almost literally out of ideas. Thanks to all the undergraduates in our lab who I have had the opportunity to train and who have helped me with my experiments. Special thanks to Mr. Andrew Beard for helping me with a lot of my studies and Mrs. Eliza Pawkey for standardizing the rat colony to a point where we always had animals at our demand. Your contribution was priceless.

Lastly, I would like to thank Dr. Sujala Pathare and Dr. Pritam Pathare for being the very first mentors of my career. I could never ask for anyone better as my first mentors. In world where everyone asks ‘what are you doing these days,’ you were the people who asked me ‘are you happy,’ and that made a world of difference to me. I would also like to thank Dr. Madhavi Indap for teaching me the true meaning of research and showing me the dedication it takes to become a researcher. You all have inspired me to do better at all times and be the best version of myself.

CHAPTER 1—INTRODUCTION

BACKGROUND AND SIGNIFICANCE

What are opioids?

Opioids are compounds or drugs which are either natural or chemical mimetics of compounds found in the opium poppy plant¹. Opioids include prescribed pain medications and illegal drugs. Prescription opioids, when used as prescribed by doctors, can treat pain and help with conditions such as post-surgical pain, severe pain due to trauma and disease, coughing, and diarrhea. Opioids are commonly administered either orally, via a skin patch below the tongue, or by injection. While some opioid drugs are made from naturally occurring plant compounds (e.g., morphine), other opioid drugs are synthetic (e.g., fentanyl) meaning they are human-made substances created in a laboratory. Heroin, an illegal street drug, is also an opioid^{1,2}. All opioids are chemically related and interact with opioid receptors on nerve cells in the body and brain. Opioid pain relievers are generally safe when taken for a short time and as prescribed by a doctor, but because they produce euphoria in addition to pain relief, they can be misused (taken in a different way or in a larger quantity than prescribed or taken without a doctor's prescription). Regular prescribed use can also lead to dependence and, when misused, opioid pain relievers can lead to addiction, overdose incidents, and deaths (**Figures 1-2**)¹⁻³.

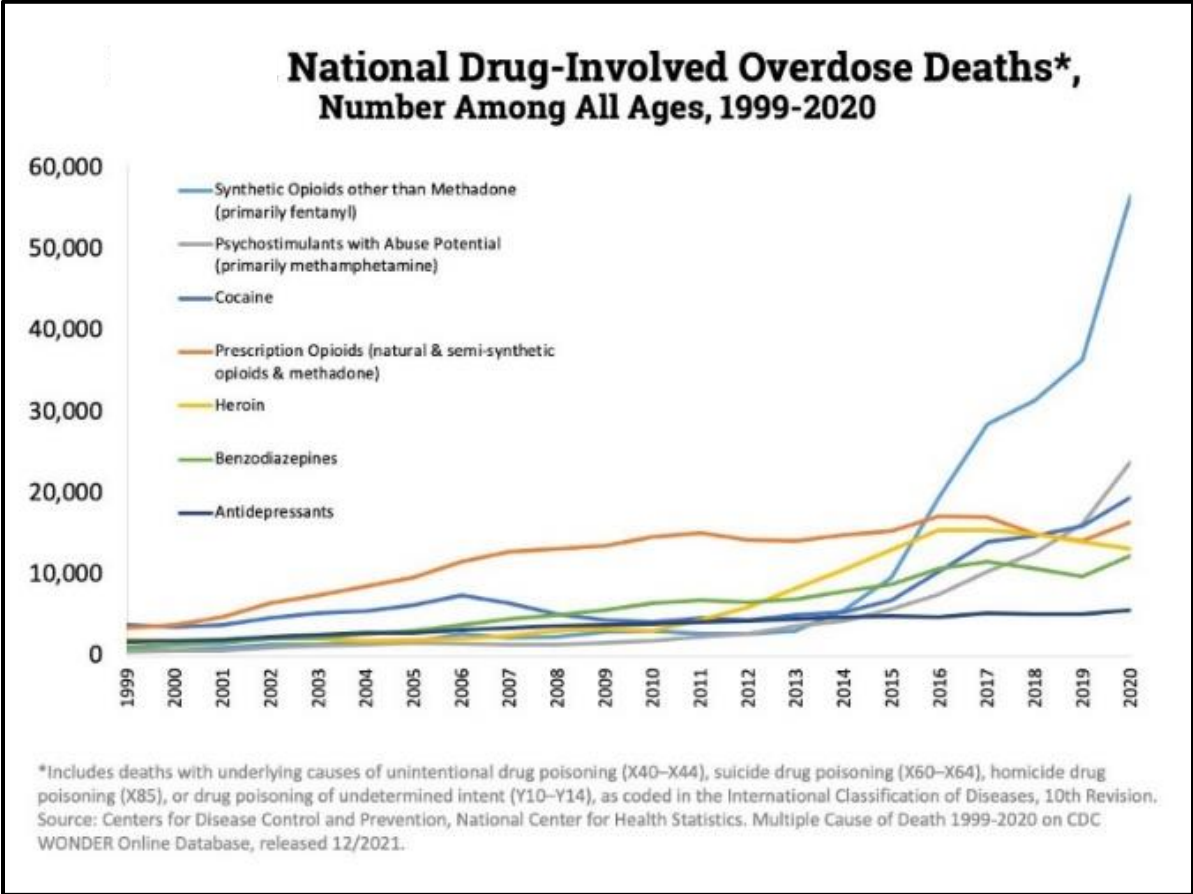


Figure 1. National drug-involved overdose deaths by specific category—number among all ages, 1999-2020. Overall, drug overdose deaths rose from 2019 to 2020, with 91,799 drug overdose deaths reported in 2020. Deaths involving synthetic opioids other than methadone (primarily fentanyl) continued to rise, with 56,516 overdose deaths reported in 2020. Those involving psychostimulants with abuse potential (primarily methamphetamine) also continued to increase to 23,837 (Source: <https://nida.nih.gov/research-topics/trends-statistics/overdose-death-rates> Fig2).

Opioid use and addiction

Opioid use disorder and opioid addiction is at an epidemic level not only in the US but is now also plaguing nations around the world. 3 million US citizens and 16 million individuals worldwide have had or currently suffer from opioid use disorder (OUD)¹. Just in the US, more than 500,000 people are dependent on heroin. A stark increase in OUD is attributed to over-prescription of opioids⁴. In the 1990s, there was a sharp increase in opioid prescriptions in response to the "pain as fifth vital sign" campaign, downplaying the abuse potential of opioids, along with aggressive marketing of drugs such as Oxycontin and Opana. Risk factors for misuse of opioids include (1) initiation at a young age, (2) previous history of illicit drug or alcohol abuse, (3) family history of illicit drug or alcohol abuse, or sexual abuse in females, (4) adverse childhood experiences, and (5) psychological comorbidities (depression, bipolar disorder, and attention deficit hyperactivity disorder)⁴.

The opioid epidemic affects every state in the US and now is driven by illicit fentanyl and fentanyl analogs, along with methamphetamine or cocaine, often in combination or in adulterated forms⁵. More than 107,000 deaths were reported in the United States between December 2020 to December 2021⁶. According to recent statistics reported by the CDC, 1.6 million people began the non-medical use of prescription opioids in 2021, with an additional 50,000 beginning the recreational use of heroin⁶. This represents a 38.4% rise from pre-COVID-19 levels, resulting in a 70% increase in emergency room visits for the treatment of overdose. Overdose deaths involving opioids—including prescription opioids, heroin, and synthetic opioids (like fentanyl)—have increased by more than 800% since 1999. Overdoses involving opioids killed nearly 69,000 people in 2020, and over 82% of those deaths involved synthetic opioids⁶.

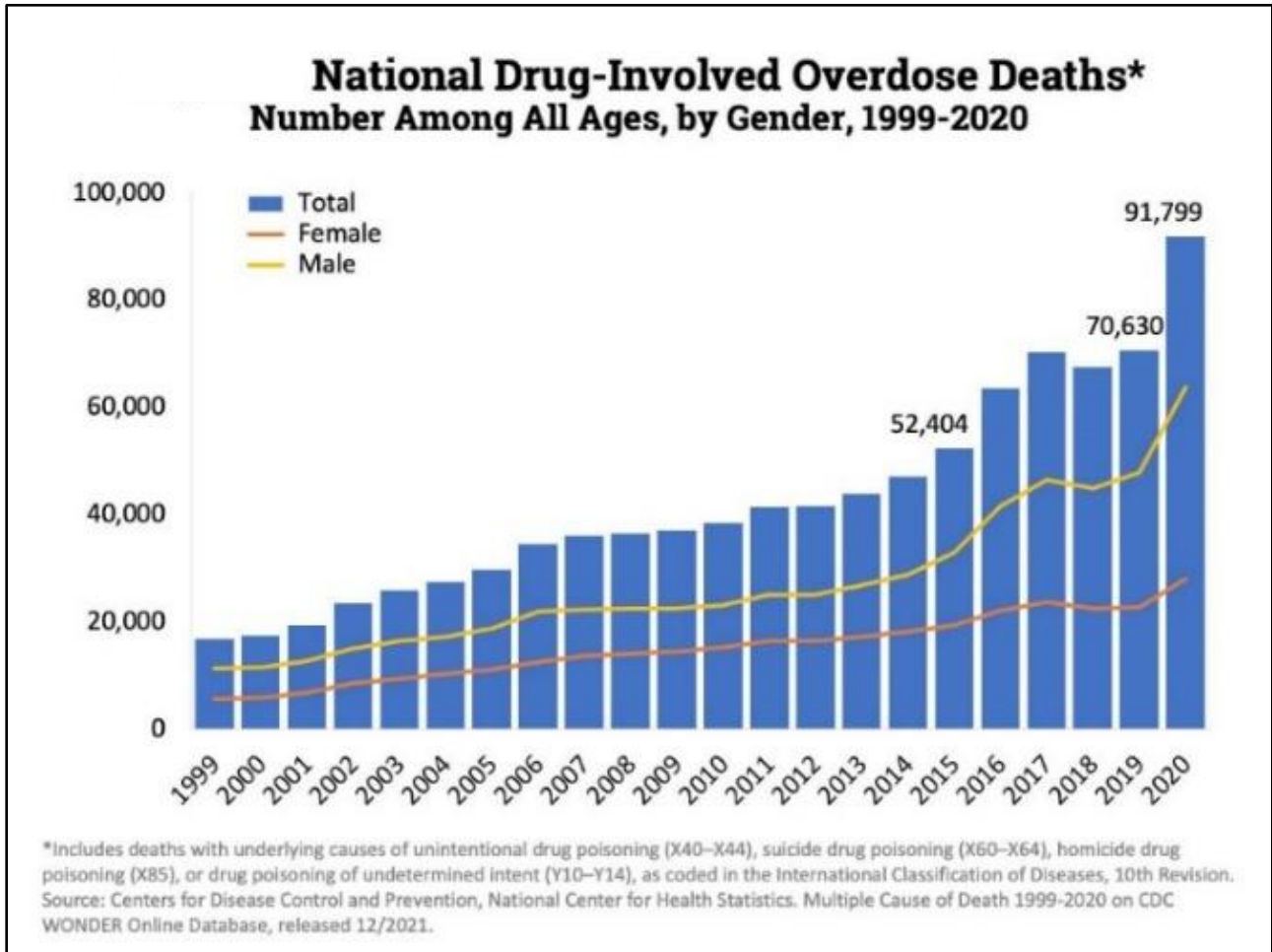


Figure 2. National drug-involved overdose deaths. Number among all ages, by sex, 1999-2020. Nearly 92,000 persons in the U.S. died from drug-involved overdose in 2020, including illicit drugs and prescription opioids. The figure above shows the total number of U.S. drug overdose deaths involving any illicit or prescription opioid drug from 1999 to 2020. The bars are overlaid by lines showing the number of deaths by sex from 1999 to 2020.

Prescription opioids are commonly administered to manage moderate to severe pain, particularly in the context of postoperative care, cancer treatment, and chronic conditions such as arthritis and osteoporosis. Beyond their analgesic effects, opioids induce a transient sense of euphoria, which, upon dissipation, can lead to significant cravings and potential misuse. Escalation of dosage, driven by the development of tolerance, can result in opioid use disorder (OUD). Upon discontinuation or inadequate dosing, individuals may experience withdrawal symptoms, including exacerbated pain, piloerection, anxiety, yawning, and gastrointestinal disturbances such as diarrhea. The risk of addiction increases substantially when opioids are consumed in a manner inconsistent with medical guidelines, such as crushing pills for intranasal or intravenous administration. This method facilitates rapid opioid delivery, heightening the risk of overdose and accelerating the onset of OUD.

Opioid pathophysiology

Opioids bind to specific receptors (mu, delta, and kappa) in the central and peripheral nervous systems which have pain, cough, and diarrhea-relieving effects. Opioids acting on these receptors can induce euphoria as well. As a result of this euphoria, individuals continue and often risk overdose to recreate the euphoria feeling. Most people who misuse opioids initiate for pain relief or to prevent withdrawal symptoms. Increasing evidence is dispelling the myth that opioids are effective long-term analgesic medications⁴. These specific opioid receptors are responsible for eliciting the following specific physiological effects:

1. **Mu:** analgesia, physical dependence, respiratory depression, miosis, euphoria, reduced GI motility, vasodilation. Peripheral mu receptors are tissue-specific with higher concentrations in bronchial smooth muscle and the digestive tract.

2. **Delta:** analgesia, antidepressant, convulsant, physical dependence, modulate mu-related respiratory depression.
3. **Kappa:** analgesia, anticonvulsant, depression, hallucination, diuresis, dysphoria, miosis, neuroprotection, sedation⁷.

Although withdrawal symptoms manifest when opioids are discontinued abruptly, withdrawal can occur with tapered cessation of medications as well. Withdrawal symptoms present in acute, subacute, and chronic phases. Most healthcare providers are aware of the acute withdrawal symptoms--hot/cold flashes, nausea, vomiting, diarrhea, sweating, lacrimation, insomnia, anxiety, generalized muscle pain, tachycardia, piloerection, and dehydration.⁴⁴

Fentanyl

Synthetic opioids such as fentanyl are most involved in overdose deaths. In 2021, nearly 71,000 drug overdose deaths involving synthetic opioids occurred in the United States alone, which is more deaths than from any other type of opioid. Synthetic opioid-involved death rates increased by over 22% from 2020 to 2021 and accounted for nearly 88% of all opioid-involved deaths in 2021⁸. The number of overdose deaths involving synthetic opioids in 2021 was nearly 23 times the number in 2013. There has been a rise in synthetic opioid related deaths that have tested positive for fentanyl and fentanyl analogs such as acetylfentanyl, furanylfentanyl, and carfentanil, which are even more difficult to detect. Fentanyl is around 50 times more potent than heroin and morphine⁹. Estimates of the potency of fentanyl analogs vary from less potent than fentanyl to much more potent than fentanyl, but there is some uncertainty because potency of illegally made fentanyl analogs has not been evaluated in humans. Carfentanil, the most potent fentanyl analog detected in the U.S., is estimated to be 10,000 times more potent than

morphine¹⁰. Moreover, fentanyl contamination of illegal drugs is also a growing concern^{11,12}. Contamination with fentanyl and its analogs in counterfeit opioid pills is contributing to deaths involving these other substances. Overdose rates in drugs mixed with opioids is at an all time high than those compared to drugs without opioids contamination^{8,9,11,12}.

Opioid induced respiratory depression

Opioid induced respiratory depression (**OIRD**) is one of the major deleterious health effects stemming from continued overuse of opioids and is leading to significant opioid overdose-related deaths¹³. Opioids elicit this effect by activating opioid receptors expressed on cells within the central and peripheral nervous system. Additionally, there are some sites outside the central nervous system, such as carotid bodies (CBs), that are involved in eliciting OIRD¹⁴. Multiple centers in the brainstem contain opioid receptors, including the pre-Bötzinger complex, parabrachial nucleus, and dorsal rostral pons, which when activated have been associated with bradypnea. **Evidence from opioid-receptor knockout mice supports a pivotal role for the mu-opioid receptor in the development of OIRD.** A very small population of mice which had their MOR knocked showed development of OIRD after application of morphine as compared to mice with their MOR intact⁷. All opioids currently prescribed for the treatment of acute or chronic pain that activate the mu-opioid receptor are known to cause respiratory depression. The magnitude of OIRD varies, however, depending on the degree of activation of the multiple intracellular pathways induced by the opioid agonist. Among a series of pathways, mu-opioid receptors engage two important signaling pathways—the G protein and β -arrestin pathways. The former pathway is associated with analgesia, the latter with opioid side-effects, including respiratory depression^{14,15}. ***Current approaches to treating OIRD and challenges involved***

Currently, the most used drug to reverse or treat opioid overdose and OIRD is naloxone, which is carried by most first responders and healthcare employees. Naloxone is administered in the nose of a patient using a nasal spray and rapidly reverses opioid overdose if administered on time. Naloxone is a competitive opioid receptor antagonist, which means that it binds to the opioid receptors competitively and prevents further binding along with reversal of opioids already bound to the receptors, thereby countering the effects of opioid overdose. Consequently, naloxone can restore normal breathing of a person who is experiencing OIRD as an effect of overdose. Naloxone is normally administered either nasally as a spray or as an injectable¹⁶⁻¹⁹.

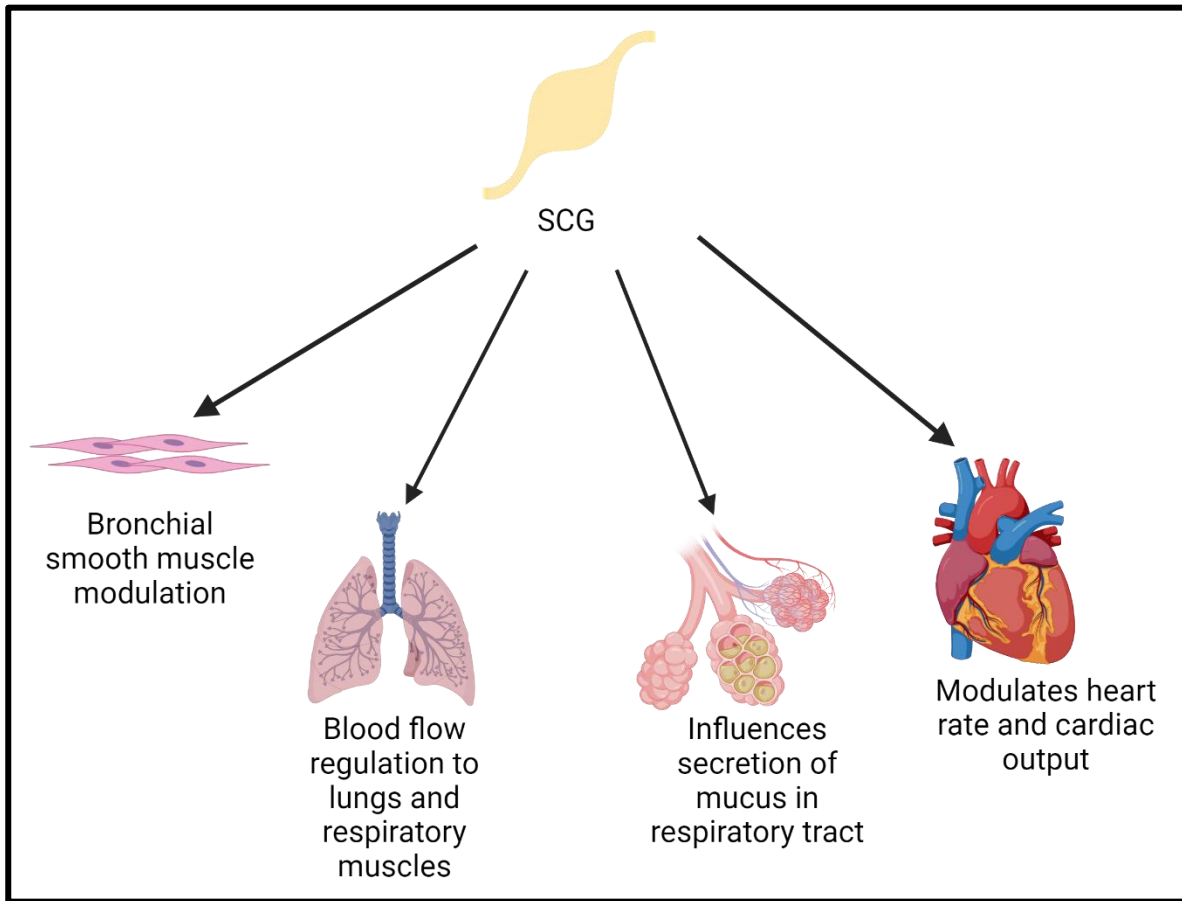
Despite being one of the most used drugs to treat overdose, naloxone is not completely safe and has some adverse effects. It is known to precipitate the withdrawal stemming from rapid replacement of opioid receptors by the opioids, making patients feel a sudden onset of withdrawal symptoms. Along with this, naloxone also inhibits the analgesic effects of the opioids which means that the pain-relieving effect of the opioids is diminished. For more potent opioids like fentanyl, a single dose of naloxone is often insufficient and multiple doses or a higher dose may need to be administered²⁰⁻²⁴.

Sympathetic nervous system and its involvement in respiratory dynamics

The sympathetic nervous system is a division of the autonomic nervous system that supplies efferent axons to all viscera of the body to constantly adjust organ function, for example during periods of stress, anxiety, physical activity, fear, or excitement. The central nervous system, including the spinal cord, gives rise to sympathetic pre-ganglionic neurons which innervate target tissues. The sympathetic preganglionic neurons primarily from the spinal cord send projections to make synapses with sympathetic postganglionic neurons located in peripheral ganglia, for example in the sympathetic chain. Axons from these sympathetic postganglionic

neurons located in the peripheral nervous system which then project to specific target tissues²⁵. The **bilateral superior cervical ganglia (SCG)** are the most rostral sympathetic ganglia, arising from the fusion of cervical ganglia C1 to C4, and supplying the head and neck (mainly carotid bodies, brainstem, tongue, and upper airway)^{26,27}. Cells present within the SCG (neurons, satellite glial cells, and small intensely fluorescent (SIF) cells) receive their preganglionic input from thoracic (T) spinal cord (T1-T4) nerves that course within the cervical sympathetic chain (CSC). The sympathetic preganglionic neurons traveling in the CSC release acetylcholine and stimulate nicotinic (N2) receptors on cells in the SCG²⁵⁻²⁸. The activated principal SCG postganglionic neurons then release norepinephrine onto numerous adrenergic receptor subtypes present on target tissues²⁵. The SCG sends postganglionic signals to the carotid body (CB) through the ganglioglomerular nerve (GGN) which modulates the carotid sinus nerve (CSN) chemosensory afferent discharge, which is further relayed to nucleus tractus solitarius (NTS) where the signal is processed, resulting in an increase in respiration²⁹. Clinical patients suffering from chronic T1-T4 spinal cord injury present with cardiorespiratory disturbances; this is consistent with diminished activity of the CSC-SCG complex including enhanced peripheral chemoreflex sensitivity, which is a major cause of sleep-disordered breathing in these patients^{30,31}. Evidence from rats has shown that mid-thoracic spinal cord injury is associated with enhanced cardiac sympathetic activity and cardiac sympathetic hyperinnervation that increases the susceptibility to life-threatening arrhythmias. In rats, hypoactivity of the CSC greatly enhances the likelihood of stroke in hypertensive models³¹. Similarly, a unilateral superior cervical ganglionectomy in rats diminished frequency (breathes/min), minute ventilation (ml/min), peak inspiratory flow (msec), and peak expiratory flow (msec) as compared to sham-operated rats³². Altogether, this evidence outlines the pathway through which the CSC-SCG

pathway modulates breathing and highlights the potential actions of opioids in the SCG in the respiratory suppression.



Figure³² 3. Role of superior cervical ganglion (SCG) in modulation of respiratory

dynamics.

Ca²⁺ as a second messenger

Second messengers are important molecules and ions that can relay signals received by cell receptors. Second messengers include a variety of molecules such as lipids, ions, and nucleotides³³. Ca²⁺ is an important messenger that is involved in numerous cellular reactions which plays an important role in stimulus responses of cells. This is achieved by keeping a constant cytoplasmic concentration and mobilization of Ca²⁺ inside the cell in response to a cellular event. Ca²⁺ as a second messenger is important in various cell types such as skeletal

muscle (contraction), smooth muscle and endothelial cells (dilation and constriction), cardiac smooth muscle cells (contraction and relaxation), pancreatic islet beta cells (insulin release), and neurons (neurotransmitter release, voltage gradation)³³⁻³⁵. Ca^{2+} plays a fundamental role in neuronal plasticity. In neurons, Ca^{2+} regulates gene expression, energy production, membrane excitability, synaptogenesis, synaptic transmission, and processes which involve learning, memory, and cell survival. Ca^{2+} signaling is achieved by modulation of extracellular Ca^{2+} concentration via opening and closing of plasma membrane (voltage gated channels, sodium calcium exchanger) and subcellular Ca^{2+} sensitive channels (ryanodine receptors on the sarcoplasmic reticulum)^{36,37}. Because of Ca^{2+} involvement in most neurological processes, even the smallest impairment in Ca^{2+} homeostasis can result in profound functional alterations. This makes Ca^{2+} one of the most important and exciting prospects of all second messengers. Our research program has established expertise in monitoring cellular Ca^{2+} and we have successfully shown its involvement in several cellular processes³⁵⁻⁴⁴.

Calcium channels and their importance in neurons

Calcium channels play a critical role in a wide range of physiological functions in cells. They include all pore-forming membrane proteins that are calcium-permeable and used for the transport of these ions across cell membranes. As an ion, calcium is unique in biological systems; this is because calcium not only functions to generate membrane potentials and electrical signals but also functions as a central cell signaling molecule. Therefore, calcium channels play an even more pivotal role in the cell by allowing for the generation of a multitude of cellular responses. Calcium channels come in many forms and are incredibly diverse in both structure and function^{33,35}.

Neuronal voltage-gated Ca^{2+} (CaV) channels play a critical role in cellular excitability, synaptic transmission, excitation–transcription coupling and activation of intracellular signaling pathways. CaV channels are multiprotein complexes and their functional expression in the plasma membrane involves finely tuned mechanisms, including forward trafficking from the endoplasmic reticulum (ER) to the plasma membrane, endocytosis and recycling. Whether genetic or acquired, alterations and defects in the trafficking of neuronal CaV channels can have severe physiological consequences^{35,36}.

Voltage-gated calcium channels (VGCCs) are the principal conduits for depolarization-mediated Ca^{2+} entry into excitable cells. Voltage-gated calcium channels have properties that ensure they are specialized for roles, for example, differences in their activation voltage threshold, their kinetic properties, and their voltage-dependence of inactivation. All these attributes contribute to the ability of the voltage-gated calcium channels to participate in different patterns of presynaptic vesicular release. These include synaptic transmission resulting from single action potentials, and longer-term changes mediated by bursts or trains of action potentials, as well as release resulting from graded changes in membrane potential in specialized sensory synapses^{36–38}.

Multiple types of VGCCs are found in neural tissues based on their biophysical and pharmacological properties: low voltage activated (LVA) T-type and high voltage-activated (HVA) L-, N-, P/Q-, and R-type channels. Calcium influx through VGCCs in different subcellular compartments of nerve cells mediates an array of cellular functions in the nervous system. For instance, L-type channels on the cell body regulate gene expression through signaling pathways. Increases in localized calcium levels in presynaptic terminals are crucial for excitation-secretion coupling mechanisms⁴⁵. The mechanisms linking calcium influx through

VGCCs to neurotransmitter release involve identifying proteins responsible for vesicle trafficking, docking, and fusion. These interactions occur during calcium-evoked exocytosis and are part of the "SNARE hypothesis." SNARE proteins, including v-SNAREs on vesicles and t-SNAREs like syntaxin on target membranes, along with NSF and SNAPs (e.g., α , β , and γ SNAPs), play key roles in vesicular docking, priming, and fusion processes. N-type VGCCs, sensitive to ω -conotoxin, bind to syntaxin, a t-SNARE on presynaptic membranes, linking VGCCs to proposed SNARE complexes involving SNAP-25 and synaptotagmin. P/Q-type VGCCs also associate with syntaxin-containing SNARE complexes in rat cerebellar synaptosomes⁴⁶. A peptide motif on N- or P/Q-type VGCCs, known as the 'synprint' site, binds to syntaxin in a calcium-dependent manner. Injecting N-type calcium channel synprint peptides into neurons led to reduced fast neurotransmitter release, indicating functional consequences of these molecular interactions. Co-expression of syntaxin with N- or P/Q-type VGCCs in *Xenopus* oocytes alters the gating properties of the channels, suggesting regulatory functions of their interaction⁴⁵⁻⁴⁷.

Calcium channels in superior cervical ganglion

Within the SCG, like in other parts of the nervous system, calcium channels are responsible for regulating the influx of calcium ions into the neuron upon depolarization. This influx of calcium ions is essential for various neuronal functions, including neurotransmitter release⁴⁸.

Voltage-gated calcium channels. These channels open in response to depolarization of the neuronal membrane. VGCCs are crucial for triggering the release of neurotransmitters from presynaptic terminals⁴⁹

Ligand-gated calcium channels. These channels are activated by the binding of specific neurotransmitters or neuromodulators. While less common in the SCG compared to voltage-gated channels, ligand-gated calcium channels can also contribute to calcium influx and subsequent neurotransmitter release in certain neuronal pathways⁵⁰⁻⁵³.

Store-operated calcium channels (SOCCs). These channels play a role in replenishing intracellular calcium stores following their depletion. While their role in the SCG may not be as extensively studied as VGCCs, SOCCs are involved in calcium signaling and homeostasis in neuronal and non-neuronal cells.

The activity of calcium channels in the superior cervical ganglion is tightly regulated and coordinated to ensure proper neurotransmission and neuronal function. Dysregulation of calcium channel activity in the SCG can lead to various neurological disorders and dysfunction in autonomic control. Therefore, understanding the role of calcium channels in the SCG is essential for elucidating the mechanisms underlying autonomic regulation and developing potential therapeutic strategies for related disorders.

Voltage-gated calcium channels are major regulators of intracellular Ca^{2+} in SCGs. Of all the calcium channels, N-type calcium channel is the main channel involved in regulation of SCG neurons. Prior experiments have shown that N-type calcium channel-expressing neurons innervate the heart in hypertensive rats. Evidence has also indicated that calcium channels contribute to ganglionic long-term potentiation⁵⁰⁻⁵³.

Calcium signaling in mu-opioid receptor signaling

Calcium signaling plays a significant role in the downstream effects of mu-opioid receptor (MOR) activation. Here's how calcium signaling is involved in MOR function:

Neurotransmitter release. Activation of MOR inhibits the release of neurotransmitters, including excitatory neurotransmitters like glutamate and substance P, as well as inhibitory neurotransmitters like gamma-aminobutyric acid (GABA). This inhibition occurs in part through the modulation of calcium influx into presynaptic terminals. MOR activation leads to the inhibition of voltage-gated calcium channels through the G beta gamma subunit, reducing calcium entry into the presynaptic terminal. This reduction in calcium influx decreases the probability of neurotransmitter release, contributing to the analgesic effects of MOR agonists⁵⁴.

Postsynaptic effects. MOR are coupled to G proteins, and their activation leads to the modulation of various intracellular signaling pathways, including those involving calcium. Upon activation, MOR can indirectly influence intracellular calcium levels through downstream signaling molecules. For example, MOR activation can inhibit adenylyl cyclase activity, leading to a decrease in intracellular cyclic AMP (cAMP) levels. This reduction in cAMP can influence calcium signaling pathways, such as those mediated by protein kinase A (PKA), which phosphorylates calcium channels and other proteins involved in calcium signaling⁵⁵.

Intracellular signaling. MOR activation can also directly influence intracellular calcium levels through signaling pathways involving phospholipase C (PLC) and inositol trisphosphate (IP3). Activation of MOR can stimulate PLC, leading to the hydrolysis of phosphatidylinositol 4,5-bisphosphate (PIP2) into diacylglycerol (DAG) and IP3. IP3 acts as a second messenger that binds to IP3 receptors on the endoplasmic reticulum, leading to the release of calcium ions from intracellular stores. This increase in intracellular calcium can modulate a range of cellular processes, including neurotransmitter release, gene expression, and synaptic plasticity^{55,56}.

Regulation of neuronal excitability. Calcium signaling downstream of MOR activation can modulate neuronal excitability in the central nervous system. Changes in intracellular calcium levels can influence the activity of ion channels, neurotransmitter receptors, and other signaling molecules involved in neuronal function. By modulating calcium signaling pathways, MOR can alter neuronal excitability and synaptic transmission, ultimately contributing to their analgesic and addictive properties.

Overall, calcium signaling plays a critical role in mediating the effects of MOR activation on synaptic transmission, neuronal excitability, and cellular signaling within the nervous system. Understanding the mechanisms underlying MOR-mediated calcium signaling may provide insights into the development of novel therapeutic strategies for pain management and opioid addiction treatment⁵⁶⁻⁵⁹.

Involvement of calcium in fentanyl mediated signaling

Calcium ions also play a significant role in the signaling pathways affected by fentanyl, a potent synthetic opioid. Here's how calcium is involved in fentanyl signaling⁶⁰.

Modulation of postsynaptic signaling. Fentanyl, like other opioids, activates opioid receptors coupled to G proteins on postsynaptic neurons. This activation leads to the inhibition of adenylyl cyclase and the opening of potassium channels, resulting in hyperpolarization of the postsynaptic neuron. Calcium ions can modulate this process by influencing the activity of various intracellular signaling pathways downstream of opioid receptor activation⁶¹.

Involvement in analgesic mechanisms. Calcium signaling pathways are involved in mediating the analgesic effects of opioids, including fentanyl. Activation of opioid receptors by

fentanyl leads to changes in calcium signaling within neurons, which can modulate neuronal excitability, synaptic transmission, and pain processing in the central nervous system⁶².

Role in opioid tolerance and dependence. Chronic exposure to opioids such as fentanyl can lead to the development of tolerance and dependence. Calcium signaling pathways are implicated in these adaptive changes in neuronal function. Prolonged activation of opioid receptors by fentanyl can lead to alterations in calcium-dependent intracellular signaling cascades, contributing to the development of tolerance and dependence.⁶³

Potential therapeutic targets. Understanding the role of calcium signaling in fentanyl signaling pathways may provide insights into potential therapeutic targets for mitigating opioid tolerance, dependence, and side effects. Modulation of calcium channels or downstream calcium-dependent signaling pathways could potentially enhance the analgesic efficacy of opioids while reducing their adverse effects and risk of dependence.

Overall, calcium signaling is intricately involved in mediating the effects of fentanyl on neuronal function and synaptic transmission. In summary, while the specific details of calcium signaling in the context of fentanyl are not as extensively studied as with other opioids, it is clear that calcium signaling plays a crucial role in mediating many of the cellular and molecular effects of fentanyl within the nervous system. Further research in this area could provide valuable insights into the mechanisms underlying fentanyl pharmacology and aid in the development of more effective and safer opioid-based therapies⁶⁰⁻⁶⁶.

Potential solution to fentanyl-induced respiratory depression?

Opioid addiction and OIRD are major problems in the US. The side-effects associated with naloxone have the research world rushing to identify an alternative agent to counter withdrawal. There is currently an urgent unmet need for development of new drugs to help counter this situation and potentially replace naloxone. Findings from our collaborators have revealed that a **novel thiol ester D-CYSee prevents the negative effects of fentanyl on breathing-minute ventilation, tidal volume, frequency of breathing and cardiovascular status (Figure 3), including mean arterial pressure (MAP), diastolic blood pressure (DBP), and systolic blood pressure (SBP) in rats without significantly affecting analgesia efficacy.** Some preliminary findings (**Figure 4**) also indicate that D-CYSee diminishes withdrawal responses including circling behavior, increase in MAP, and apneas. In anesthetized and freely moving rats, D-CYSee reverses the deleterious effects of morphine on the arterial blood gas chemistry and breathing. Moreover, preliminary findings from our lab demonstrate that D-CYSee successfully reverses the fentanyl mediated effects on the $i[Ca^{2+}]$ in cells isolated from the SCGs (figure 34-36).

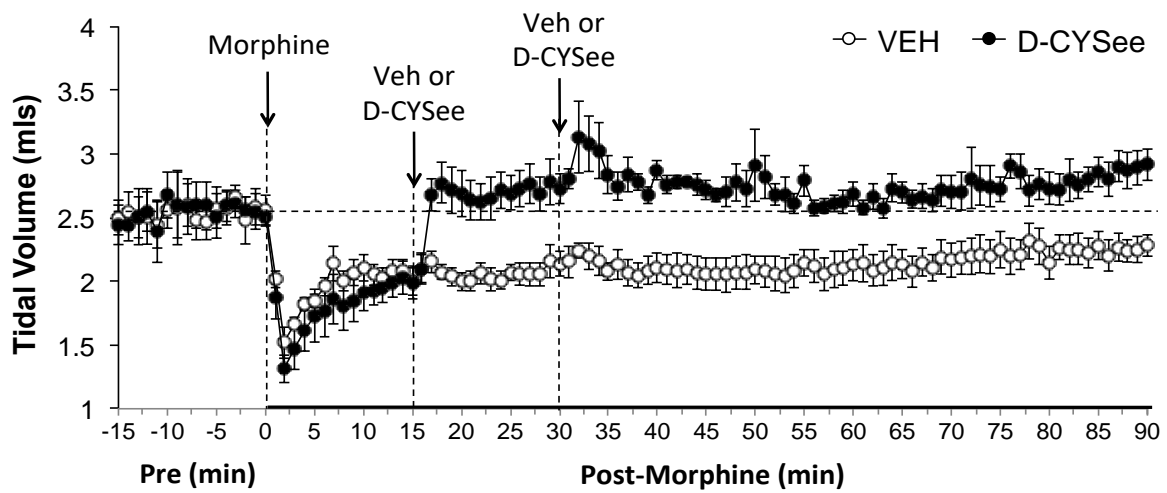


Figure 4. Changes in tidal volume (left panel) elicited by IV injections of vehicle (VEH, saline, IV), D-CYSee (500 μ mol/kg), or D-cysteine (500 μ mol/kg) in morphine (10 mg/kg, IV)-treated rats. The data are mean \pm SEM. There were 9 rats receiving each treatment. *P < 0.05, significant response

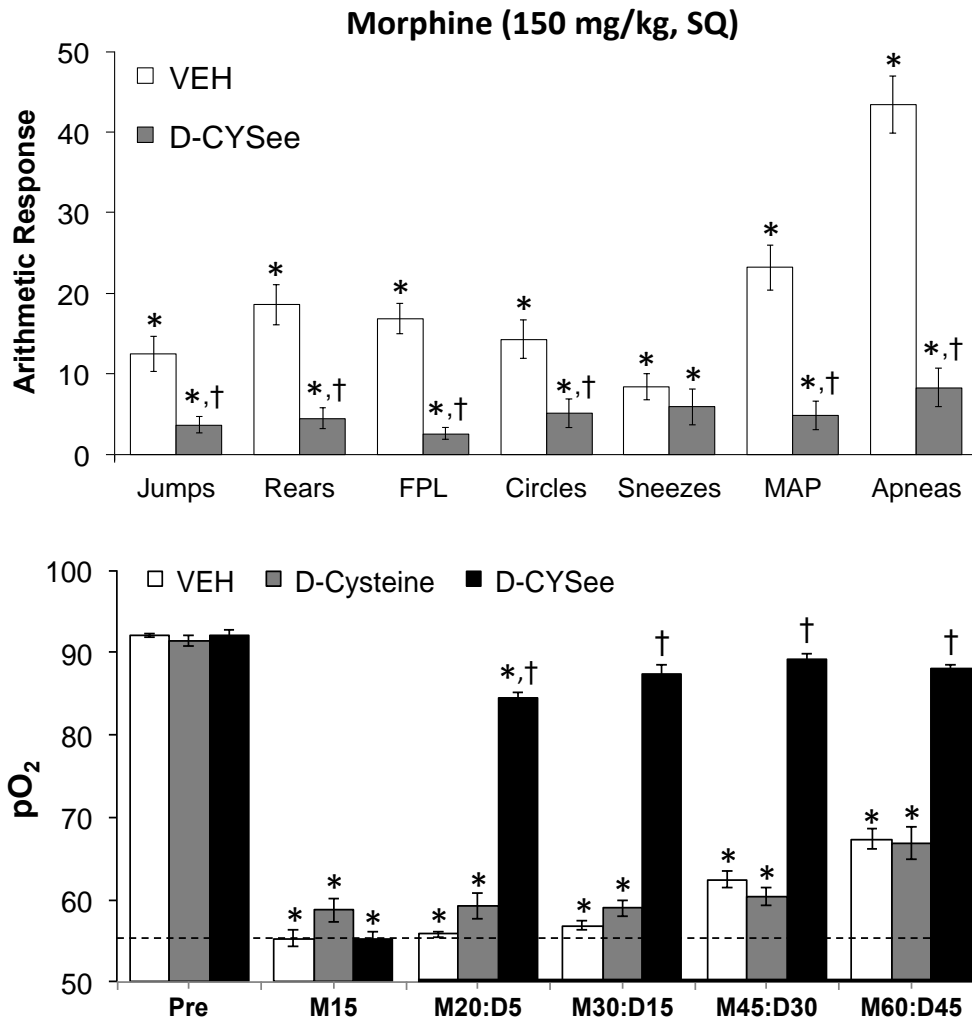


Figure 5. Withdrawal behaviors elicited by naloxone HCl (1.5 mg/kg, IP) in rats treated for 24h with a subcutaneous depot of morphine (150 mg/kg) with or without continuous infusion of D-CYSee (20 μ mol/kg/h, IV).

Previous evidence generated using patch clamp has shown that activation of the MOR directly leads to the suppression of the **N-Type Ca²⁺ channel** currents in neurons. This activity is attributed to the MOR Gβγ subunit⁶⁷⁻⁷⁰. Our data has also shown that inhibition of the N-Type Ca²⁺ channel using specific inhibitors completely inhibits the spontaneous i[Ca²⁺] activity in the cells isolated from SCG. We have also observed identical inhibition of i[Ca²⁺] activity after application of fentanyl in these cells. **Altogether, this data indicates that a VGCC is directly involved in regulating the i[Ca²⁺] activity and that fentanyl modulates this activity by activating the MOR. Along with this, we also hypothesize that since D-CYSee reverses the fentanyl-mediated effects on i[Ca²⁺] activity whereas naloxone will have no effect on fentanyl mediated suppression of the activity.**

CHAPTER II—METHODS

PART I: DRIVERS OF INTRINSIC Ca^{2+} ACTIVITY

Rationale: Importance of Ca^{2+} in neurons

Calcium (Ca^{2+}) is a universal second messenger that regulates the most important activities of all eukaryotic cells. It is of critical importance to neurons as it participates in the transmission of the depolarizing signal and contributes to synaptic activity. Neurons have thus developed extensive and intricate Ca^{2+} signaling pathways to couple the Ca^{2+} signal to their biochemical machinery. Ca^{2+} influx into neurons occurs through plasma membrane receptors and voltage-dependent ion channels^{37,38}. The release of Ca^{2+} from the intracellular stores, such as the endoplasmic reticulum, by intracellular channels also contributes to the elevation of cytosolic Ca^{2+} . Inside the cell, Ca^{2+} is controlled by the buffering action of cytosolic Ca^{2+} -binding proteins and by its uptake and release by mitochondria. The uptake of Ca^{2+} in the mitochondrial matrix stimulates the citric acid cycle, thus enhancing ATP production and the removal of Ca^{2+} from the cytosol by the ATP-driven pumps in the endoplasmic reticulum and the plasma membrane. A Na^+/Ca^{2+} exchanger in the plasma membrane also participates in the control of neuronal Ca^{2+} . The impaired ability of neurons to maintain an adequate energy level may impact Ca^{2+} signaling; this occurs during aging and in neurodegenerative disease processes³⁹.

High-intensity Ca^{2+} signaling necessitates high ATP consumption to restore basal (low) intracellular Ca^{2+} levels after Ca^{2+} influx through plasma membrane receptor and voltage-dependent ion channels. Ca^{2+} influx may also lead to increased generation of mitochondrial reactive oxygen species (ROS). Impaired abilities of neurons to maintain cellular energy levels and to suppress ROS may impact Ca^{2+} signaling during aging and in neurodegenerative disease processes. Advances in understanding the molecular regulation of Ca^{2+} homeostasis and how it is perturbed in neurological disorders may lead to therapeutic strategies that modulate neuronal Ca^{2+} signaling to enhance function and counteract disease processes. The spatiotemporal patterns of intracellular Ca^{2+} signals, and the ultimate cellular biological outcome, are also dependent upon termination mechanism, such as Ca^{2+} buffering, extracellular extrusion, and intra-organelle sequestration. Because of the central role played by Ca^{2+} in neuronal physiology, it is not surprising that even modest impairments of Ca^{2+} homeostasis result in profound functional alterations. Despite their heterogeneous etiology neurodegenerative disorders, as well as the healthy aging process, are all characterized by disruption of Ca^{2+} homeostasis and signaling.

Calcium binds to calmodulin and stimulates the activity of a variety of enzymes, including calcium-calmodulin kinases and calcium-sensitive adenylate cyclases. These enzymes transduce the calcium signal and affect short-term biological responses, such as the modification of synaptic proteins and long-lasting neuronal responses that require changes in gene expression. Recent studies of calcium signal-transduction mechanisms have revealed that, depending on the route of entry into a neuron, calcium differentially affects processes that are central to the development and plasticity of the nervous system, including activity-dependent cell survival, modulation of synaptic strength, and calcium-mediated cell death³⁶⁻⁴⁰.

The role and importance of calcium in SCG and fentanyl mediated signaling has been well defined above (Chapter 1). Fentanyl's modulation of calcium makes it a relevant second messenger that reflects cellular activity. Tracking changes in intracellular calcium in response to fentanyl, D-CYSee, and naloxone can provide us with valuable insights into how the signaling is taking place. Hence, I selected methods to probe SCG response to opioids using specifically targeted indices of Ca^{2+} dynamics. Specifically, I utilized rat SCG cells to probe the ability of fentanyl to alter $i[Ca^{2+}]$.

Rat model

Sprague Dawley rats are a commonly used strain of laboratory rat in biomedical research.

Origin. Sprague Dawley rats were developed by Sprague Dawley, Inc. in the early 20th century. They were selectively bred from Wistar rats, another commonly used laboratory rat strain^{71,72}.

Characteristics. Sprague Dawley rats are albino rats, meaning they have white fur and pink eyes due to a lack of melanin. They have a docile temperament, making them relatively easy to handle and work with in laboratory settings^{73,74}.

Size. As adults, Sprague Dawley rats typically weigh between 250-600 grams, with males usually being larger than females. They are considered a medium-sized rat strain^{73,74}.

Use in research. Sprague Dawley rats are widely used in various fields of biomedical research, including toxicology, pharmacology, physiology, neuroscience, and behavioral studies. Their popularity stems from their relatively calm nature, adaptability, and availability from commercial suppliers^{75,76}.

Health and reproduction. Sprague Dawley rats are known for their robust health and reproductive capabilities, which make them suitable for breeding and longitudinal studies. They have a relatively short gestation period of about 21-23 days and produce litters ranging from 6 to 12 pups on average.

Genetic Variability. While Sprague Dawley rats are considered an inbred strain, there can still be some genetic variability between individuals due to genetic drift or minor genetic differences maintained intentionally or unintentionally in breeding colonies^{75,76}.

Handling and Husbandry. Proper care and husbandry practices are essential for maintaining the health and well-being of Sprague Dawley rats in laboratory settings. This includes providing appropriate housing conditions, diet, environmental enrichment, and veterinary care.

Overall, Sprague Dawley rats are valuable animal models for studying various physiological, pharmacological, and pathological processes, contributing significantly to scientific advancements and the development of medical treatments and therapies⁷⁷.

Surgical isolation of superior cervical ganglion tissue

To test my hypothesis, I started by isolating primary cells from SCG tissue. Working with primary neurons has an advantage over cell lines as the model mimics more than 90% of what happens *in vivo*. Also, we consciously chose to keep the entire network of neurons and glial cells intact instead of working with only neurons and eliminating glial cells as is commonly the case. Keeping the entire cellular composition of the tissues intact in culture will help replicate all the signaling mechanisms involved *in vivo*.

Male and female Sprague Dawley (SD) rats (4/sex) of approximately 6-8 weeks old were procured from Charles River labs and housed in biological sciences animal handling room for acclimatization for 2 weeks. After 2 weeks the male and female rats were paired together for breeding to acquire pups of desired age. The gestation of these animals was approximately 21-25 days after which pups were born. Newborn pups of postnatal day 0-3 were used to isolate cells. The remaining pups were maintained in the colony for future propagation of animals. All the procedures were carried out using the protocol (519 DD21-09) approved by the Kent State University institutional animal care and use committee (IACUC).

The pups were transferred to the lab in secondary containment for isolation of cells. After transfer of pups to the laboratory room, the isolation procedure was started by decapitating the pups using a guillotine. The head and neck region was used to isolate SCG tissue. The head was then transferred to a surgery bed and was fixed on the bed using 22-gauge needles. Fine scissors and fine tip forceps (Fine Science Tools, Foster City, CA) were prepared by washing and dipping them in 70% alcohol and drying them inside the hood under UV light. The surgery bed with the fixed head was mounted under a surgical microscope (Olympus) to aid with isolation. Ice-cold phosphate buffered saline (PBS; containing NaCl, KCl, Na₂HPO₄, K₂HPO₄) was added to the surgery bed to prevent the head from drying out. Carefully with a fine surgical scissor, the skin flap on the neck was removed followed by the esophagus. This revealed the carotid artery to which the SCG tissue is attached. Using fine tip forceps and scissors, the tissue was separated from the carotid artery and the SCG tissue was dissected from the root and transferred to a tube containing ice-cold Leibowitz 15 medium (L-15; ThermoFisher Scientific) with antibiotic for further processing. SCG tissue from both sides of the head was isolated from 6 rats.

Isolation of cells from superior cervical ganglion

SCG tissue transferred to ice-cold L-15 medium was used as a starting material for cell isolation. The tube was transferred to a hood where all further processing was conducted. The L-15 medium was decanted from the tube using a 1ml pipette using care to not disturb the tissue. After the tube was empty, pre-warmed 2 ml collagenase type 1 (2.5mg/ml; Worthington labs) was added to the tube and incubated in a 37°C water bath for 15 minutes. The tube was again transferred to the hood after 15 minutes and collagenase was discarded carefully to avoid disturbing the tissue. Pre-warmed 2ml trypsin (2.5mg/ml; Thermofisher Scientific) was added to the tube and incubated in a 37°C water bath for 30 minutes. After the trypsin treatment, the trypsin was discarded and pre-warmed complete L-15 medium (L-15 base media 10% FBS, 1% antibiotic antimycotic, 1% glutamax, 1% glucose and 50ng/ml nerve growth factor) was added for a 5-min incubation in the hood to halt the trypsin reaction. After 5 minutes, the medium was discarded and fresh 1ml medium was added to the tube. Using a 1 ml pipette, the tissue was triturated to release all the cells from the tissue into the medium. An additional 2ml of the medium was added to the tube to make the final volume to 3 ml. Poly-d-lysine (PDL) coated glass coverslips were prepared in advance and kept available for plating. Briefly, 1 glass coverslip was added to each well of a 6-well plate. 1mg/ml PDL in bolare buffer (Borax, sodium tetraborate decahydrate) was added to each well; cultures were incubated in the refrigerator overnight. On the next day, the PDL was discarded; the coverslips were washed with distilled water 3 times and allowed to dry overnight under the hood with UV turned on. 500ul of cell suspension was added to each coverslip and incubated in a 5% CO₂ environment for 1 hour to allow for cell attachment. After 1 hour, 1.5 ml of more medium was added to each well making

the total volume 2 ml. The cells were incubated for 12 days with fresh media being added to the cells every other day and used for either Ca^{2+} imaging or immunofluorescence.

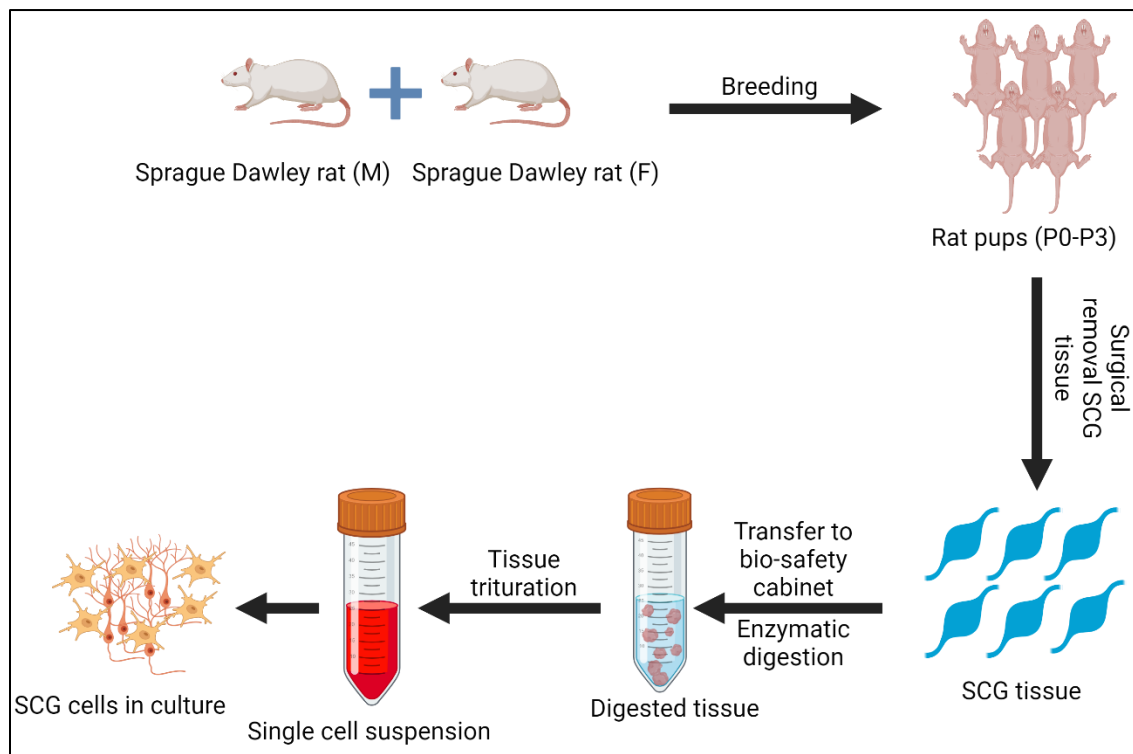


Figure 6. Schematic representation of superior cervical ganglia (SCG) cell isolation from rat pups

Real-time Ca²⁺ imaging

Since we focus on Ca²⁺ as a second messenger, our primary data comes from experiments with real-time Ca²⁺ imaging. This is a sophisticated tool that allows us measure changes in intracellular Ca²⁺ in response to the exposure to drugs and conditions in real time. 12-day cultured cells were once again used as a starting material. The cells were loaded with a calcium indicator dye Cal520AM (2mM; AAT Bioquest) in fresh medium and incubated for 1 hour in 5% CO₂ environment. After this, the cells were washed with fresh medium by replacing half the medium 3 times to remove any unbound dye and incubated again for half hour. In the meantime, all the drugs were prepared in tyrodes buffer (NaCl, KCl, CaCl₂, MgCl₂, HEPES, 4% horse serum, 5mM glucose). Since I was characterizing the intrinsic Ca²⁺ activity, I wanted to observe changes in the intracellular calcium in response to (1) calcium removal, (2) L-type calcium channel blocker (verapamil 1,50, 100mM), (3) N-type calcium channel blocker (ω -conotoxin 1, 50, 100nM), (4) sodium channel blocker (tetrodotoxin 1, 50, 100nM), and (5) neuronal gap junction blocker (quinine hydrochloride 1, 50, 100uM). All concentration of drugs were prepared in tyrodes buffer as detailed above.

Once the cells were ready to image, the coverslips were transferred to Nikon Ti2 inverted fluorescence microscope for experimentation. The coverslip was mounted on the microscope using a coverslip mount (Warner Instruments LLC) which had notches for entry and exit of the drugs to be tested. The prepared drugs were transferred to an automatic perfusion system (Warner Instruments LLC) which provided us control over dispensing each drug at the desired concentration and duration. There was a perfusion drain set up as well to remove the excess drug solutions and maintain a constant volume of the drug on the cells. The cells and the drugs were maintained at 37°C for the entire duration of the experiment. The experiments were set up for 25

minutes with the first 5 minutes of control tyrodes buffer followed by increasing concentrations of drug (dose response), with each drug concentration lasting 5 minutes, followed by the final 5 minutes of drug washout. Once the appropriate dosage of the drug was determined, a final drug concentration was determined and an experiment with just the final drug concentration was conducted again for 25 minutes, with first 5 minutes of control followed by two 5-min intervals (10 min total) of drug exposure, and then the final 10 mins (again, two 5-min intervals) of washout. The responses of cells to all drug exposures were assessed using the same protocol (i.e., five 5-min intervals) while the fluorescence was recorded using the Nikon ti2 software.

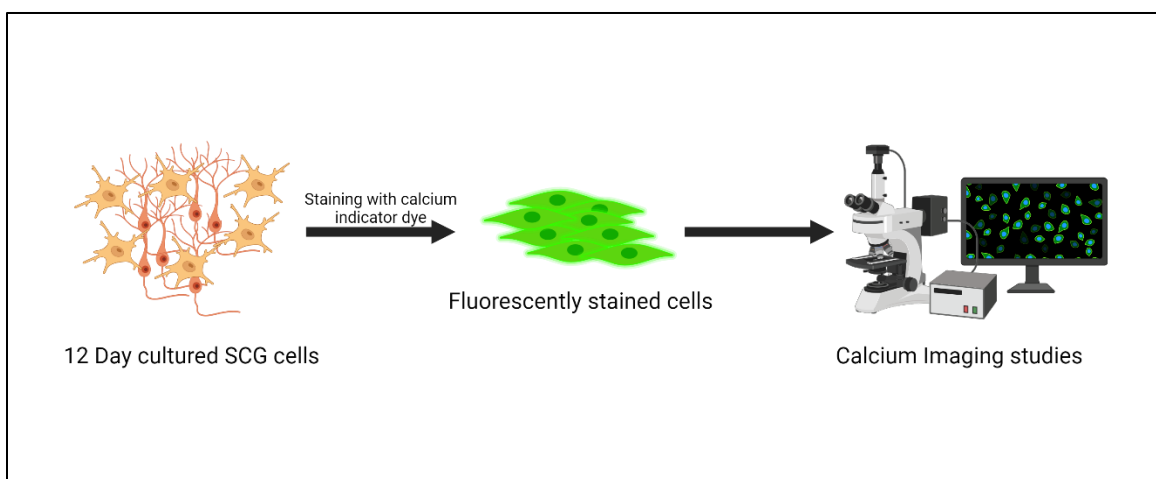


Figure 7. Schematic representation of real time Ca^{2+} imaging; superior cervical ganglia (SCG)

Data analysis

The recorded data was analyzed using the Nikon ti2 analysis software to extract the photometric data. The photometric data was then used to analyze Ca^{2+} fluorescence using ORIGIN LABS analysis software, details of which will be explained below.

Initial studies in our lab using NeuO and SR101 labeling involved manual annotation for cellular identification and drawing of cell regions of interest (ROIs). This method demonstrated poor reproducibility, with significant discrepancies between different labelers. To address this, we developed an automated, high-speed, standardized, and reproducible imaging analysis

pipeline. This pipeline utilizes macro methods in NIS Elements Advanced Research (AR) to automatically identify the soma of NeuO+ and SR101+ cells. Mean intensity values were generated after identification of two different cell types (neurons and glia) and separated the cell activities into their own categories. This generated photometric data which was then transferred to a text file for further detection of major activity phenotypes.

Following this, all the analysis was completed using Originpro2022B. Due the complex nature of the data, a full script was written to identify the photometric data. The script ran a linear regression to extract the mean intensity values from the photometric data and generated an image of different activity phenotypes detected. These were then categorized as Increase (increase in activity), Active (active cells), Decrease (decrease in activity), and Subthreshold (no activity) over the 5 phases of the experiment. The analysis chain provided photometric frequency data which was used as the main parameter to test whether the drugs displayed a significant effect on the activity as compared to control. The frequency data from each of the five phases was plotted against each other and a 3-way ANOVA was run with a 99.99% significance level. Each of the phases involving drug experiments was compared to the first control phase to show significance during changes in each phase. In the data involving control experiments the ANOVA was set in a way to show significant changes if any during the entire 25-minute experiment. The data also accounted for outliers. The outlier detection tool in Originpro2022B was used to carefully to detect and demarcate the outliers in each data set. The summary bar graphs (shown in the Chapter 3) were plotted after running ANOVA in each experiment and significance of each data set was determined. The parameters used for running the 3-way ANOVA were phase 1 against all the other phases individually to detect variances in the frequency of phases 2-1 (drug and washout) as compared to phase 1 (control)

***PART II: FENTANYL AND NALOXONE: DOES NALOXONE ALONE ALTER SCG
CALCIUM ACTIVITY?***

One of my primary goals was to determine the ability of fentanyl to change intracellular calcium activity. We have long known that naloxone is currently the only FDA approved drug to treat an opioid overdose case. In all cases involving OIRD and OUD, first responders inject naloxone to counter the effects of fentanyl. Naloxone acts as a competitive inhibitor of the MOR, which is also the receptor through which fentanyl elicits its actions. Recent reports have started outlining the side-effects of naloxone, which might outweigh its benefits¹⁸. Conversely, there have been no studies outlining the effects of naloxone by itself. **This study aims to determine the effects of fentanyl and naloxone on the intrinsic calcium activity of cells isolated from SCG tissue. This study also aims to determine whether naloxone can reverse the fentanyl mediated effects on intrinsic calcium activity of cells isolated from SCG tissue.**

Surgical isolation of superior cervical ganglion tissue

To test my hypothesis, I started by isolating primary cells from SCG tissue, as described above. Newborn pups of postnatal day 0-3 were used to isolate cells. All the procedures were carried out using the protocol (519 DD 21-09) approved by the Kent State University institutional animal care and use committee (IACUC). The pups were transferred to the lab in secondary containment for isolation of cells, and SCG tissue was obtained and cultured as described above. SCG tissue from both sides of the head was isolated from 6 rats for cell culture and real time Ca²⁺ imaging. Processing of SCG tissue was conducted as described above.

Real-time Ca²⁺ imaging and analysis

Measurement of Ca²⁺ fluorescence and subsequent analyses were completed as described above.

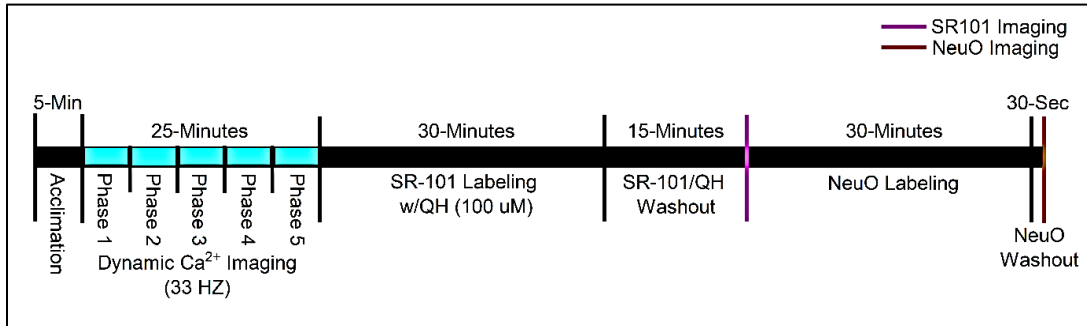


Figure 8. Real time Ca²⁺ imaging timeline.

CHAPTER III – RESULTS

PART I: CHARACTERIZATION OF INTRINSIC Ca^{2+} ACTIVITY

Real-time Ca^{2+} imaging

The main aim of this experiment was to understand what drives the intrinsic Ca^{2+} activity in the SCG cells. Moreover, we wanted to discern whether it was neurons or the glial cells acting as the driving force for the Ca^{2+} activity in and to deduce whether there was any difference in the calcium activity.

Cultured SCG cells showed intrinsic calcium activity

During 25 minutes of control, drug-free conditions, cells showed stable Ca^{2+} activity, observed in both neurons and glia as seen from the traces in **Figure 9**, below. In all phases (i.e., 1-5, delineated by color in Figure 5), SCG cultures show a very stable Ca^{2+} activity evident in both the neurons and glial cells. Comprehensive analysis of the changes in frequency was completed to detect the major activity phenotypes that were observed in **Figure 9**. Each of the five experimental phases is denoted by a different color to easily identify changes in the activity in these phases. The blue and red squares in the first two phases show a close look at the Ca^{2+}

spikes during the experiment. I completed a comprehensive analysis of the changes in frequency to detect the major activity phenotypes that were observed in the cells. **Figures 10A and 10B** present this analysis of major activity phenotypes under control, drug-free conditions in NeuO-labeled neurons and SR101-labeled glia from the SCG. The study categorizes this cellular activity across five phases, highlighting the stability and changes in activity levels over time without pharmacological intervention.

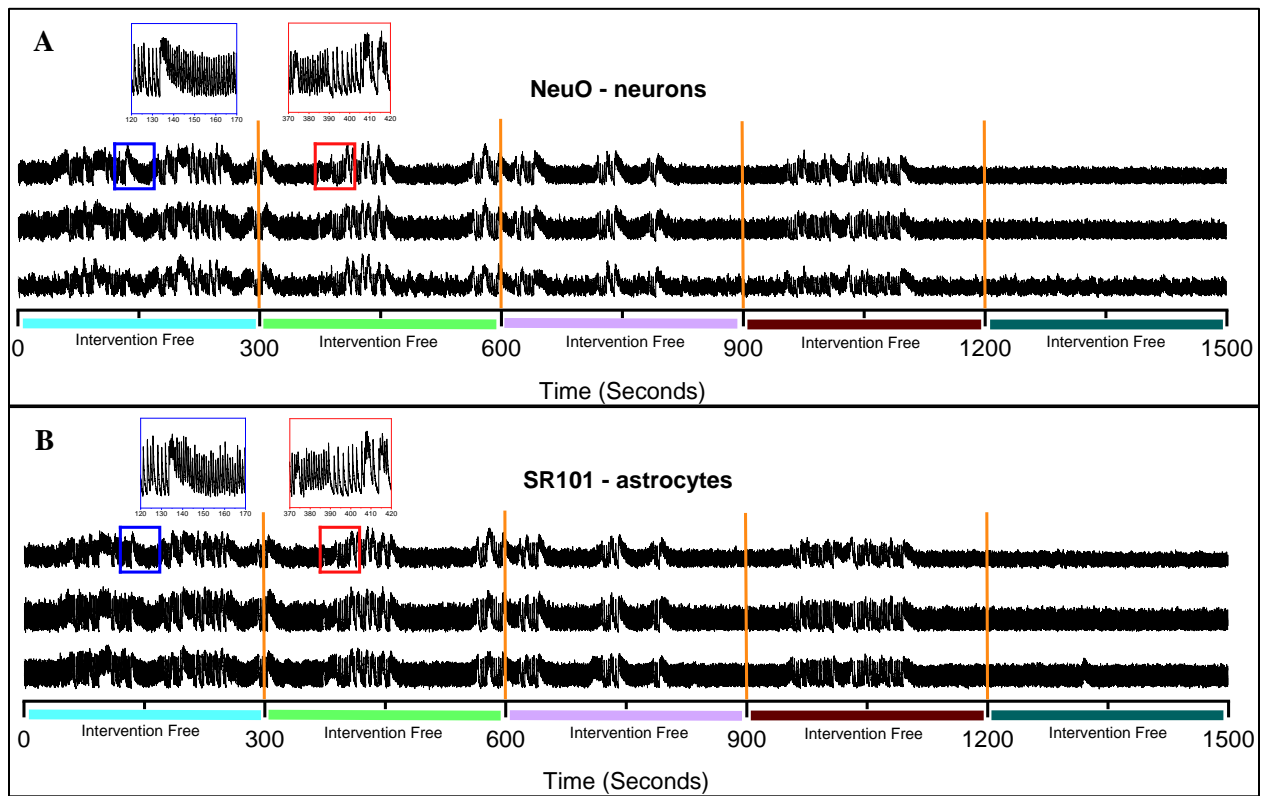


Figure 9. Typical traces depicting the effects of control drug free intervention in NeuO-labeled neurons (A) and SR101 labeled astrocytes (B) show consistent activity throughout all 5 phases.

In Phase 1, all 127 neurons (100%) and 47 glia are classified as active, indicating a baseline level of activity. There are no cells in the subthreshold category, showing that initially, all cells exhibit significant activity above the threshold frequency of 0.0132 Hz. As the study progresses to Phase 2, the classification remains unchanged: all cells continue to be classified as active (127 neurons, and 47 glia, 100%). In phase 3, 126 neurons (99.2%) remain classified as active, but one neuron (0.8%) showed a decrease in activity whereas all 47 glia (100%) remain classified as active. This small shift indicates the beginning of variability in neuronal responses but not in glia. By Phase 4, the number of cells with decreased activity increases slightly to neurons 4 (3.1%), and glia 3 (6.4%) while the majority (123 neurons, 96.9% and 44 glia 93.6%) remain active. No cells fall into the "Subthreshold" or "Increase" categories, suggesting a trend towards a slight reduction in activity for a small subset of cells. In Phase 5, all cells (127 neurons, and 47 glia 100%) exhibit no significant change in activity, reinforcing the trend observed in earlier phases. There are no cells with increased activity or in the Subthreshold category.

Major activity phenotypes detected: The pie chart in **Figure 10B, section 3a** summarizes the overall distribution of major activity phenotypes across all phases. The overwhelming majority of neurons (96.1%) and glia (93.6%) remain active throughout all 5 phases, while a small fraction of neurons (3.1%) and glia (6.4%) showed a decrease in activity, and only 0.8% neurons exhibit no change.

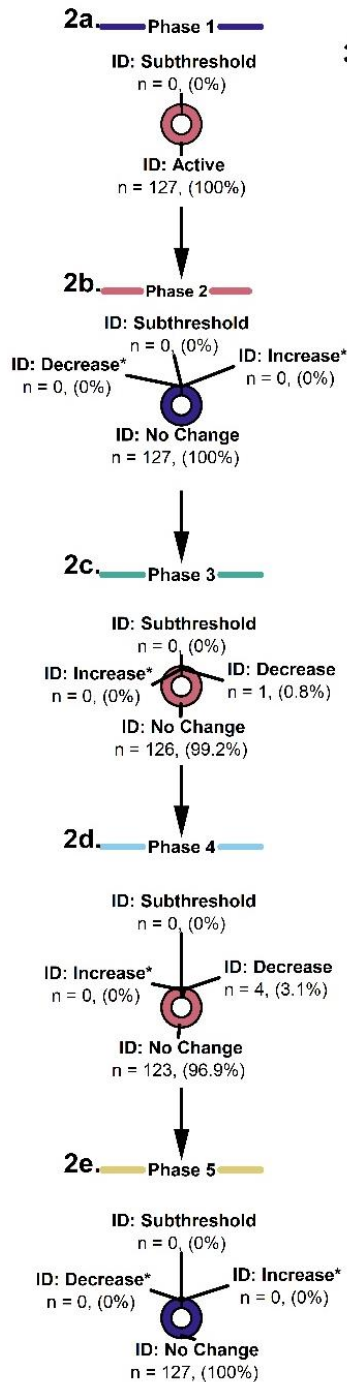
Bar graphs (**Figure 10A, sections 4a and 4b**) illustrate the frequency of neuronal activity (Hz) across phases, showing minor but significant changes in certain phases. These graphs highlight the dynamic yet stable nature of cellular activity under control conditions, with slight decreases observed in specific phases.

Comparisons between different phases, specifically Phase 1 versus Phase 5 (**Figure 10A, section 5a**) and Phase 2 versus Phase 4 (**Figure 10A, section 5b**), further emphasize the minor fluctuations in cellular activity. In the comparison of Phase 1 versus Phase 5, most neurons showed no change (45 neurons, 35.4%) or a decrease in activity (81 neurons, 63.8%), with only one neuron (0.8%) becoming subthreshold. Similarly, the majority of glia showed no change (19 glia, 40.4%) or a decrease in activity (27 glia, 57.4%) with only 1 glia (2.1%) becoming subthreshold. Similarly, in Phase 2 versus Phase 4, 46 neurons (36.2%) and 46 glia (97.9%) showed no change, while 80 neurons (63%) and no glia exhibit a decrease in activity. The analysis reveals that under control, drug-free conditions, most cells maintain their initial active state across multiple phases. A small subset shows a slight decrease in activity, indicating minimal variability in cellular responses over time. The data suggests a high level of stability in cellular activity in the absence of pharmacological intervention, with only minor changes detected in later phases. Overall, this detailed examination of neuronal activity phenotypes under control conditions provides valuable insights into the baseline behavior of cells, highlighting their inherent stability.

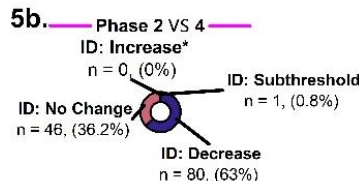
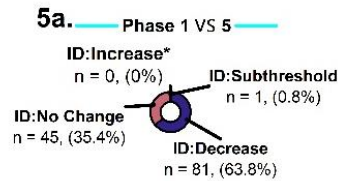
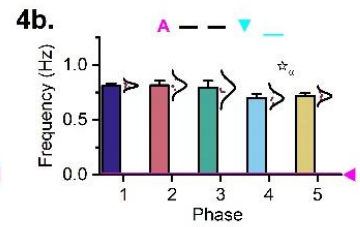
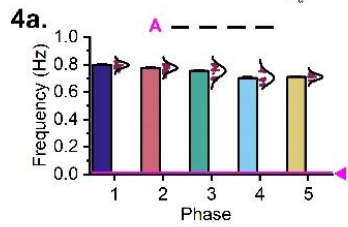
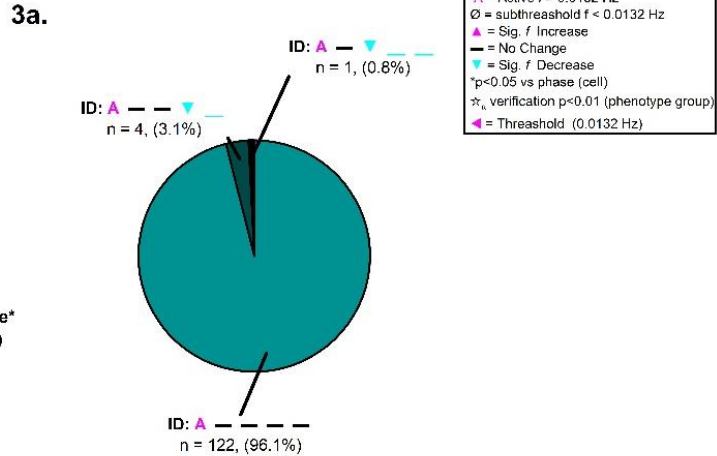
A

Major activity phenotypes under control drug free conditions in NeuO labelled neurons

1. Cell labeling: NeuO



Major activity phenotypes detected (%_{total} > 3)



B

Major activity phenotypes under control drug free conditions in SR101 labelled glia

1. Cell labeling: SR101

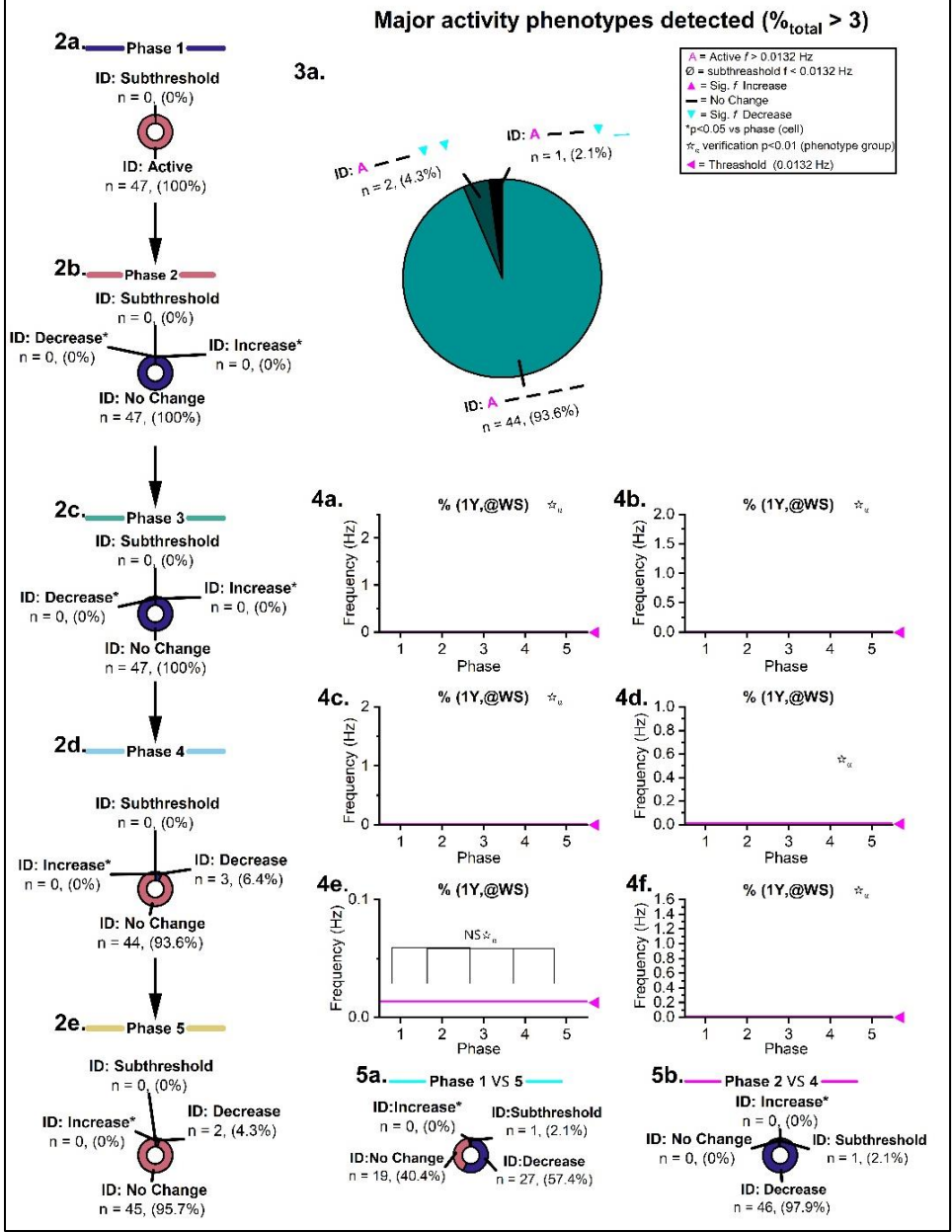


Figure 10. Detailed analyses revealing the major activity phenotypes detected in neurons (A) and glia (B) under drug free control, conditions. Section 2 (a-e) depicts the changing activity levels of the cells in all the phases. The pie chart (3a) categorizes the major activity phenotypes, and section 4 shows bar graphs of the most observed phenotypes detected. Section 5 shows a phase comparison in the changes in activity between Phases 1 and 5 and Phases 2 and 4, which showed that under control conditions, there were no significant changes in phase 1 and 5 and 2 and 4.

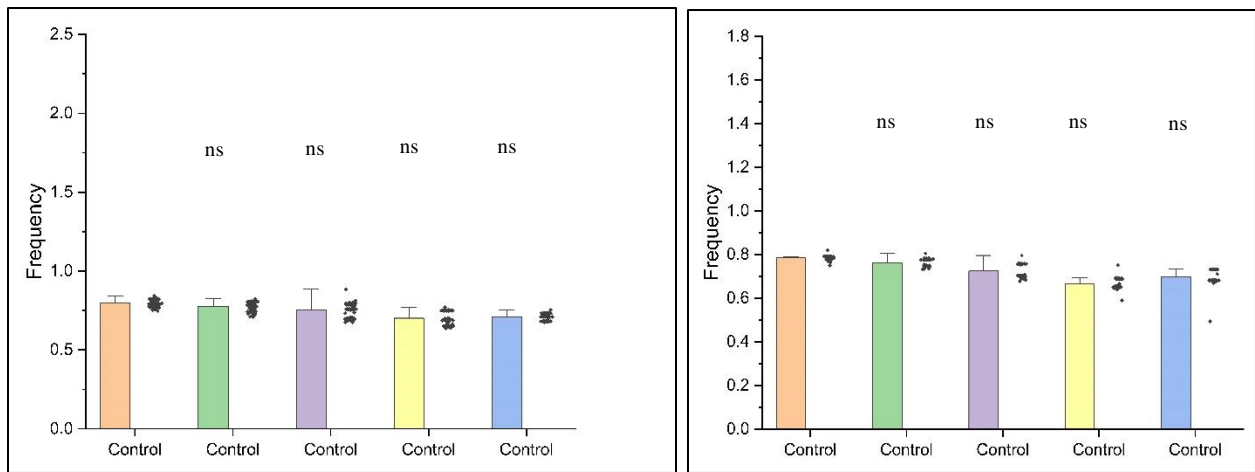


Figure 11: Summary graphs of superior cervical ganglia (SCG) neurons and glia under control conditions depicting consistent activity throughout all 5 phases. ^{ns} Not significantly different compared to phase 1 control ($p > 0.01$).

Extracellular calcium is crucial for the activity

Figure 12 shows representative traces of the intrinsic Ca^{2+} activity observed in cells isolated from SCGs under Ca^{2+} -free conditions. As observed from the traces, under Ca^{2+} -free conditions the cells, both neurons (**Figure 12A**) and astrocytes (**Figure 12B**) display an inhibition of the activity starting from Phase 2 where Ca^{2+} buffer is introduced, and continuing onto Phase 3. After re-introduction of Ca^{2+} starting fin Phase 4, the intrinsic activity re-emerges, nearly

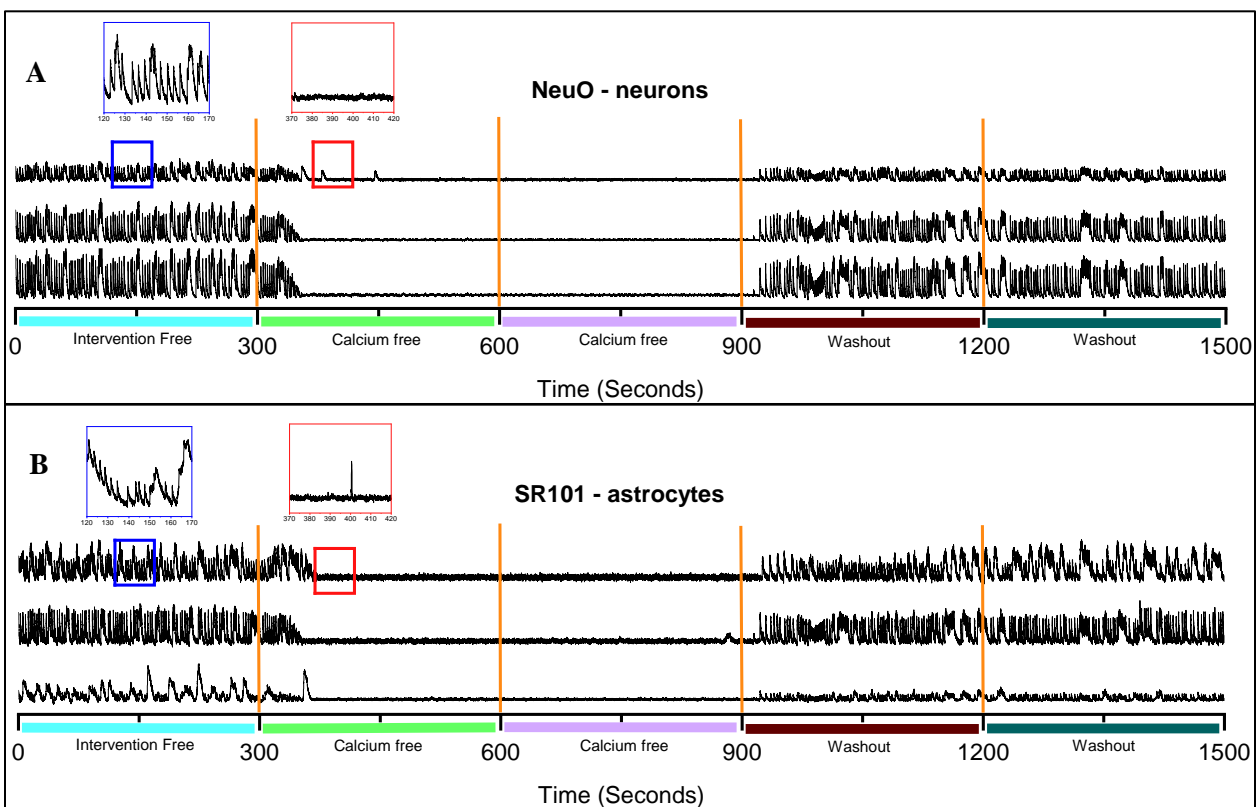


Figure 12. Typical traces depicting the effects of Ca^{2+} -free medium in NeuO-labeled neurons (A) and SR101 labeled astrocytes (B) show inhibition of activity in Ca^{2+} -free Phases (2 and 3) with return to control levels in washout Phases (4 and 5).

reaching control levels by Phase 5. This signifies the importance of extracellular Ca^{2+} in normal functioning of the intrinsic Ca^{2+} activity.

Figure 13 presents a comprehensive analysis of the major activity phenotypes detected after the removal of calcium (Ca^{2+}) in NeuO-labeled neurons (**Figure 13A**) and SR101-labeled glia (**Figure 13B**) from the SCG. The study tracked changes in neuronal activity across five distinct phases, each phase revealing different phenotypic characteristics and firing frequencies.

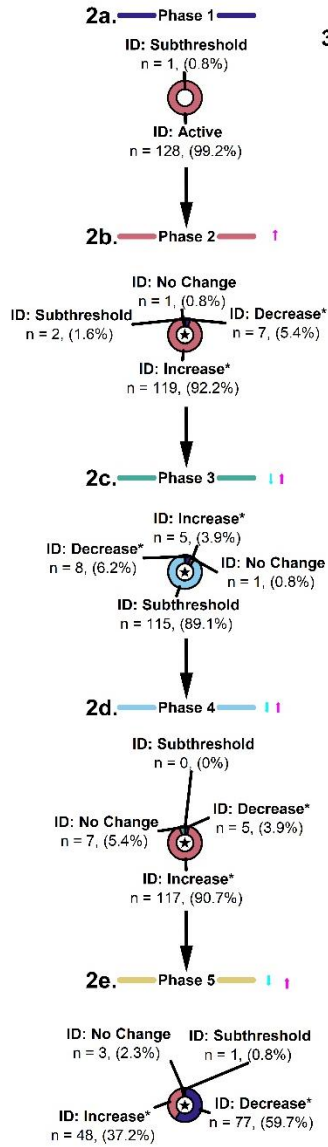
In Phase 1, most cells were categorized as Active (257 cells, 99.2%), with only one neuron and 1 glial cell labeled as "Subthreshold" (0.8%). As the study progressed to Phase 2, with the removal of extracellular Ca^{2+} there was a diversification in activity phenotypes: 2 neurons (1.6%) and 3 glia (2.3%) showed no change, 1 neuron (0.8%) and 3 glia (2.3%) remained subthreshold, 7 neurons (5.4%) and 23 glia (17.7%) exhibited a significant decrease in activity, and a substantial 119 neurons (92.2%) and 101 glia (77.7%) displayed increased activity. This shift indicates an early response to the removal of Ca^{2+} from the buffer. Phase 3, with the continuation of Ca^{2+} free medium, saw a significant shift in activity, with 5 neurons (3.9%) and 20 glia (15.4%) showing decreased activity, 1 neuron (0.8%) maintaining the same activity level, and a notable 115 neurons (89.1%) and 106 glia (81.5%) falling into the subthreshold category. This marked reduction in activity suggests a strong inhibitory effect in this phase. By Phase 4, no neurons but only 3 glia (2.3%) were subthreshold, while 7 neurons (5.4%) and 13 glia (10%) showed no change, 5 neurons (3.9%) and 2 glia (1.5%) exhibited decreased activity, and a dominant 117 neurons (90.7%) and 112 glia (86.2%) showed increased activity, reflecting a resurgence in neuronal activity. Phase 5 continued to show dynamic changes, with 3 neurons (2.3%) and 5 glia (3.8%) exhibiting no change, 1 neuron (0.8%) and 1 glia (0.8%) categorized as subthreshold, 48 neurons (37.2%) and 70 glia (53.8%) showing increased activity, and 77 neurons (59.7%) and 54 glia (41.5%) demonstrating a significant decrease in activity.

The comparative analysis between phases, particularly Phase 1 versus Phase 5 and Phase 2 versus Phase 4, highlighted the transitions in cellular behavior, with varying proportions of neurons and glia showing increased, decreased, or unchanged activity levels. The bar graphs in **Figure 13**, section 4 illustrate frequency changes across different phases, highlighting significant variations in activity phenotypes. The data indicated that while a large proportion of cells initially remained active or increased in activity following Ca^{2+} removal, subsequent phases saw a significant shift towards decreased or subthreshold activity. These findings suggest a complex, phased response of the cells to the absence of Ca^{2+} involving both inhibitory and excitatory adjustments over time. Overall, **Figure 13** provides a detailed and dynamic picture of cellular activity changes in response to calcium removal, showcasing the intricate nature of neuronal adaptation.

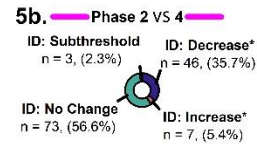
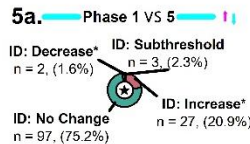
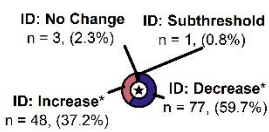
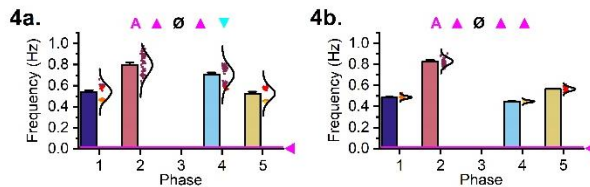
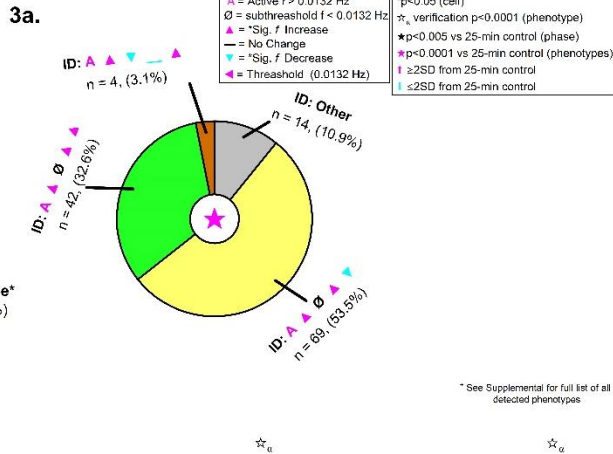
A

Major activity phenotypes detected after removal of Ca²⁺ in NeuO labelled neurons from superior cervical ganglion

1. Cell labeling: NeuO
 $n_{\text{cell}} = 2148$, $n_{\text{phenotypes}} = 112$
 cells removed = 116



Major activity phenotypes detected (%_{total} > 3)



B

Major activity phenotypes detected after removal of Ca in SR101 labelled glia from superior cervical ganglion

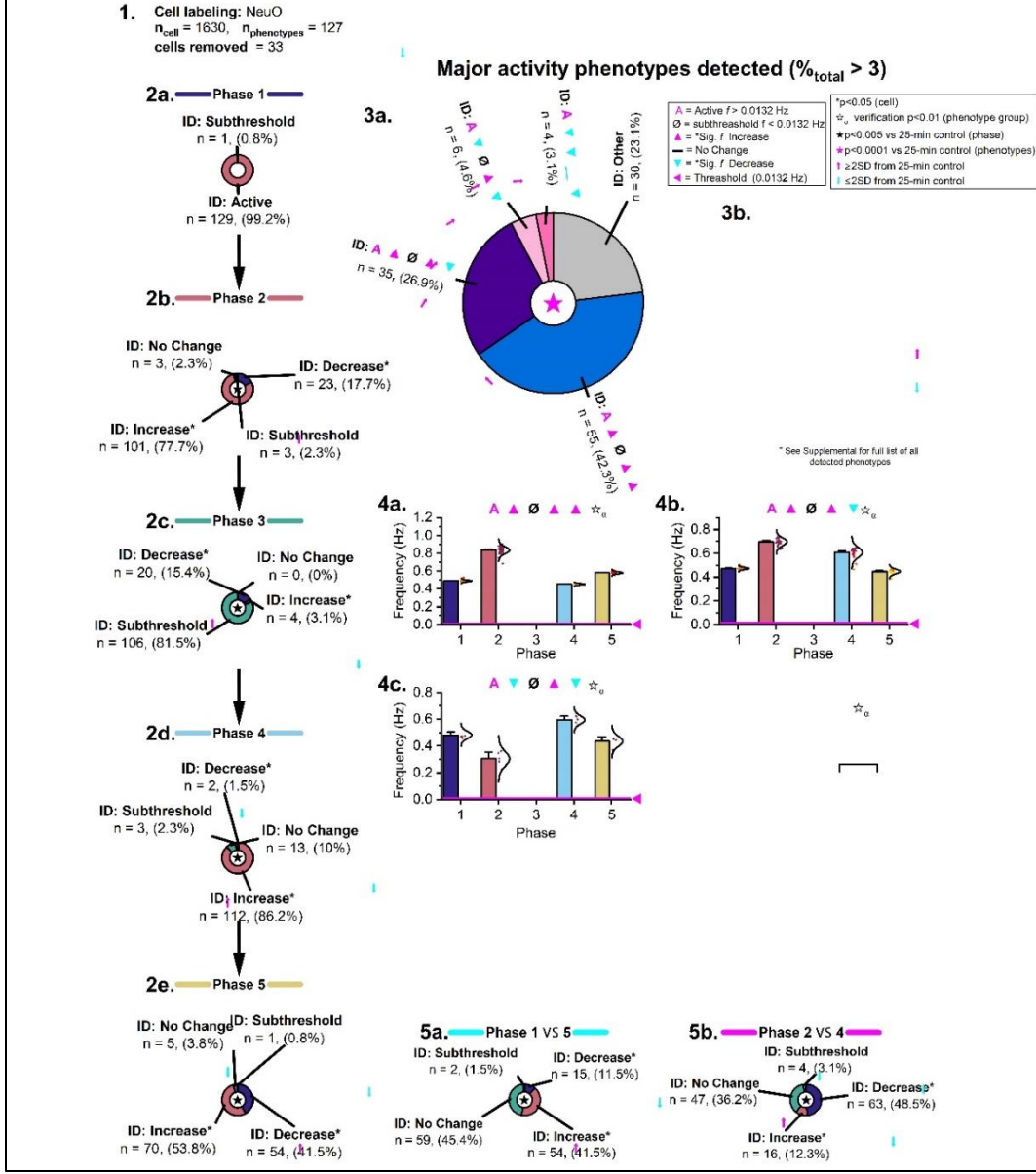


Figure 13. Detailed analyses revealing the major activity phenotypes detected in neurons (A) and glia (B) under drug-free, control conditions. Section 2 (a-e) depicts the changing activity levels of the cells in all the phases. The pie chart (section 3a) categorizes the major activity phenotypes and section 4 shows bar graphs of the most observed phenotypes detected.

Section 5 shows a phase comparison in the changes in activity between Phases 1 and 5 and Phases 2 and 4.

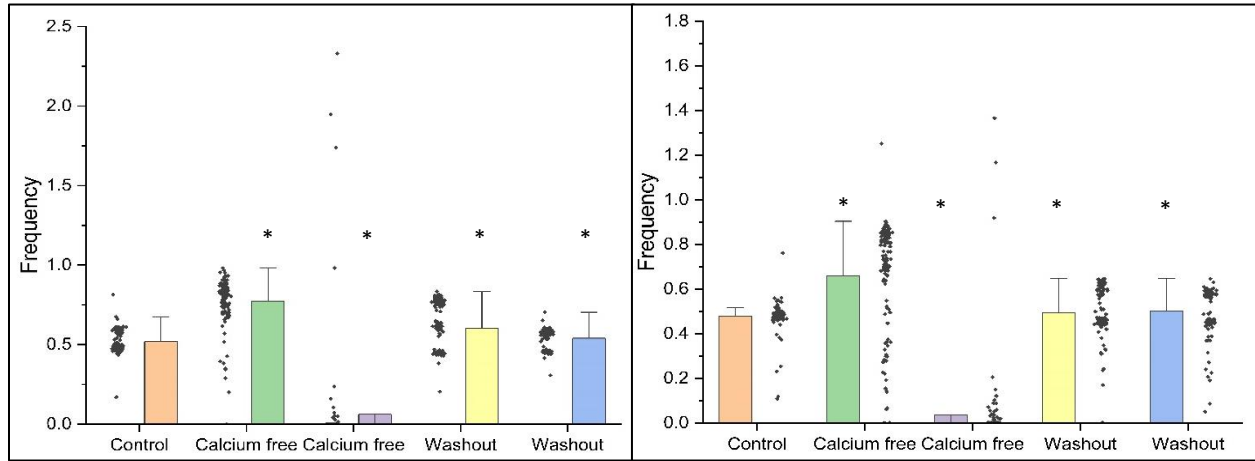


Figure 14: Summary graphs of superior cervical ganglion (SCG) neurons and glia after removal of extracellular Ca^{2+} . *Significantly different compared to control in phase 1 ($p < 0.01$).

N-type calcium channel is partly involved in regulating the activity

Figure 15 shows representative traces of the intrinsic Ca^{2+} activity observed in cells isolated from SCGs after application of single dose of conotoxin (50nM). As is observed from the traces, 50nM conotoxin added at the start of Phase 2 induced a complete inhibition of the activity in Phases 2 and 3, respectively, in both neurons (**Figure 15A**) and astrocytes (**Figure 15B**). The activity returned to control levels after washout of conotoxin in Phases 4 and 5, indicating involvement of N-type calcium channel as one driver of calcium activity.

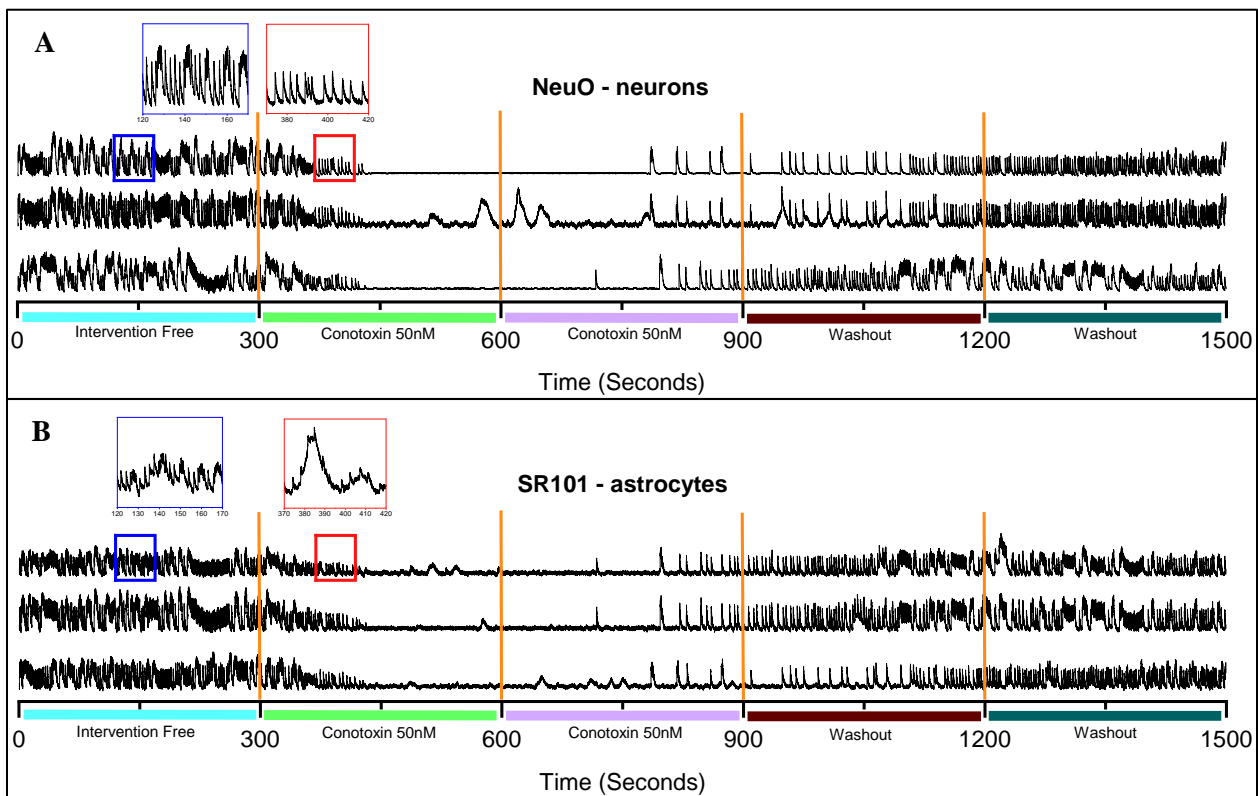


Figure 15. Typical traces depicting the effects of conotoxin (50nM) in NeuO-labeled neurons (A) and SR101 labeled astrocytes (B) show inhibition of activity in conotoxin phases (2 and 3) with return to control levels in washout phases (4 and 5).

NeuO-labeled neurons. Initially, in Phase 1, most NeuO-labeled neurons (98.7%) were active, with a small fraction (1.3%) at subthreshold levels. As the conotoxin is applied, Phase 2 reveals a significant shift, where 97.4% of neurons exhibit decreased intrinsic Ca^{2+} activity; there are minimal increases (0.7%) or no changes (0.7%) observed. This pattern of decreased activity persists into Phase 3, with 96.7% of neurons still showing decreased activity and 2% showing no change. By Phase 4, there is a notable change: 46.4% of neurons exhibited increased activity, while 51.6% remain unchanged. The increased neuronal activity continued in Phase 5 with a significant number of neurons (77.8%) showing increased activity and 20.3% remaining unchanged. The pie chart (**Figure 15A, section 3a**) summarizes these findings, showing that 49.7% of neurons experienced significant decreases in activity, 25.5% showed increases, and 18.6% fell into other categories. Comparative analyses (**Figure 15A, sections 5a and 5b**) highlight substantial decreases between Phases 1 and 5 and between Phases 2 and 4. Frequency changes (**Figure 15A, sections 4a-c**) show significant variations, particularly in Phases 2 and 4.

SR101-labeled glia. SR101-labeled glial cells show different activity patterns compared to cultured SCG neurons. In Phase 1, 94.5% of glial cells are active, and 5.5% were inactive. With conotoxin application, Phase 2 revealed a dramatic shift, with 85.2% of cells showing decreased activity, 8.9% becoming inactive, and only 2.6% showing increased activity. Phase 3 showed a slight shift: 83.4% of cells remained decreased, 4.8% are inactive, and 2.2% showed increased activity. In Phase 4, the activity levels diversify: 63.1% of cells remained unchanged, 24.4% increase, and 9.6% are inactive. By Phase 5, a majority (80.8%) of glial cells exhibited decreased activity, 7.4% were inactive, and 63.1% showed increased activity. The pie chart (**Figure 15B, section 3a**) indicates that 56.6% of cells experienced a significant decrease, 24.6% showed increases, and 10% fell into other categories. Comparative analyses (**Figure 15B,**

section 5a and 5b) reveal notable decreases between Phases 1 and 5 and between Phases 2 and 4. Changes in frequency depicted in the bar graphs (**Figure 15B, sections 4a-f**) depict significant fluctuations, especially in Phases 2 (introduction of conotoxin) and 4 (washout of conotoxin), reflecting the dynamic response of glial cells to conotoxin.

Together, these analyses reveal the differential impact of 50 nM conotoxin on NeuO-labeled neurons and SR101-labeled glial cells. NeuO-labeled neurons initially show a marked decrease in activity upon conotoxin application, but many eventually exhibit increased activity by the later phases. In contrast, SR101-labeled glial cells show a pronounced and sustained decrease in activity with yadda-toxin, with fewer cells transitioning to an increased activity state. This contrast highlights the cell type-specific responses to conotoxin, with neurons showing a more dynamic range of activity changes compared to the more consistently decreased activity in glial cells with conotoxin. The frequency changes across phases in both cell types underscore the nuanced and phase-dependent effects of conotoxin on cellular activity.

A

Major activity phenotypes after application of 50nM conotoxin in NeuO labelled neurons

1.

Cell labeling: NeuO

2a. Phase 1

ID: Subthreshold

n = 2, (1.3%)

ID: Active

n = 151, (98.7%)

2b. Phase 2

ID: No Change

n = 1, (0.7%)

ID: Subthreshold

n = 2, (1.3%)

ID: Increase*

n = 1, (0.7%)

ID: Decrease*

n = 149, (97.4%)

2c. Phase 3

ID: Increase*

n = 0, (0%)

ID: Subthreshold

n = 2, (1.3%)

ID: No Change

n = 3, (2%)

ID: Decrease*

n = 148, (96.7%)

2d. Phase 4

ID: Decrease*

n = 0, (0%)

ID: Subthreshold

n = 3, (2%)

ID: No Change

n = 79, (51.6%)

ID: Increase*

n = 71, (46.4%)

2e. Phase 5

ID: Subthreshold

n = 2, (1.3%)

ID: No Change

n = 31, (20.3%)

ID: Decrease*

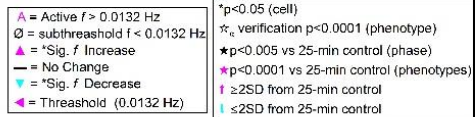
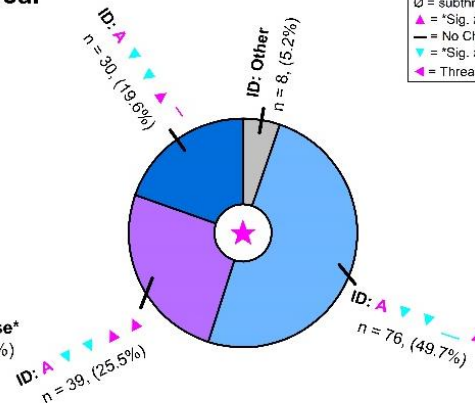
n = 1, (0.7%)

ID: Increase*

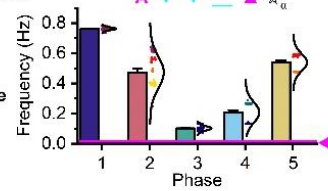
n = 119, (77.8%)

Major activity phenotypes detected (%_{total} > 3)

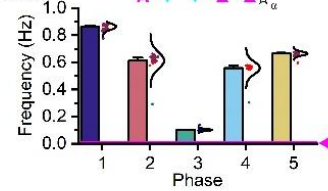
3a.



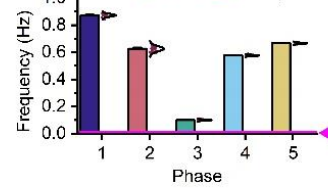
4a.



4b.



4c.



5a. Phase 1 VS 5

ID: Increase*

n = 0, (0%)

ID: Subthreshold

n = 3, (2%)

ID: Increase*

n = 2, (1.3%)

ID: Decrease*

n = 148, (96.7%)

5b. Phase 2 VS 4

ID: Subthreshold

n = 4, (2.6%)

ID: No Change

n = 67, (43.8%)

ID: Decrease*

n = 77, (50.3%)

ID: Increase*

n = 5, (3.3%)

B

Major activity phenotypes after application of 50nM conotoxin in SR101 labelled glia

1. Cell labeling: SR101

2a. Phase 1

ID: Inactive
n = 15, (5.5%)

ID: Active
n = 256, (94.5%)

2b. Phase 2

ID: No Change
n = 9, (3.3%)

ID: Inactive
n = 24, (8.9%)

ID: Increase*
n = 7, (2.6%)

ID: Decrease*
n = 231, (85.2%)

2c. Phase 3

ID: No Change
n = 13, (4.8%)

ID: Inactive
n = 26, (9.6%)

ID: Increase*
n = 6, (2.2%)

ID: Decrease*
n = 226, (83.4%)

2d. Phase 4

ID: Decrease*
n = 8, (3%)

ID: Increase*
n = 66, (24.4%)

ID: Inactive
n = 26, (9.6%)

ID: No Change
n = 171, (63.1%)

2e. Phase 5

ID: Inactive
n = 20, (7.4%)

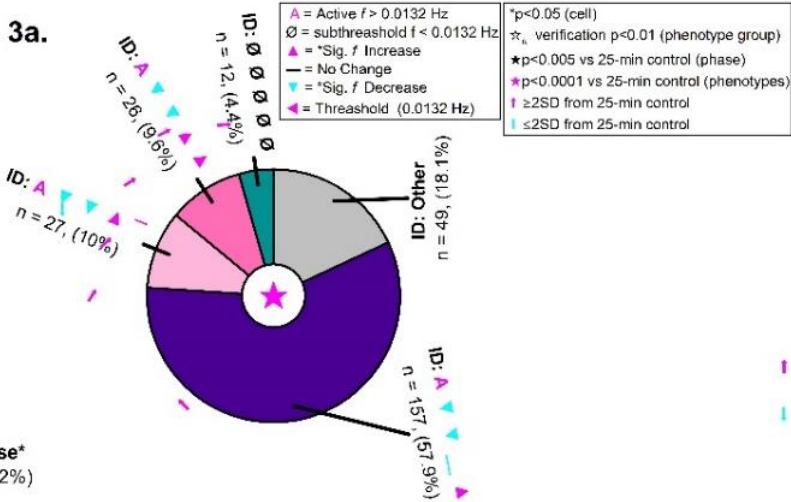
ID: No Change
n = 42, (15.5%)

ID: Decrease*
n = 6, (2.2%)

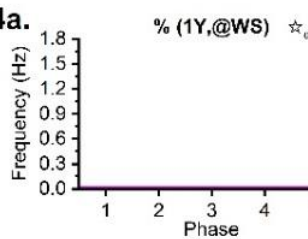
ID: Increase*
n = 203, (74.9%)

Major activity phenotypes detected (%_{total} > 3)

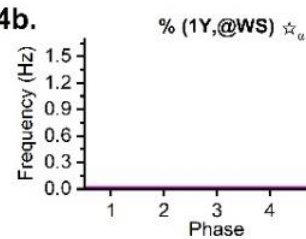
3a.



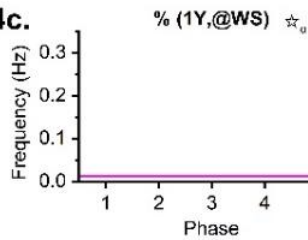
4a.



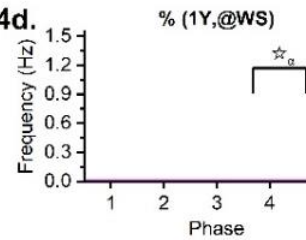
4b.



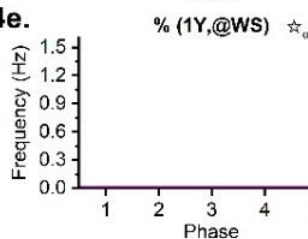
4c.



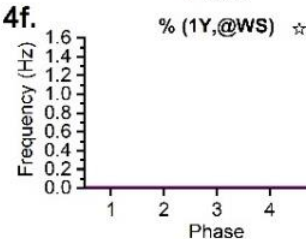
4d.



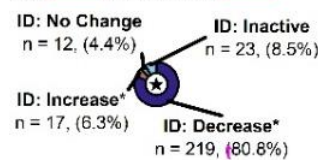
4e.



4f.



5a. Phase 1 VS 5



5b. Phase 2 VS 4

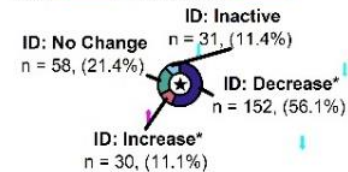


Figure 16. Detailed analyses revealing the major activity phenotypes detected in neurons (A) and glia (B) under 50nM conotoxin conditions. Section 2 (a-e) depicts the changing activity levels of the cells in all the phases. The pie chart (section 3a) categorizes the major activity phenotypes and section 4 shows bar graphs of the most observed phenotypes detected. Section 5 shows a phase comparison in the changes in activity between Phases 1 and 5 and Phases 2 and 4.

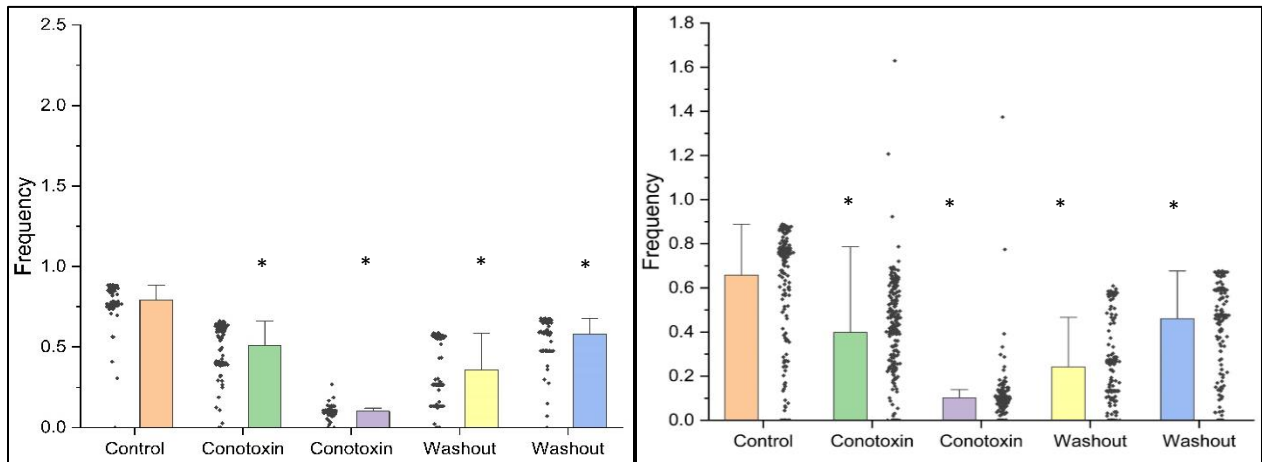


Figure 17: Summary graphs of superior cervical ganglion (SCG) neurons and glia after application of N-type calcium channel blocker conotoxin. *Significantly different compared to control in phase 1 ($p < 0.01$).

L-type Calcium channel drives the activity

Figure 18 shows representative traces of the intrinsic Ca^{2+} activity observed in cells isolated from SCGs after application of single dose of verapamil (50 μM), the L-type calcium channel blocker. As is observed from the traces, 50 μM verapamil induced a complete inhibition of the activity in Phases 2 and 3 respectively in both neurons (**Figure 18A**) and astrocytes (**Figure 18B**). The activity started resuming in Phase 4 and returned to control levels after washout of verapamil in Phase 5, indicating involvement of L-type calcium channel in driving the activity.

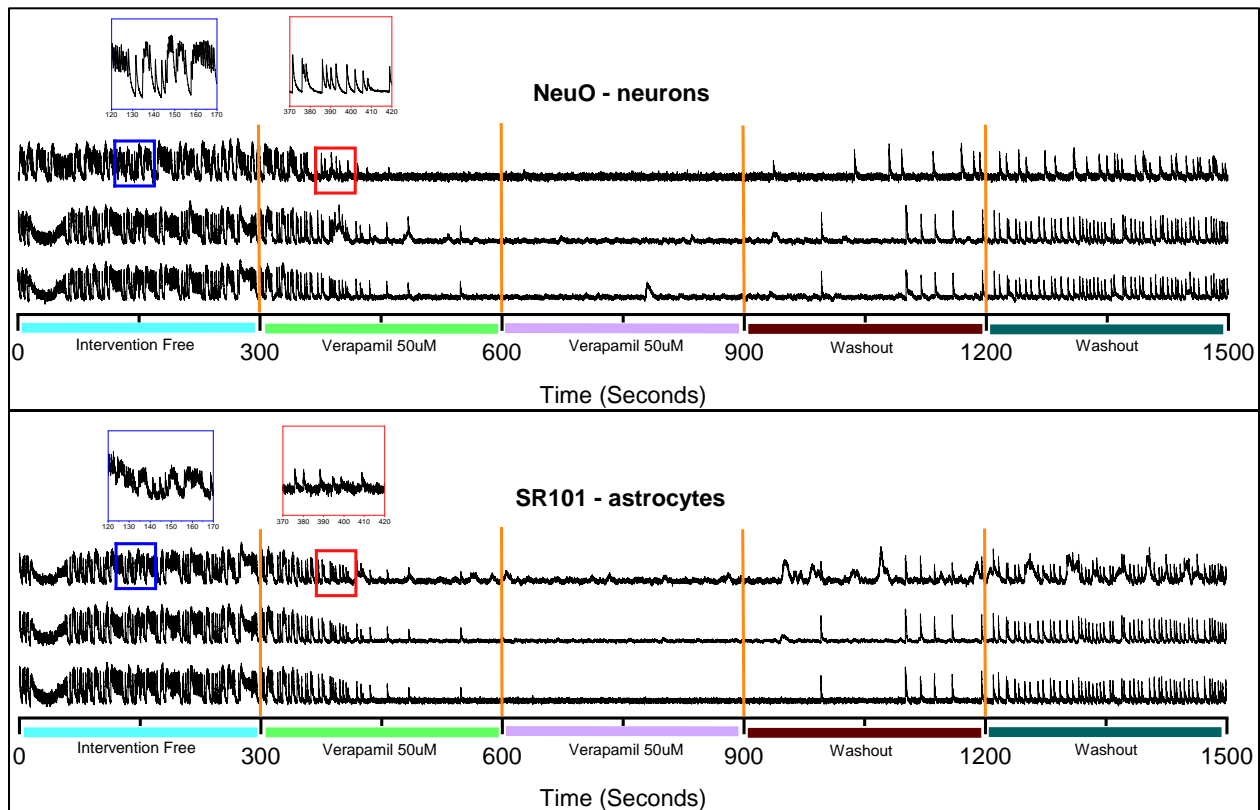


Figure 18. Typical traces depicting the effects of verapamil (50uM) in NeuO-labeled neurons (A) and SR101-labeled astrocytes (B) show inhibition of activity with verapamil in Phases 2 and 3, with a partial return to control levels in washout (Phases 4 and 5).

Figure 19 provides a detailed analysis of cellular activity phenotypes in NeuO-labeled neurons (**Figure19A**) and SR101-labeled glia (**Figure 19B**) after exposure to 50 μ M verapamil, tracked over five experimental phases.

Phase-by-Phase Analysis: Phase 1 began with all 98 neurons (100%) and 170 glia (100%) classified as active, indicating a uniform baseline of high activity. There were no cells exhibiting subthreshold activity, implying that all cells are above the threshold of activity from the start, in Phase 2, all the neurons (100%) showed a decrease in their activity, while we saw 168 glia (98.8%) decreased with only 1 cell (0.6%) showing subthreshold activity. This suggests that verapamil had started to induce a noticeable impact on the cells, yet cells were still able to maintain their initial high activity state. Phase 3 marks the first significant shift in cellular behavior. Here, 98% of the neurons and 98% glia fell below subthreshold levels in activity, indicating the inhibitory effect of verapamil. Only 1% of neurons and 2.4% glia showed an increase in activity, and another 1% remained unchanged. The changes in activity during this phase clearly showed that verapamil started to suppress cellular activity significantly for most cells. In Phase 4, however, the trend changed to increased activity, with 98% of neurons and 93% glia continuing to exhibit increased activity levels. Additionally, 2% of neurons and 1.2% of glia now fell into the subthreshold category, indicating their activity had dropped below the baseline threshold. No neurons and glia remain unchanged in this phase, underscoring the pervasive effect of verapamil. The intrinsic Ca^{2+} during Phase 5 (final washout) revealed that most neurons (95.9%) and glia (95%) maintained their increased activity levels from the previous phase.

However, 4.1% of neurons exhibited an increase in activity, suggesting some late-stage variability in response to verapamil. No neurons but 3 glia (1.8%) remained at the subthreshold level, and there are no further changes in most cells, indicating a stabilization of verapamil's impact.

Summary and comparative analysis. The pie chart (**Figure 19, section 3a**) synthesizes these findings, showing that 94.9% of neurons and 89% glia experienced a decrease in activity. A small fraction, 3.1% (neurons) and 12.4% (glia), exhibited other phenotypes. This distribution highlights the dominant effect of verapamil in reducing cellular activity across the population. The bar graph (**Figure 19, section 4a**) illustrates frequency changes across the five phases, with significant activity reductions, particularly between Phases 2 and 4. This confirms the substantial impact of verapamil on cellular activity suppression. Comparative analyses (**Figure 19, sections 5a and 5b**) between different phases reveal pronounced decreases in activity. Between Phase 1 and Phase 5, 99% of neurons and 97% glia showed decreased activity, with only 1% neurons and 2.4% glia at subthreshold levels. Similarly, comparisons between Phase 2 and Phase 4 show that 99% of neurons and 97% glia demonstrate decreased activity, with no neurons and glia remaining unchanged.

Conclusion. The application of 50 μ M verapamil (L-type calcium channel blocker) led to a significant and sustained decrease in cellular activity, beginning in Phase 3 and continuing through Phase 5. The dominant phenotype is a marked reduction in activity, affecting nearly all cells. This consistent decrease highlights verapamil's potent effect in modulating neuronal excitability, underscoring its potential for influencing neuronal activity dynamics in experimental settings. The detailed phase-by-phase analysis and comparative studies further reinforce the significant role of L-type calcium channel in regulating calcium activity in SCG neurons.

A

Major activity phenotypes after application of 50uM verapamil in NeuO labelled neurons

1.

Cell labeling: NeuO

2a. Phase 1

ID: Subthreshold
n = 0, (0%)

ID: Active
n = 98, (100%)

2b. Phase 2

ID: Increase*
n = 0, (0%)

ID: Subthreshold
n = 0, (0%)

ID: No Change
n = 0, (0%)

ID: Decrease*
n = 98, (100%)

2c. Phase 3

ID: No Change
n = 0, (0%)

ID: Increase*
n = 1, (1%)

ID: Decrease*
n = 1, (1%)

ID: Subthreshold
n = 96, (98%)

2d. Phase 4

ID: Decrease*
n = 2, (2%)

ID: Subthreshold
n = 0, (0%)

ID: No Change
n = 0, (0%)

ID: Increase*
n = 96, (98%)

2e. Phase 5

ID: Subthreshold
n = 0, (0%)

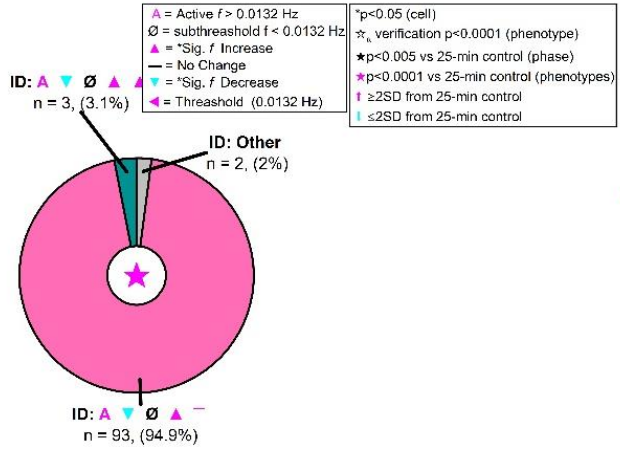
ID: Decrease*
n = 0, (0%)

ID: Increase*
n = 4, (4.1%)

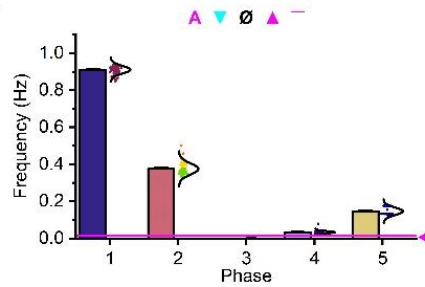
ID: No Change
n = 94, (95.9%)

Major activity phenotypes detected (%_{total} > 3)

3a.



4a.



5a. Phase 1 VS 5

ID: Increase*
n = 0, (0%)

ID: No Change
n = 0, (0%)

ID: Decrease*
n = 97, (99%)

ID: Subthreshold
n = 1, (1%)

5b. Phase 2 VS 4

ID: No Change
n = 0, (0%)

ID: Increase*
n = 0, (0%)

ID: Decrease*
n = 97, (99%)

ID: Subthreshold
n = 1, (1%)

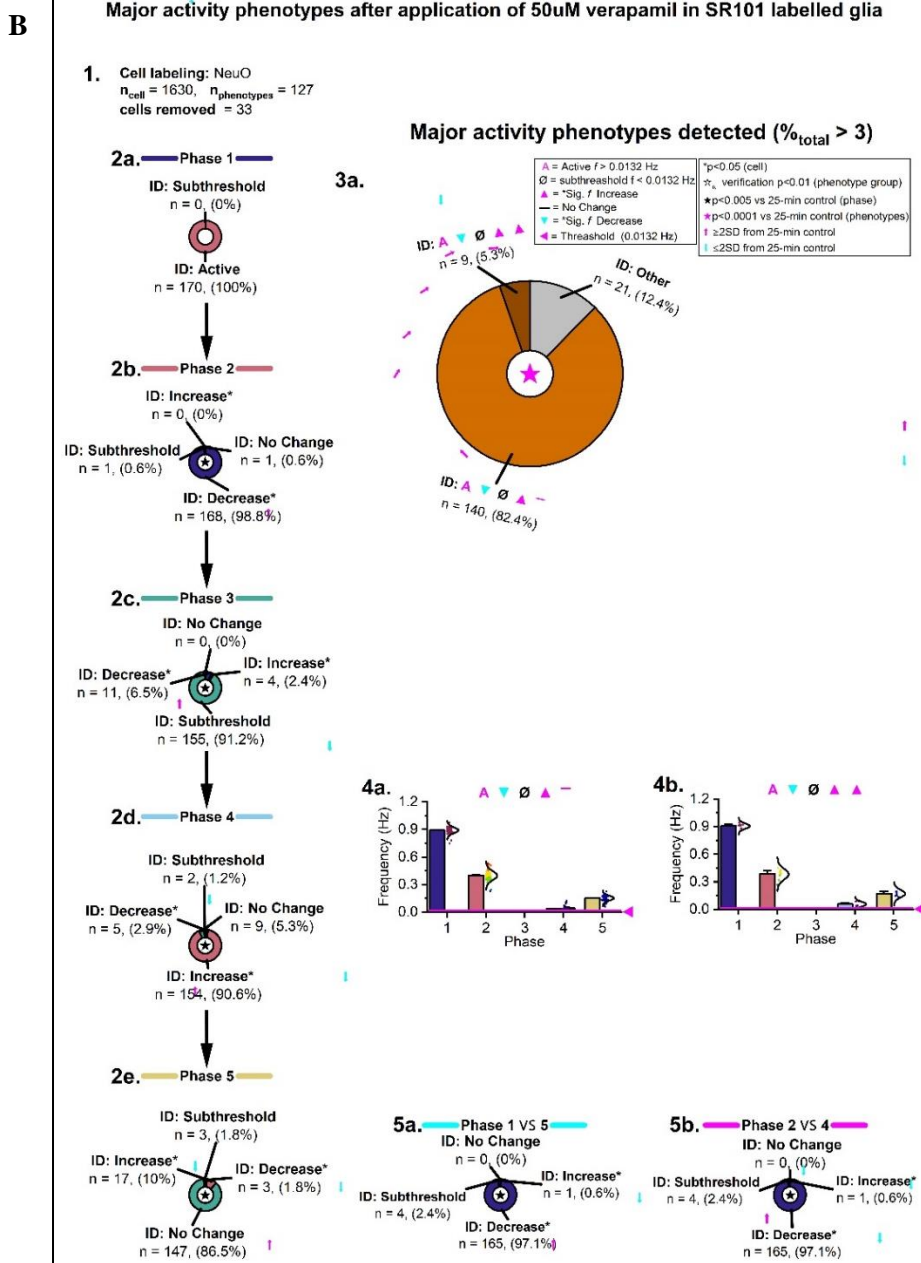


Figure 19. Detailed analyses revealing the major activity phenotypes detected in neurons (A) and glia (B) under 50uM verapamil control conditions. Section 2 (a-e) depicts the changing activity levels of the cells in all the phases. The pie chart (section 3a) categorizes the

major activity phenotypes, and section 4 shows bar graphs of the most observed phenotypes detected. Section 5 (a-b) shows a phase comparison in the changes in activity between Phases 1 and 5 and Phases 2 and 4.

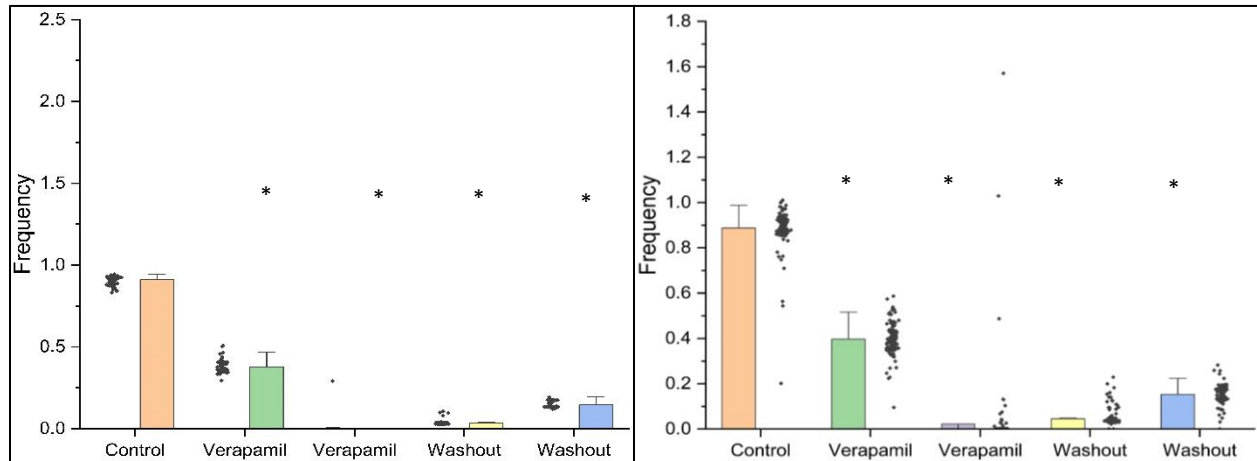


Figure 20. Summary graphs of superior cervical ganglion (SCG) neurons and glia after application of L-type calcium channel blocker verapamil. *Significantly different compared to control in phase 1 ($p < 0.01$).

Sodium channels are implicated in neurotransmitter release

Figure 21 shows representative traces of the intrinsic Ca^{2+} activity observed in cells isolated from SCGs after application of single dose of tetrodotoxin (50nM). As is observed from the traces, 50nM tetrodotoxin induced a complete inhibition of the activity in Phases 2 and 3 respectively in both neurons (**Figure 21A**) and astrocytes (**Figure 21B**). The activity began to resume in Phase 4 and returned to control levels after washout of tetrodotoxin in Phase 5.

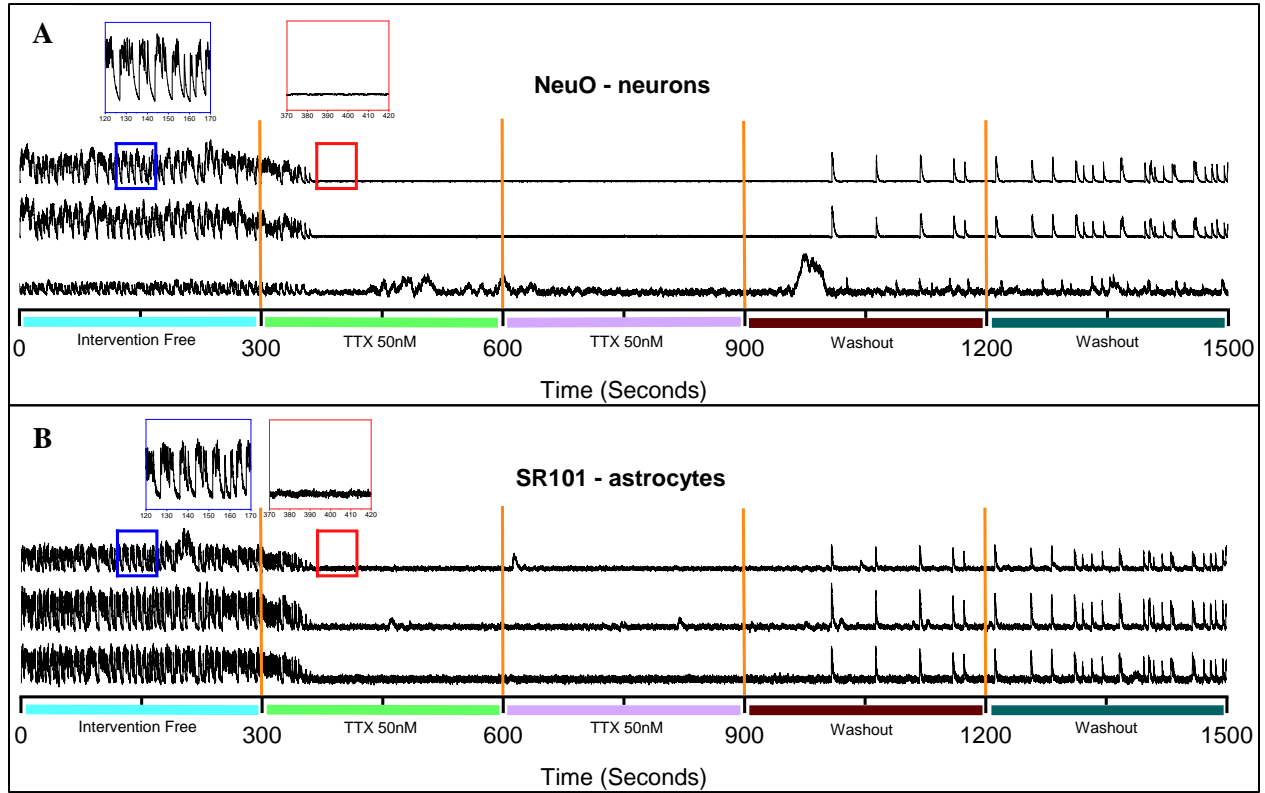


Figure 21. Typical traces depicting the effects of tetrodotoxin (50nM) in NeuO-labeled neurons (A) and SR10- labeled astrocytes (B) show inhibition of activity in tetrodotoxin phases (2 and 3) with partial return to control levels in washout phases (4 and 5).

Figure 22 presents detailed analyses of neuronal (**Figure 22A**) and glial (**Figure 22B**) cell activity phenotypes following the application of 50 nM tetrodotoxin, which is a sodium channel inhibitor.

NeuO-labeled neurons. Initially, in Phase 1, all NeuO-labeled neurons (100%) were active, with no neurons at subthreshold level. As the tetrodotoxin is applied, Phase 2 revealed a significant shift, where 86.8% of neurons exhibited decreased activity with 2.2% falling below the subthreshold level and 11% showing no change. This pattern of decreased activity persists into Phase 3, with 95.6% of neurons falling below subthreshold activity, 1.1% showing a decrease, and 3.3% showing an increase. By Phase 4, there was a notable change: 95.6% of neurons exhibit increased activity, while 2.2% remain unchanged and 2.2% showed a decrease. This pattern continued in Phase 5 with a significant number of neurons (94.5%) showing no change in activity and 5.5% decreasing their activity. The pie chart (**Figure 22A, section 3a**) summarizes these findings, showing that 82.4% of neurons experienced significant decreases in activity, and 7.7% fell into other categories. Comparative analyses (**Figure 22A, sections 5a and 5b**) highlight substantial decreases between Phases 1 and 5 and between Phases 2 and 4. Frequency changes (**Figure 22A, section 4a-c**) showed significant variations, particularly in Phases 2 and 4.

SR101-labeled glia. SR101-labeled glial cells show different activity patterns compared to neurons. In Phase 1, 100% of glial cells were active, and none were inactive. With tetrodotoxin application in Phase 2, glial cell activity underwent a dramatic shift, with 87.5% of cells showing decreased activity, 2% becoming inactive, and only 1% showing increased activity. Phase 3 showed a slight shift: 94% of cells fell below subthreshold, 1.5% decreased, and 3% show increased activity. In Phase 4, the activity levels diversify: 93.5% of cells showed an

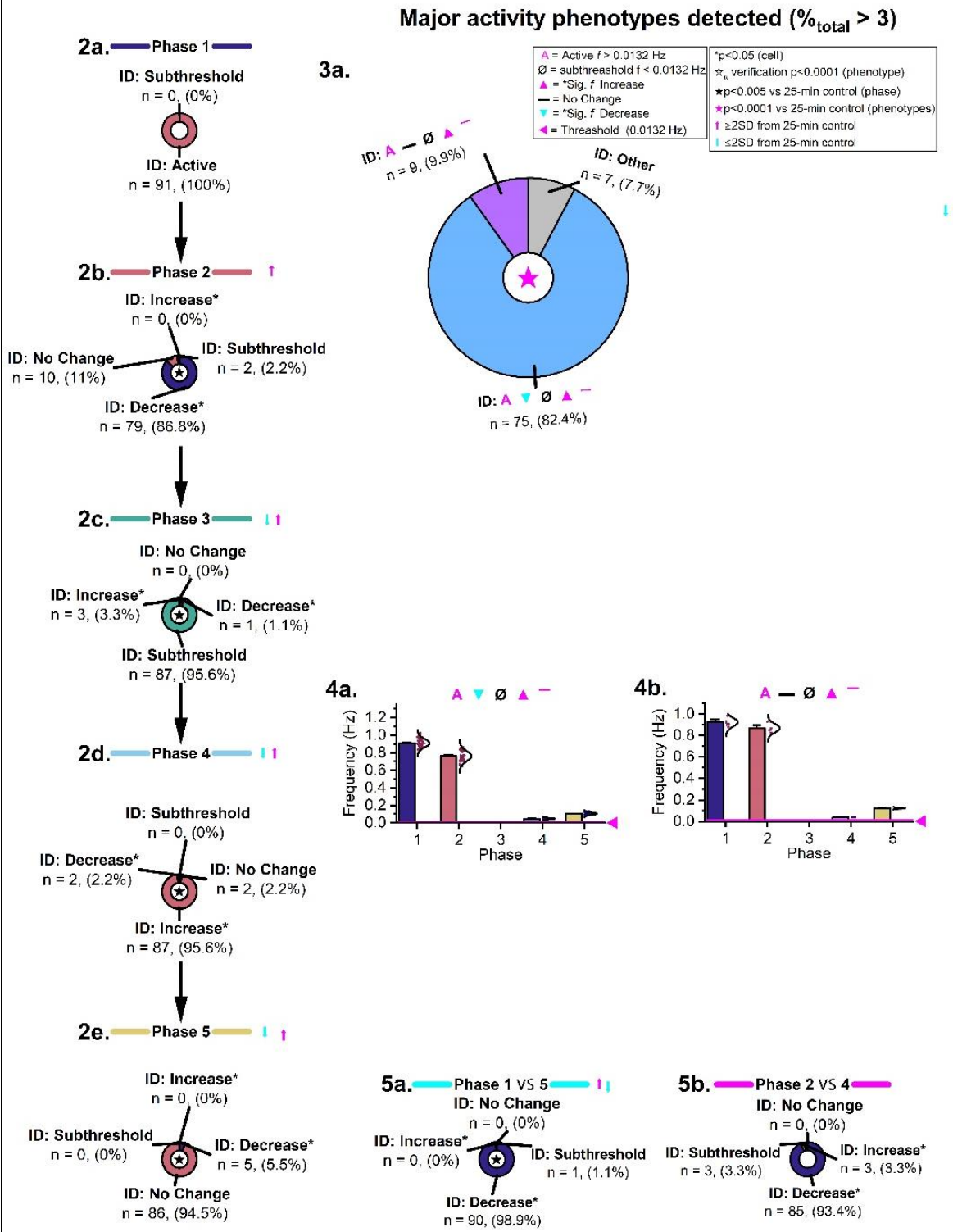
increase, 4.5% decrease, and 1% were inactive. By Phase 5, a majority (93.5%) of glial cells exhibited no change activity, 1% were inactive, and 0.5% showed increased activity. The pie chart (**Figure 22B, section 3a**) indicates that 81.5% of cells experienced a significant decrease, 9% showed no change, and 9.5% fell into other categories. Comparative analyses (**Figure 22B, sections 5a and 5b**) reveal notable decreases between Phases 1 and 5 and between Phases 2 and 4. Frequency changes (**Figure 22BA, section 4a-f**) depict significant fluctuations, especially in Phases 2 and 4, reflecting the dynamic response of glial cells to conotoxin.

Together, these analyses reveal the differential impact of sodium channel inhibition on NeuO-labeled neurons and SR101-labeled glial cells. NeuO-labeled neurons and SR101 labeled glia initially show a marked decrease in activity upon tetrodotoxin application, but many eventually exhibit increased activity by the later phases. Sodium channels have been shown to be important for regulation of action potential firing. The effect of inhibition of sodium channels on the calcium activity further cements its role in modulation of intracellular calcium.

A

Major activity phenotypes after application of 50nM tetrodotoxin in Neuro Labelled neurons

1. Cell labeling: NeuO



B

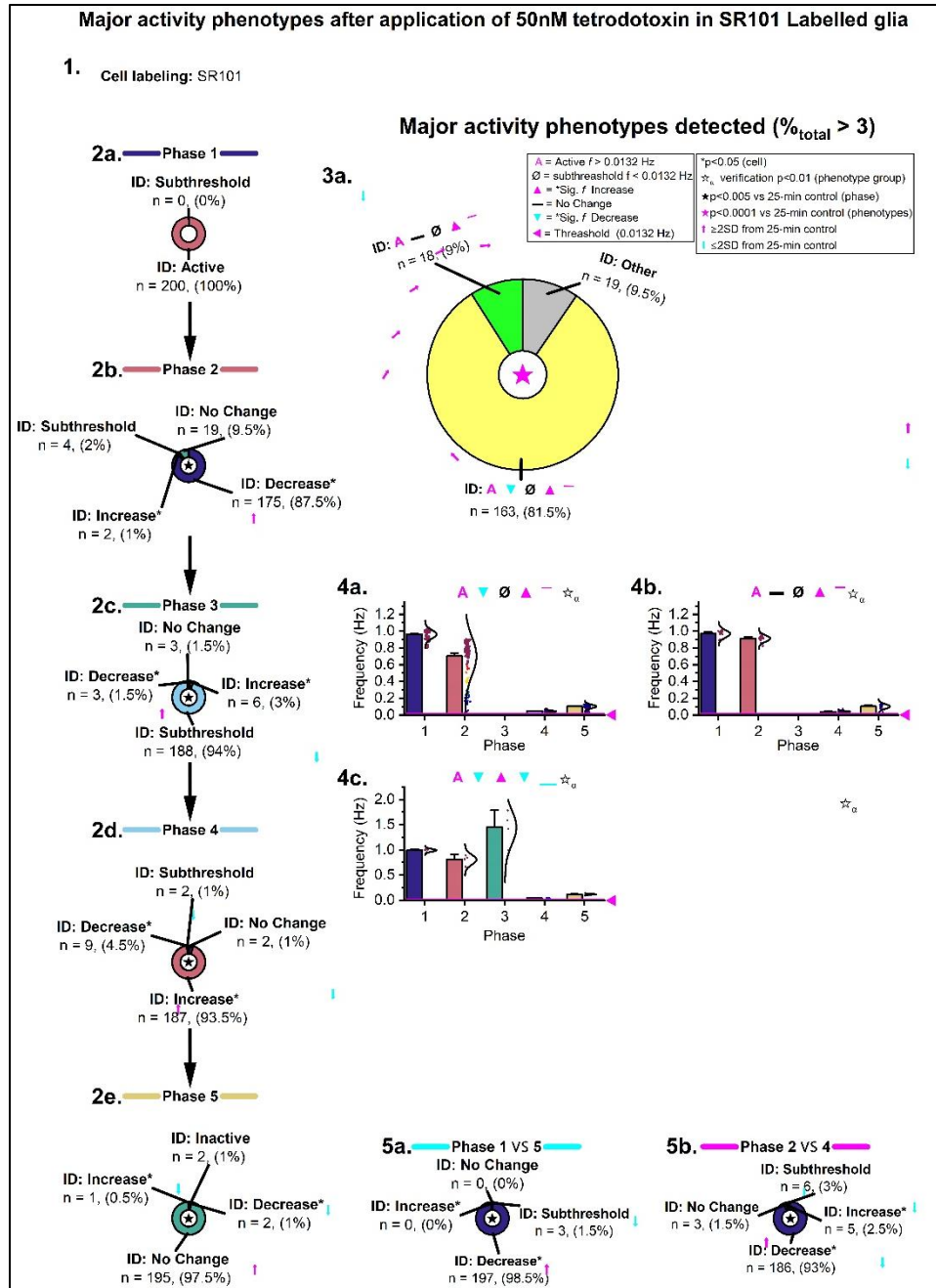


Figure 22. Detailed analyses revealing the major activity phenotypes detected in neurons (A) and glia (B) under 50nM tetrodotoxin conditions. Section 2 (a-e) depicts the changing activity levels of the cells in all the phases. The pie chart (3a) categorizes the major activity

phenotypes and section 4 shows bar graphs of the most observed phenotypes detected. Section 5 shows a phase comparison in the changes in activity between Phases 1 and 5 and Phases 2 and 4.

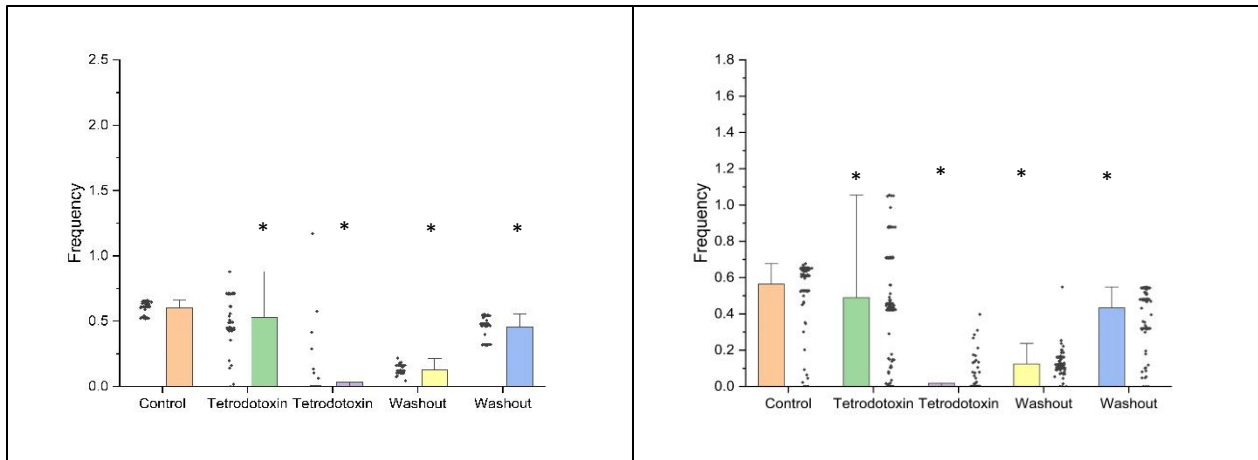


Figure 23. Summary graphs of superior cervical ganglion (SCG) neurons and glia after application of sodium channel blocker tetrodotoxin. *Significantly different compared to control in phase 1 ($p < 0.01$).

PART II: FENTANYL D-CYSEE AND NALOXONE

Fentanyl inhibits intrinsic calcium activity

Figure 24 shows representative traces of the intrinsic Ca^{2+} activity observed in cells isolated from superior cervical ganglion (SCG) after application of single dose of fentanyl (100nM). As is observed, respectively, in both neurons (**Figure 24A**) and astrocytes (**Figure 24B**). The activity returned to control levels after washout of fentanyl in Phases 4 and 5, indicating involvement of mu-opioid receptor in driving the activity.

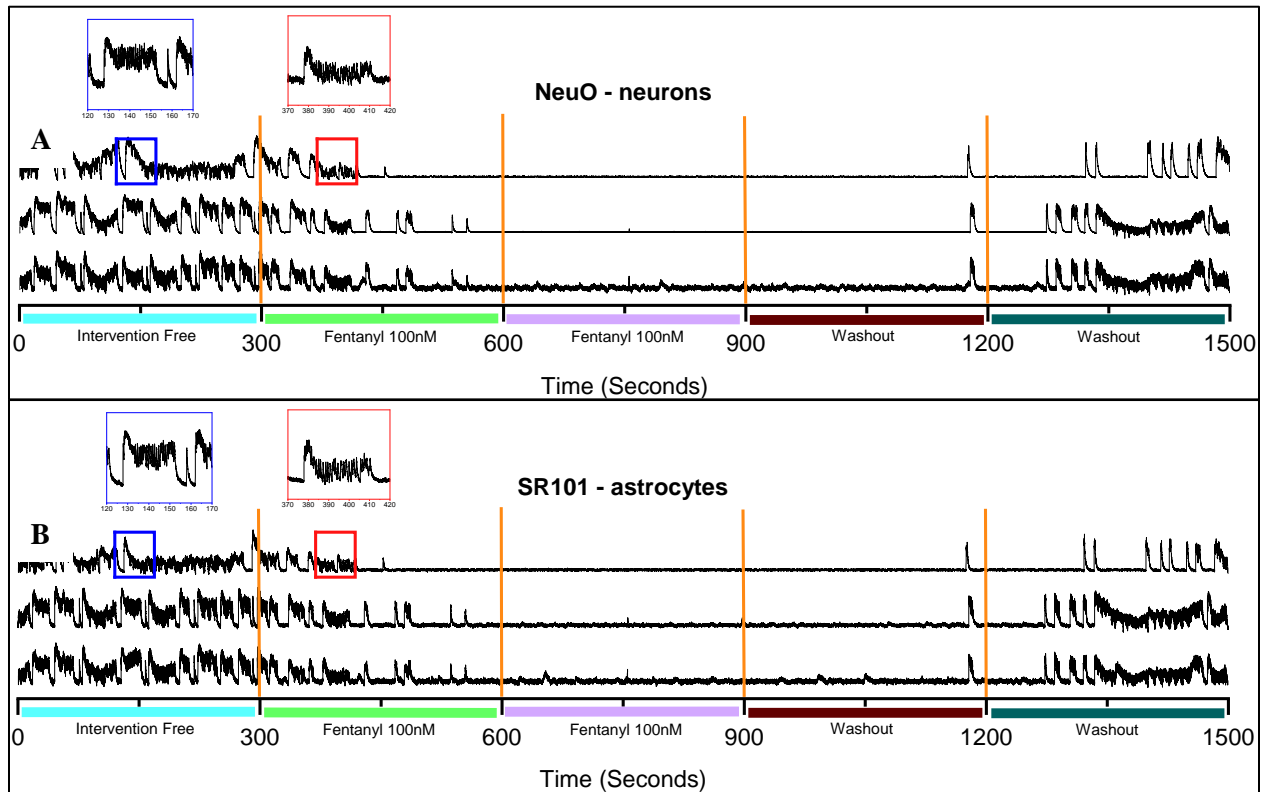


Figure 24. Responses to fentanyl (100 nM). Typical traces depicting the effects of fentanyl (100nM) in NeuO-labeled neurons and SR101 labeled astrocytes show inhibition of activity in fentanyl Phases (2 and 3) with partial return to control levels in washout Phases (4 and 5).

Figure 25 depicts the results from the analysis of major activity phenotypes in NeuO labelled neurons (**Figure 26A**) and SR101 labelled glia (**Figure 26B**) labeled cells after the application of 100nM fentanyl

NeuO-labeled neurons. The results indicate a significant impact of 100nM fentanyl perfused in Phase 2 and 3 on NeuO-labeled neurons across different Phases. Initially, in Phase 1, all 251 neurons were active, with no subthreshold activity observed. However, in Phase 2, there was a notable shift, with 96.8% (243 neurons) showing decreased activity, 2.8% (7 neurons) exhibiting subthreshold activity, and only 0.4% (1 neuron) maintaining no change. This pattern continued in Phase 3, where most neurons (91.2%, 229 neurons) showed decreased activity, with a smaller proportion (3.2%, 8 neurons) showing an increase in activity, and 2% (5 neurons) remaining unchanged.

By Phase 4, a significant number of neurons (76.5%, 192 neurons) exhibited an increase in activity, while 16.7% (42 neurons) were subthreshold. A minimal 4.8% (12 neurons) demonstrated no change. In Phase 5, the pattern shifted again, with 63.3% (159 neurons) showing no change, 20.3% (51 neurons) exhibiting an increase in activity, 15.9% (40 neurons) being subthreshold, and 0.4% (1 neuron) showing a decrease in activity. The frequency analysis across these Phases highlighted significant changes, with notable variations in the active, subthreshold, significant increase, no change, and significant decrease phenotypes.

Comparing Phase 1 and Phase 5, 74.5% (187 neurons) showed a decrease in activity, 18.3% (46 neurons) maintained no change, and 6.4% (16 neurons) demonstrated an increase in activity. Between Phase 2 and Phase 4, 53.8% (135 neurons) had no change, 23.5% (59 neurons) showed a decrease in activity, and 19.1% (48 neurons) exhibited subthreshold activity. These

results suggest a dynamic response of NeuO labeled neurons to fentanyl, with Phases of increased and decreased activity indicating the drug's modulatory effects on neuronal excitability.

SR101-labeled glia. The application of 100nM fentanyl (Phase 2 and 3, washout phase 4 and 5) also significantly affected SR101 labeled glia. In Phase 1, all 270 glial cells were active. Phase 2 showed a marked change, with 74.4% (209 cells) exhibiting decreased activity, 10.7% (29 cells) showing a significant increase in activity, 4.1% (11 cells) maintaining no change, and 3.7% (10 cells) being subthreshold. In Phase 3, most glial cells (90%, 243 cells) were subthreshold, with 3.3% (9 cells) showing a decrease in activity and 2.2% (6 cells) demonstrating an increase in activity.

In Phase 4, 59.6% (161 cells) had no change, 32.2% (87 cells) exhibited a decrease in activity, 5.6% (15 cells) were subthreshold, and 2.6% (7 cells) showed no change. By Phase 5, 34.1% (92 cells) had decreased activity, 15.6% (42 cells) showed no change, 7% (19 cells) demonstrated an increase in activity, and 2.6% (7 cells) were subthreshold. The frequency analysis indicated significant changes across Phases, with phenotypic distributions suggesting shifts in glial cell activity in response to fentanyl.

Between Phase 1 and Phase 5, 80.8% (219 cells) showed a decrease in activity, 21.4% (58 cells) had no change, and 6.3% (17 cells) exhibited an increase in activity. Comparing Phase 2 and Phase 4, 69.6% (188 cells) had no change, 42.2% (114 cells) showed a decrease in activity, and 4.1% (11 cells) exhibited subthreshold activity. These results highlight the differential response of SR101 labeled glia to fentanyl, with significant shifts towards decreased activity and

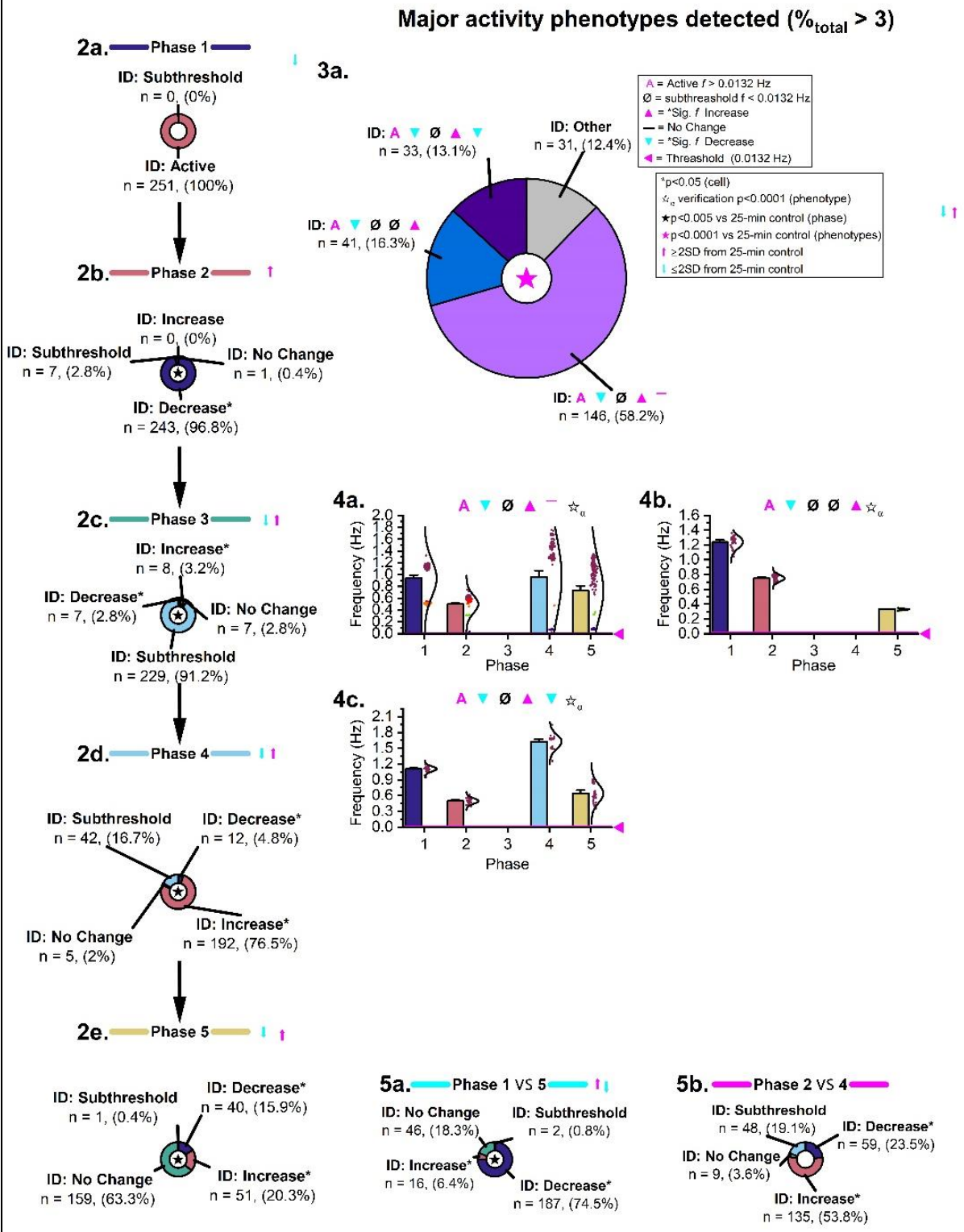
subthreshold states, indicating the drug's profound impact on glial cell function and activity patterns.

Summary. The application of 100nM fentanyl resulted in significant changes in activity phenotypes in both NeuO-labeled neurons and SR101-labeled glia. Both cell types demonstrated a trend towards increased subthreshold and decreased activity Phases over time, indicating a pronounced effect of fentanyl on reducing SCG cellular activity. The shifts in activity were more marked in neurons compared to glia, suggesting differential sensitivity or response dynamics between these cell types to fentanyl exposure. The detailed phenotypic analysis across different Phases highlights the drug's impact on cellular excitability and activity patterns.

A

Major activity phenotypes detected in NeuO labeled neurons after application of 100nM fentanyl

1. Cell labeling: NeuO



B

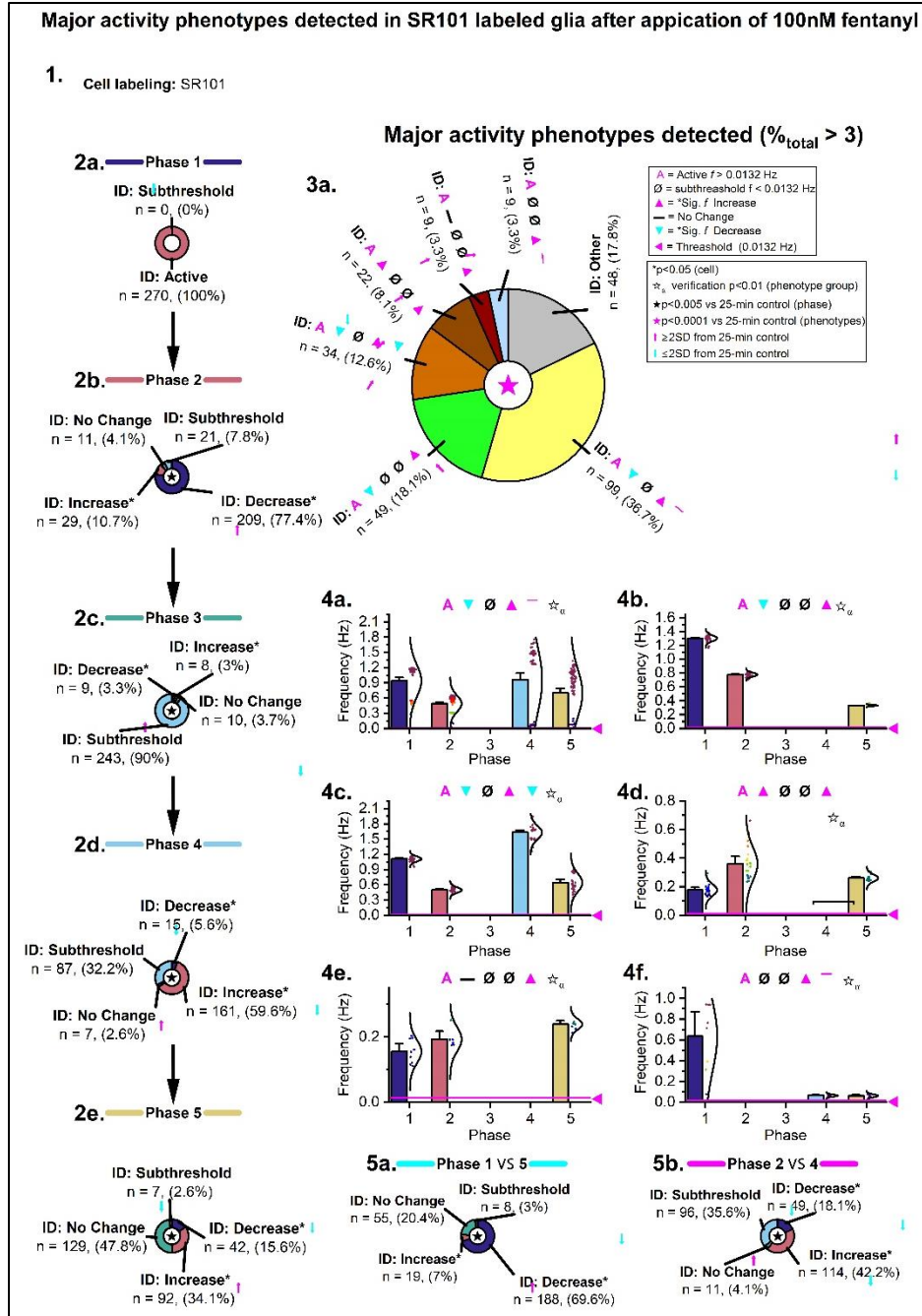


Figure 25. Detailed analyses revealing the major activity phenotypes detected in neurons (A) and glia (B) under 100nM fentanyl control conditions. Section 2 (a-e) depicts the changing activity levels of the cells in all the Phases. The pie chart (3a) categorizes the major activity phenotypes and section 4 shows bar graphs of the most observed phenotypes detected.

Section 5 shows a Phase comparison in the changes in activity between Phases 1 and 5 and Phases 2 and 4.

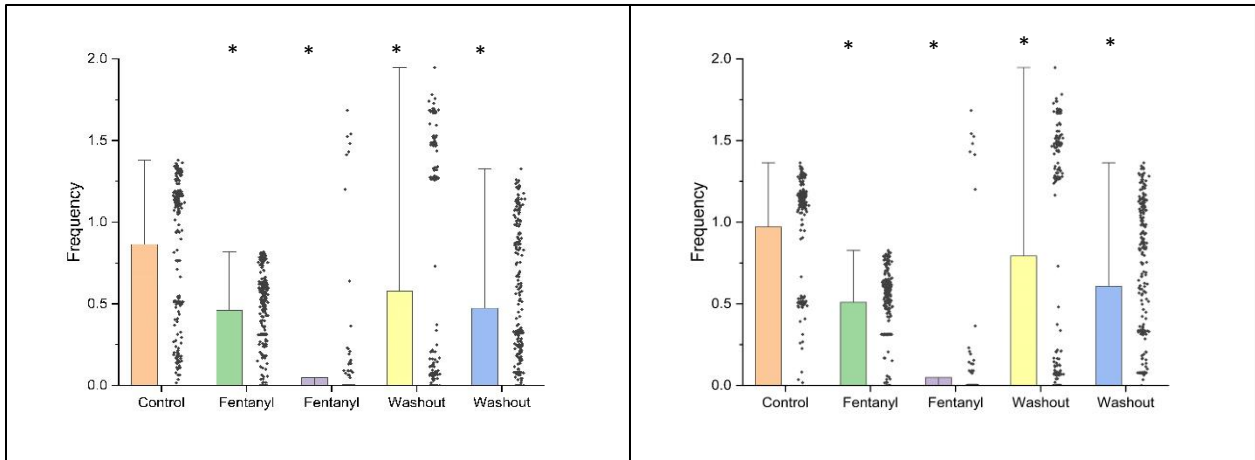


Figure 26. Summary graphs of superior cervical ganglion (SCG) neurons and glia after application of 100nM fentanyl. *Significantly different compared to control in phase 1 ($p < 0.01$).

Naloxone inhibits intrinsic calcium activity

Figure 27 shows representative traces of the intrinsic Ca^{2+} activity observed in cells isolated from SCG after application of single dose of naloxone (100uM). As observed from the traces, 100uM naloxone completely inhibited the SCG cellular activity in Phase 2 and 3 in both neurons (**Figure 27A**) and glia (**Figure 27B**) which returned to control levels after washout in Phase 4 and 5.

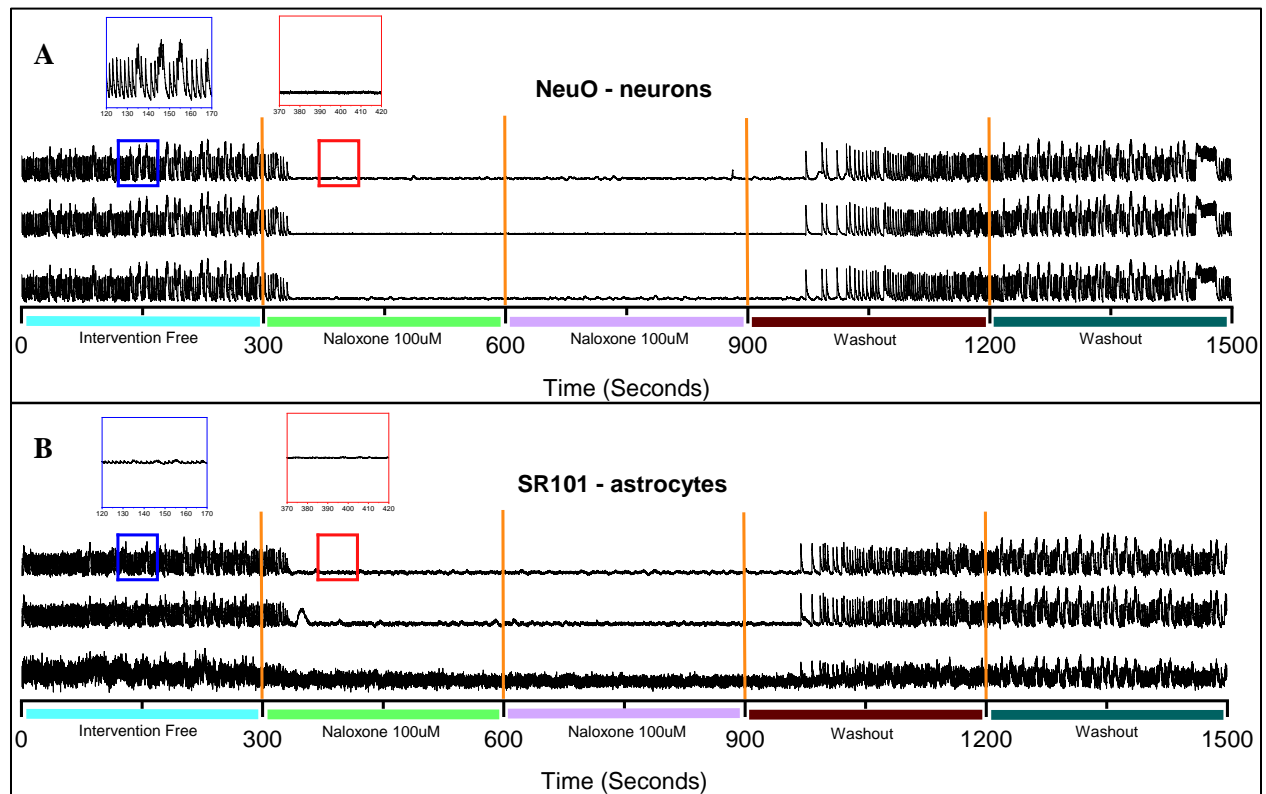


Figure 27. Responses of SCG cells to naloxone (100 uM). Typical traces depicting the effects of single dose naloxone (100uM) in NeuO-labeled neurons (**A**) and SR101 labeled astrocytes (**B**). Naloxone showed complete inhibition of the activity in Phases 2 and 3 with return to control levels in Phase 4 and 5.

Figure 28 depicts the results from the analysis of major activity phenotypes in NeuO- (**Figure 28A**) and SR101- (**Figure 28B**) labeled cells after the application of 100uM naloxone.

Phase Analysis: Phase 1. Initially, in Phase 1 (drug-free control), 97% (162 neurons) and 95.5% (63 glia) were active, while 3% (5 neurons) and 4.5% (3 glia) exhibited subthreshold activity.

Phase 2. As the experiment progressed to Phase 2 (fentanyl 100nM), a significant shift occurred. The majority of neurons (75.4%, 126 neurons) and glia (59.1%, 39 glia) showed a decrease in activity. Concurrently, 19.8% (33 neurons) and 4.5% (3 glia) maintained no change, 3.6% (6 neurons) and 10.6% (7 glia) were subthreshold, and 1.2% (2 neurons) and 25.8% (17 glia) exhibited an increase in activity.

Phase 3. In Phase 3 (fentanyl 100nM), the decrease in activity remained dominant, with 97.6% (163 neurons) and 87.9% (58 glia) showing decreased activity. Only a small proportion of neurons and glia demonstrated other activity patterns: 1.2% (2 neurons) and 4.5% (3 glia) showed an increase, and another 1.2% (2 neurons) and 4.5% (3 glia) showed no change. No neurons exhibited subthreshold activity while 87.9% glia exhibited subthreshold activity at this Phase.

Phase 4. Moving into Phase 4 (washout), 97% (162 neurons) and 87.9% (58 glia) showed an increase in activity, 1.8% (3 neurons) and 9.1% (9 glia) were subthreshold, 0.6% (1 neuron) and 3% (2 glia) had no change, and another 0.6% (1 neuron) while no glia showed decreased activity. This indicates a shift back towards increased cellular activity.

Phase 5. Finally, in Phase 5 (washout), 98.2% (164 neurons) and 83.3% (55 glia) showed an increase in activity, 1.2% (2 neurons) whereas 7.6% (5 glia) were subthreshold, and 0.6% (1 neuron) while 3% (2 glia) maintained no change.

Phenotypic distribution: The pie charts in Figure 29 A and B, section 3a, show the major activity phenotypes detected. The most notable phenotype, encompassing 74.3% of neurons (124 neurons) and 50% of glial cells (33 glia), was the combination of significant decrease with application of naloxone in Phase 2 followed by a further decrease with application of naloxone in Phase 3. This was followed by the “other” category at 6% (10 neurons) 16.7% (11 glia), with a smaller portion of the neurons and glia distributed among the other phenotypes.

Frequency analysis: The frequency analysis (Figure 29A and B sections 4a and 4b) across the Phases indicates variations in cellular firing rates. Initially, in Phase 1, cells’ firing frequency was high, corresponding to the high percentage of active cells. As Phases progressed, fluctuations in frequency were observed, particularly noticeable during transition periods of increased or decreased activity.

Comparative phase analysis: Comparing Phase 1 to Phase 5 (Figure 29 A and B section 5a), 63.5% of neurons (106) and 45.5% of glial cells (30) showed an increase in activity, 32.9% of neurons (55) 33.3% of glia (22) had no change, and 3.6% of neurons (6) 10.6% of glia (7) exhibited subthreshold activity. Comparing Phase 2 (naloxone) to Phase 4 (naloxone washout) (5b), 70.1% of neurons (117) while 62.1% of glia (42) showed no change in activity, 19.8% of neurons (33) whereas 1.5% of glia (1) showed a decrease, 4.2% of neurons (7) and 13.6% of glia (9) were subthreshold, and 6% of neurons (10) and 22.7% of glia (15) exhibited an increase in activity.

Summary: The application of 100 μ M naloxone induced significant shifts in the cellular activity. While most cells started in an active state, a substantial proportion shifted to decreased activity in the early phases (2 and 3) with the application of naloxone to the cells, with a notable

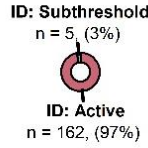
recovery towards increased activity in later phases after washout of naloxone. The frequency analysis supports these transitions, showing significant fluctuations aligned with the phases of activity. The comparison between different phases highlights the dynamic response of cells to naloxone, illustrating the drug's impact on neuronal excitability and activity patterns.

A

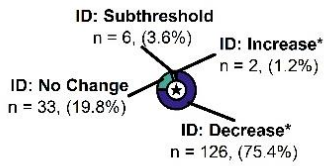
Major activity phenotypes detected in NeuO labeled neurons after application of 100uM naloxone

1. Cell labeling: NeuO

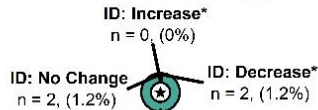
2a. Phase 1



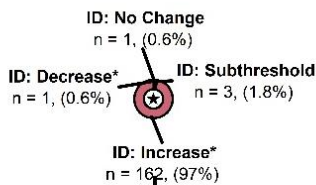
2b. Phase 2



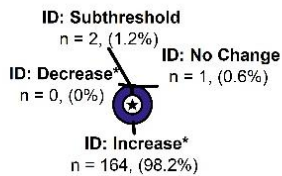
2c. Phase 3



2d. Phase 4

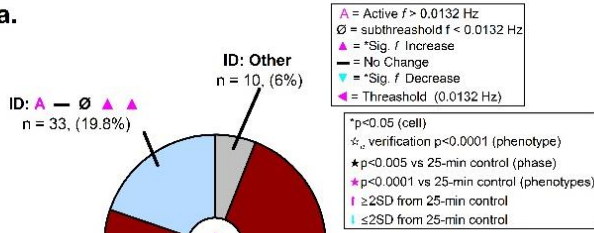


2e. Phase 5

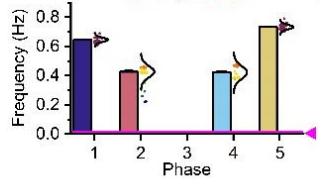


Major activity phenotypes detected (%total > 3)

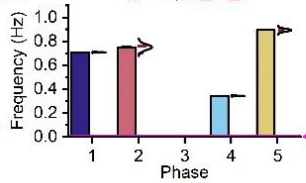
3a.



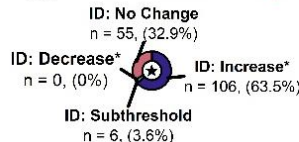
4a.



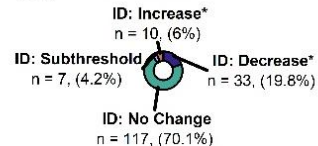
4b.



5a. Phase 1 VS 5



5b. Phase 2 VS 4



Section 5 shows a phase comparison in the changes in activity between Phases 1 and 5 and Phases 2 and 4.

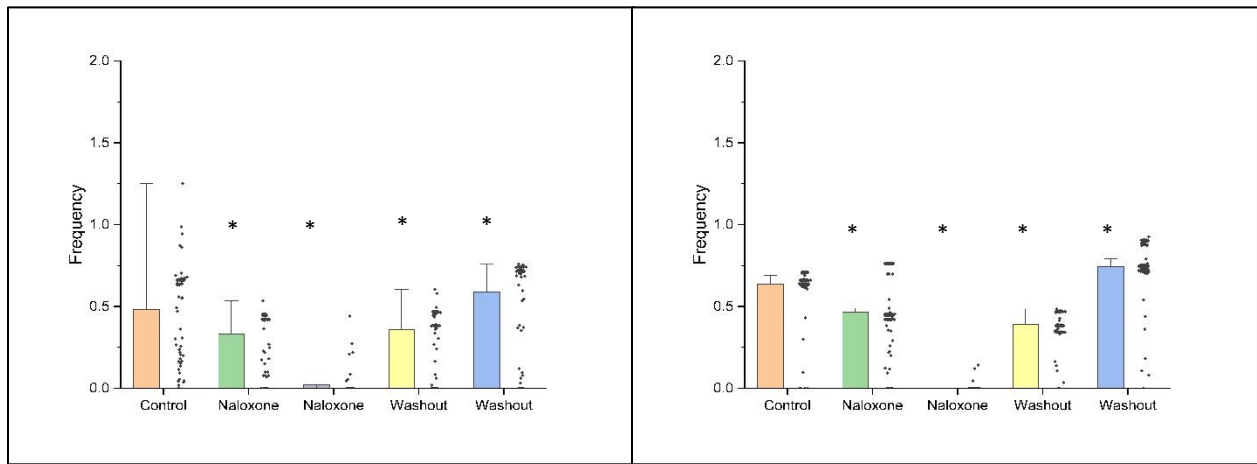


Figure 29. Summary graphs of superior cervical ganglion (SCG) neurons and glia after application of 100uM naloxone. *Significantly different compared to control in phase 1 ($p < 0.01$).

D-CYSee has no significant effect on the intrinsic calcium activity

Figure 30 shows representative traces of the intrinsic Ca^{2+} activity observed in cells isolated from SCG after application of single dose of D-CYSee (100uM). As observed from the traces, 100uM D-CYSee showed a slight decrease in the activity in Phases 2 and 3 in both neurons (**Figure 30A**) and astrocytes (**Figure 30B**) with return to washout levels in Phases 4 and 5. D-CYSee had no other significant effect on the activity, however.

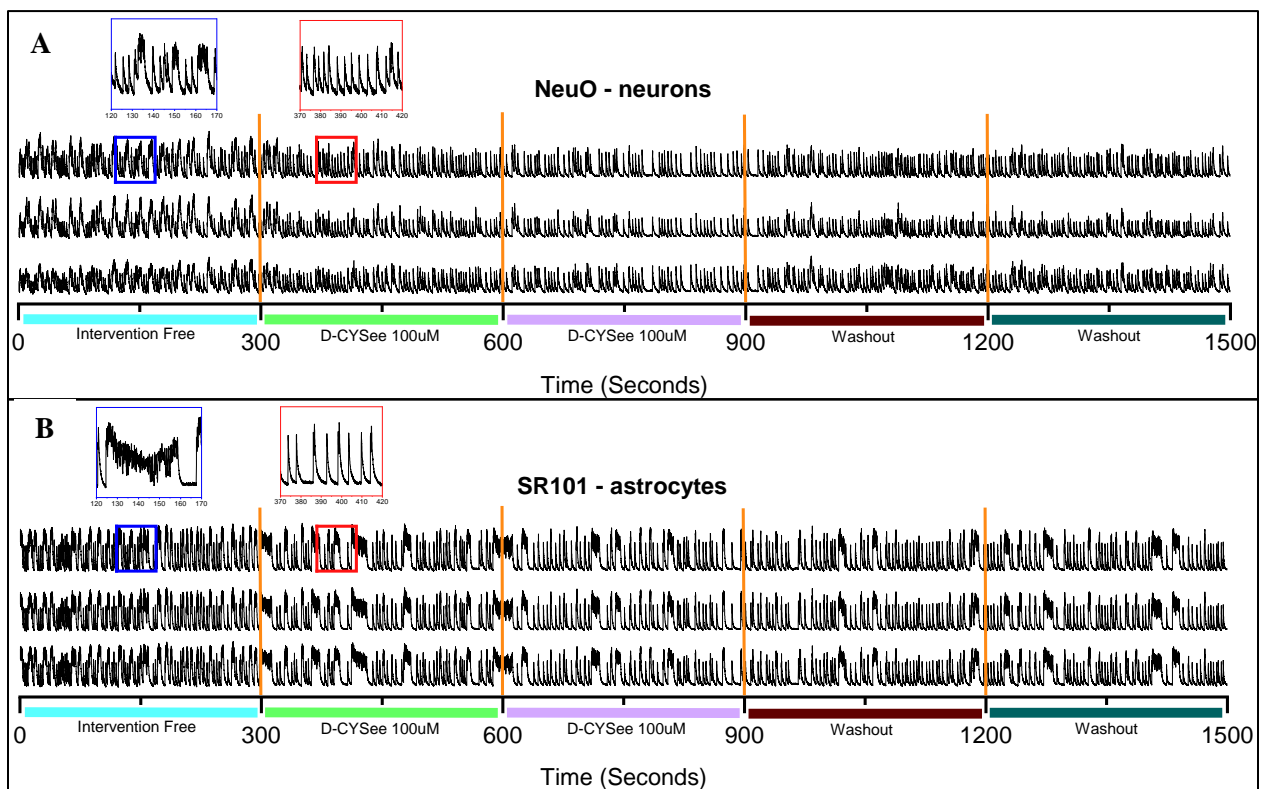


Figure 30. Typical traces depicting the effects of D-CYSee (100uM) in NeuO-labeled neurons (A) and SR101-labeled astrocytes (B) show slight decrease in activity in D-CYSee Phases (2 and 3) with return to control levels in washout Phases (4 and 5).

Figure 31 depicts the results from the analysis of major activity phenotypes in NeuO (**A**) and SR101 (**B**) labeled cells after the application of 100uM naloxone.

NeuO-labeled neurons. D-CYSee did not have a significant effect on the activity in the NeuO-labeled neurons. In Phase 1 (drug-free control) 98.8% neurons were active whereas only 1.2% of them exhibited a subthreshold activity. In Phase 2, after application of 100uM D-CYSee, 95.2% neurons displayed a decrease in activity with 1.2% remaining subthreshold. While 3.6% neurons showed no change, there were no neurons which showed an increase in activity. Phase 3 (D-CYSee 100uM) also showed a similar pattern with 94% cells continuing to decrease their activity, with 4.2% cells showing no change, and the number of subthreshold cells remaining constant at 1.2%. By Phase 4 (initial washout), 38.3% cells began to show an increase in activity, with 34.7% cells showing no change in activity. 25.7% of cells showed some decrease in activity, with 1.2% cells remaining subthreshold. The pattern of cell activity remained similar in Phase 5 (final washout) as well.

Comparing Phase 1 (drug-free) to Phase 5 (final drug washout), 95% cells showed a decrease in activity, with only 1.2% of cells showing an increase in activity, and 3% cells being subthreshold. Comparing Phase 2 (D-CYSee 100uM) to Phase 4 (initial washout), 55.7% neurons showed a decrease in activity, with 41.3% cells showing no change, and 1.8% neurons being subthreshold. These results suggest that neuron activity was not significantly affected by application of D-CYSee. The neurons only showed a slight decrease in activity, but an extremely small number of neurons were subthreshold as early as Phase 1, indicating no effect of D-CYSee on this subpopulation of neurons. In short, D-CYSee alone did not appear to have a significant effect on neuronal excitability.

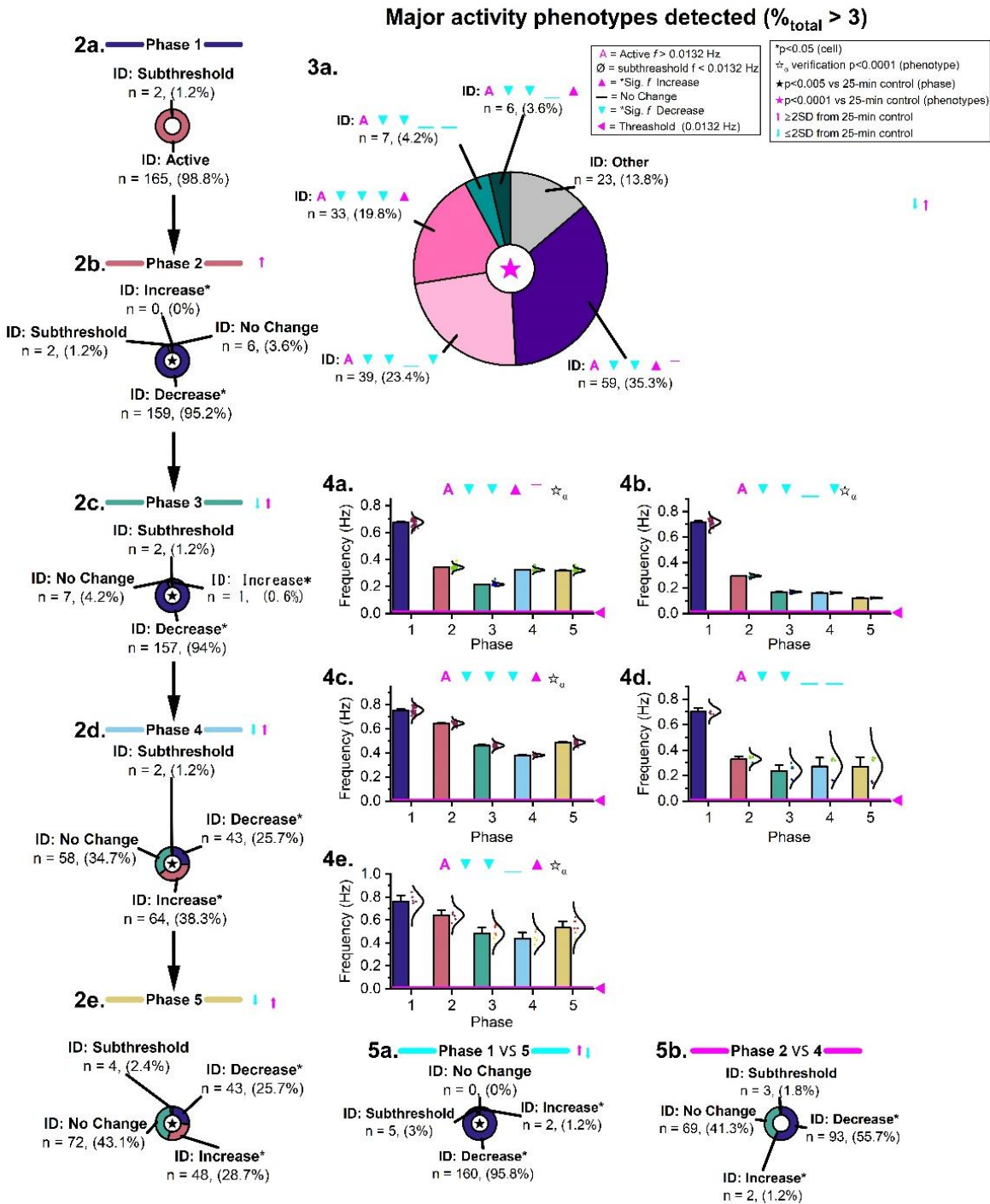
SR101-labeled glia. The results indicate that D-CYSee did not have a significant effect on the activity in the SR101-labeled glia. In Phase 1 (drug-free control), 98.8% glia were active whereas only 1.2% of the glial cells exhibited a subthreshold activity. In Phase 2, after application of 100uM D-CYSee, 95.9% of the glia displayed a decrease in activity, with 1.2% remaining subthreshold. While 2.9% of the glia showed no change in activity, there were no glia which showed increased activity. Phase 3 (D-CYSee 100uM) also showed a similar pattern with 98.2% of cells continuing to decrease their activity. A small number of glia showed an increase in activity, whereas the number of cells exhibiting subthreshold activity remained the same. By Phase 4 (initial washout), 24.6% of the glia began to show an increase in activity with 22.2% of glia showing no change in activity. 52% of glia continued to show some decrease, with 1.2% of glial cells remaining subthreshold. In Phase 5 (final washout), 52% cells showed an increase in activity, whereas 28.7% of glia showed no change, and 18% continued to decrease in activity.

Between Phase 1 (drug-free) and Phase 5 (final washout), 97.1% of glia showed a decrease in activity, and a small fraction of glia (1.2%) showing an increase, with 1.8% cells showing subthreshold activity. Comparing Phase 2 (D-CYSee 100uM) and Phase 4 (initial washout), 72.5% glia showed a decrease, 24% glia showed a decrease in activity, and 1.8% (11 cells) exhibited subthreshold activity. These results indicate the just like the results seen in neurons D-CYSee did not appear to have a significant effect on the glia by itself. There was only a slight decrease in activity seen just like that seen in neurons.

A

Major activity phenotypes detected in NeuO labeled neurons after application of 100uM D-CYSee

1. Cell labeling: NeuO



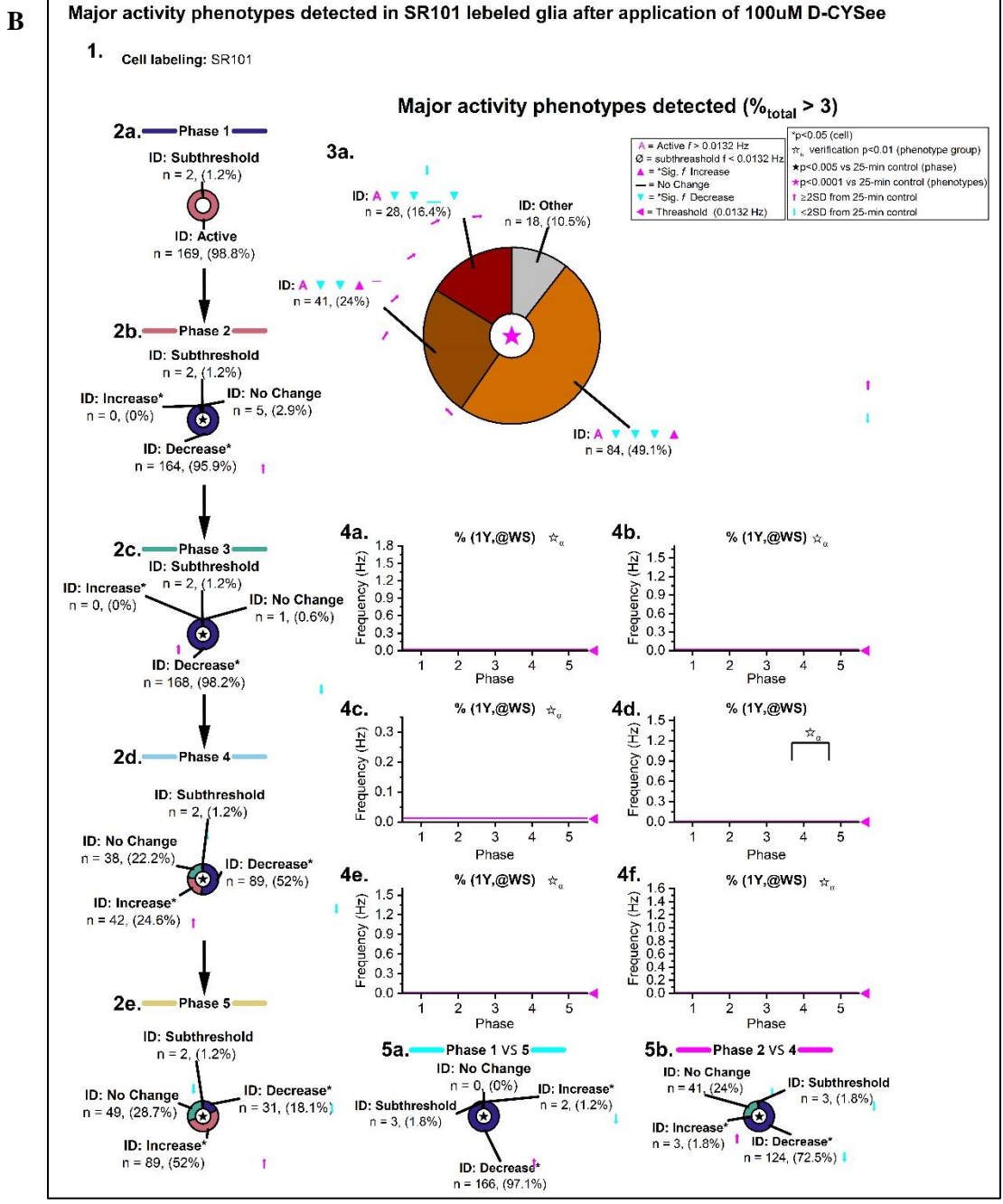


Figure 31. Detailed analyses revealing the major activity phenotypes detected in neurons (A) and glia (B) under 100uM D-CYSee conditions. Section 2 (a-e) depicts the changing activity levels of the cells in all the Phases. A pie chart (3a) categorizes the major activity

phenotypes and section 4 shows bar graphs of the most observed phenotypes detected. Section 5 shows a Phase comparison in the changes in activity between Phases 1 and 5 and Phases 2 and 4.

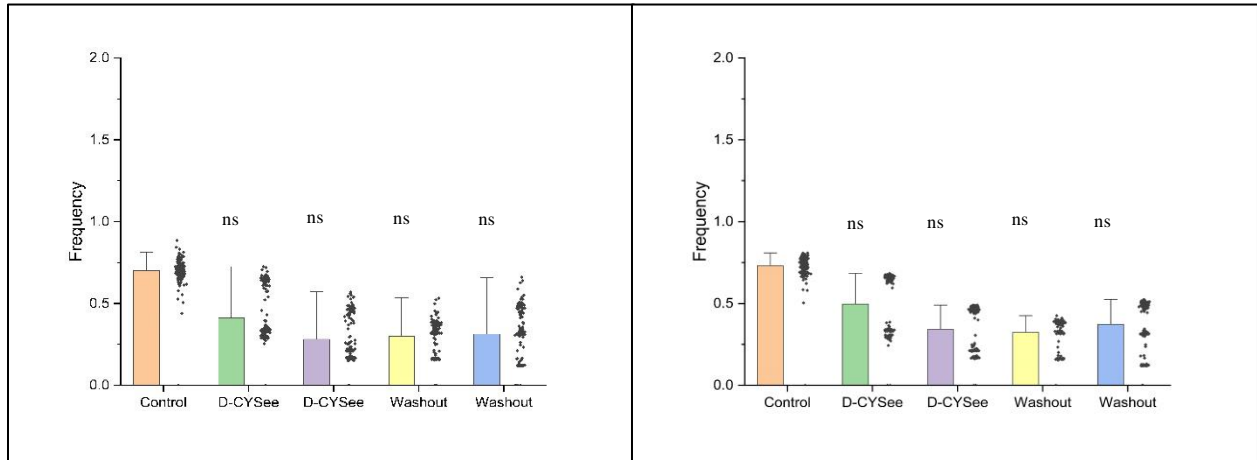


Figure 32. Summary graphs of SCG neurons and glia after application of 100uM D-CYSee. ^{ns}

Not significantly different compared to phase 1 control ($p > 0.01$).

D-CYSee successfully reversed fentanyl-mediated effects on intrinsic calcium activity

Figure 33 shows representative traces of the intrinsic Ca^{2+} activity observed in cells isolated from SCG after application of D-CYSee in presence of fentanyl. As is observed from the traces, 100nM fentanyl completely inhibited cellular activity in Phase 2, which was partially

A restored after application of 100uM D-CYSee in presence of fentanyl in Phase 3. After washout of D-CYSee in Phase 4, fentanyl again inhibited cellular activity, with the activity partially returning to control levels after washout of both drugs in Phase 5.

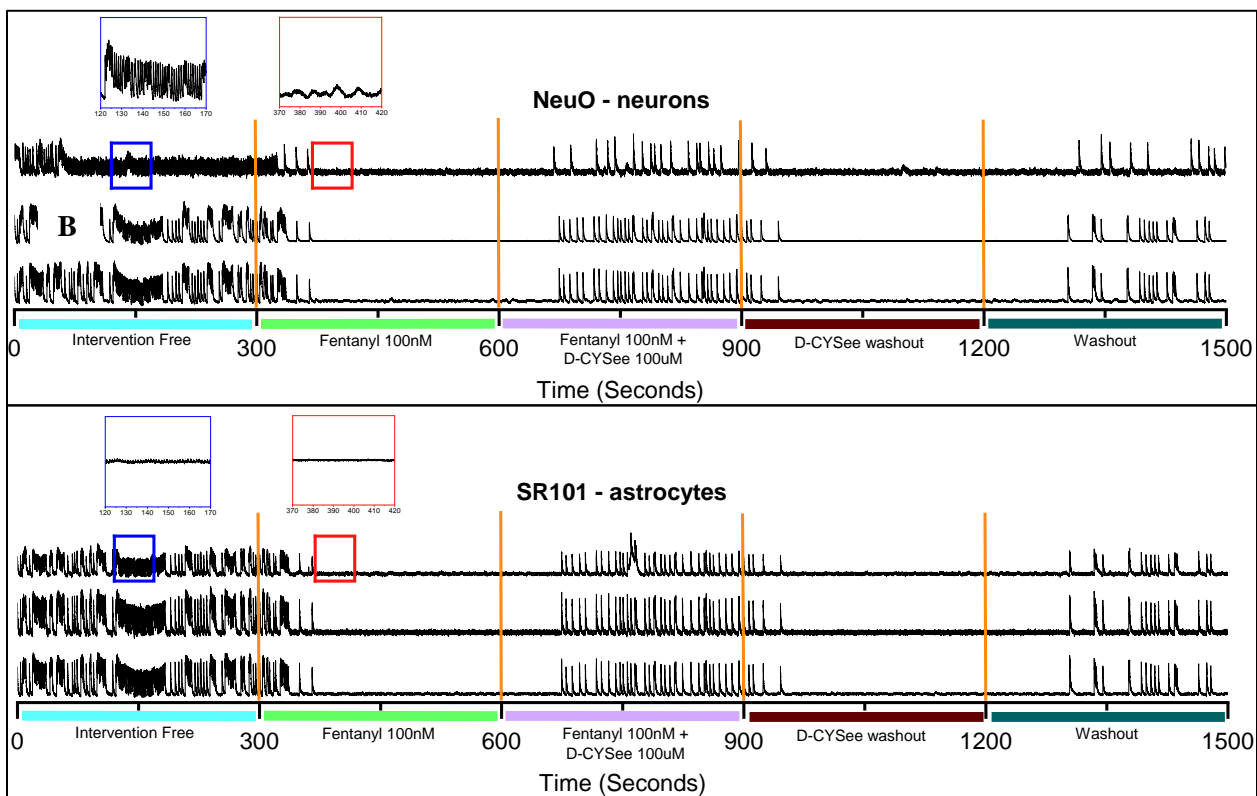


Figure 33. Typical traces depicting the effects of D-CYSee (100uM) in presence of fentanyl (100nM) in NeuO-labeled neurons and SR101 labeled astrocytes. Fentanyl displayed inhibition of activity in Phase 2 which was partially restored after addition of D-CYSee in presence of fentanyl in Phase 3 which was re-inhibited after washout of D-CYSee only in Phase 4 and a partial return to control level after complete washout of both drugs in Phase 5.

Figure 34. Effect of D-CYSee in presence of fentanyl. Typical traces depicting the effects of D-CYSee (100uM) in presence of fentanyl (100nM) in NeuO-labeled neurons and SR101 labeled astrocytes. Fentanyl displayed inhibition of activity in Phase 2 which was partially restored after addition of D-CYSee in presence of fentanyl in Phase 3 which was re-inhibited after washout of D-CYSee only in Phase 4 and a partial return to control level after complete washout of both drugs in Phase 5.

NeuO-labeled neurons: D-CYSee in presence of fentanyl

Figure 34A outlines the major activity phenotypes detected in NeuO-labeled neurons after the application of D-CYSee in the presence of fentanyl. Initially, all 143 SCG neurons were active in Phase 1 (drug free), with no subthreshold activity observed (**section 2a**). In Phase 2, the introduction of fentanyl resulted in 3.2% of neurons exhibiting an increase in activity, while 8.2% showed a decrease. As the experiment progressed to Phase 3, introduction of D-CYSee in presence of fentanyl 1.4% of neurons displayed a subthreshold response, 4.2% showed an increase, and a notable 22.5% showed a decrease in activity (**section 2C**). By Phase 4, after washing out D-CYSee with fentanyl still intact 29.6% of neurons were subthreshold, 20.0% exhibited a significant decrease, while 30.4% showed a significant increase in activity. In Phase 5, after washout of both drugs 12.5% of neurons were subthreshold, 6.2% showed an increase, and 11.6% exhibited a decrease in activity (**section 2e**).

Figure 34 presents the overall cell-activity phenotypes detected. The most predominant phenotype was a decrease in activity, observed in 43% of the neurons, while 25% displayed an increase, 15% showed subthreshold activity, and the remaining 12% did not change. Figures 4a to 4f illustrate the frequency changes across the Phases, showing varying activity patterns with

significant changes occurring between Phases 2 and 3. These results indicate that in phase 2 after application of fentanyl the intrinsic Ca^{2+} was inhibited which was at least partially reversed after application of D-CYSee in phase 3 with fentanyl still being present.

SR101-labeled glia - D-CYSee in presence of fentanyl

In the SR101-labeled glia, **Figure 34B**, section 2a indicates that all 238 cells were initially active with no subthreshold activity in Phase 1 (drug free). In Phase 2, upon applying fentanyl, 2.1% of the cells exhibited a subthreshold response, 14.3% showed a significant increase in activity, and 13.6% displayed a decrease (**Figure 34B**, section 2b). Moving to Phase 3 after application of D-CYSee in presence of fentanyl, most cells, 20.0%, showed a decrease in activity, while 8.2% displayed a significant increase and 6.1% showed subthreshold activity (section 2c). By Phase 4, after D-CYSee washout with fentanyl still present a large portion of cells, 24.0%, exhibited a decrease in activity, while 13.0% showed subthreshold responses, and 11.3% displayed a notable increase in activity. In Phase 5, after complete drug washout, 3.4% of cells exhibited subthreshold activity, 8.6% showed a notable decrease, and 10.2% displayed a notable increase in activity (**Figure 34B**, section 2e).

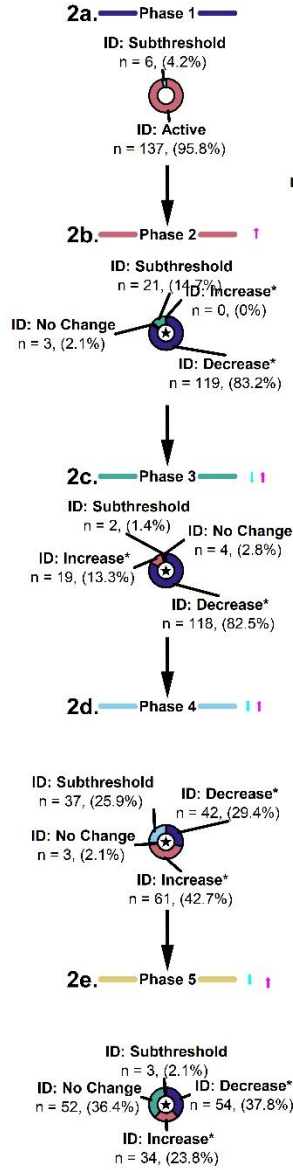
The overall phenotypes detected are summarized in **Figure 34B**, section 3a. The predominant phenotype was a decrease in activity after application of fentanyl, observed in 42% of the cells, followed by an increase in 27% of cells after application of D-CYSee in presence of fentanyl, and 15% showing subthreshold activity. Sections 4a to 4f of **Figure 34B** illustrate the frequency changes across the Phases, highlighting significant changes between Phases 2 (fentanyl) and 3 (fentanyl+D-CYSee).

Overall, the application of D-CYSee in the presence of fentanyl caused significant alterations in neuronal and glial activity, with a substantial portion of cells showing decreased activity, subthreshold responses, or increased activity, depending on the Phase of the experiment. Just like in neurons fentanyl inhibited intrinsic Ca^{2+} activity after its introduction in Phase 2 which was at least partially reversed after addition of D-CYSee in presence of fentanyl in phase 3. These results conclusively show that D-CYSee was able to reverse fentanyl mediated inhibition not only in neurons but also in glia isolated from the superior cervical ganglion.

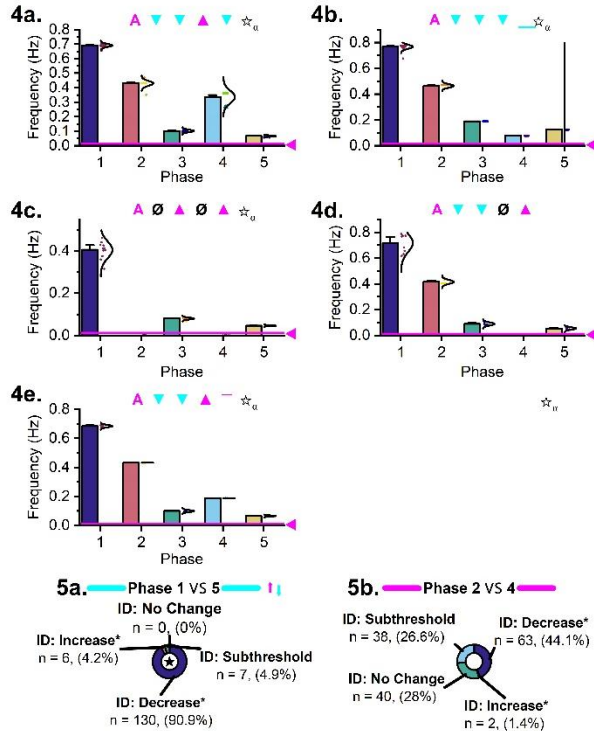
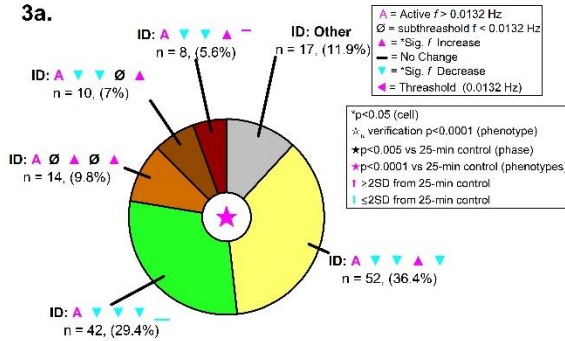
A

Major activity phenotypes detected in NeuO labeled neurons after application of D-CYSee in presence of fentanyl

1. Cell labeling: NeuO



Major activity phenotypes detected (%total > 3)



B

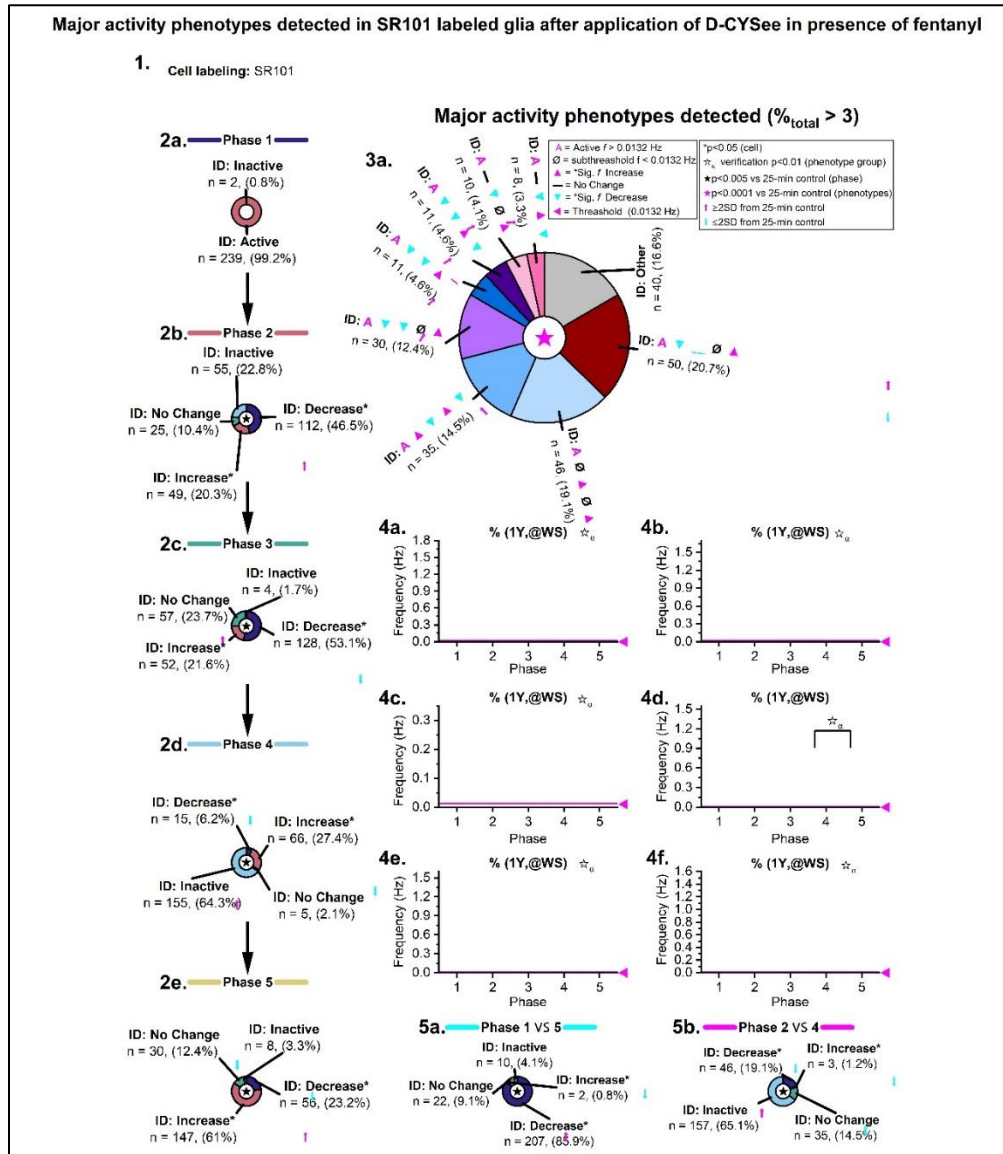


Figure 34. Detailed analyses revealing the major activity phenotypes detected in neurons (A) and glia (B) after application of D-CYSee in presence of fentanyl. Section 2 (a-e) depicts the changing activity levels of the cells in all the Phases. The pie chart (3a) categorizes the major activity phenotypes and section 4 shows bar graphs of the most observed phenotypes detected. Section 5 shows a Phase comparison in the changes in activity between Phases 1 and 5 and Phases 2 and 4

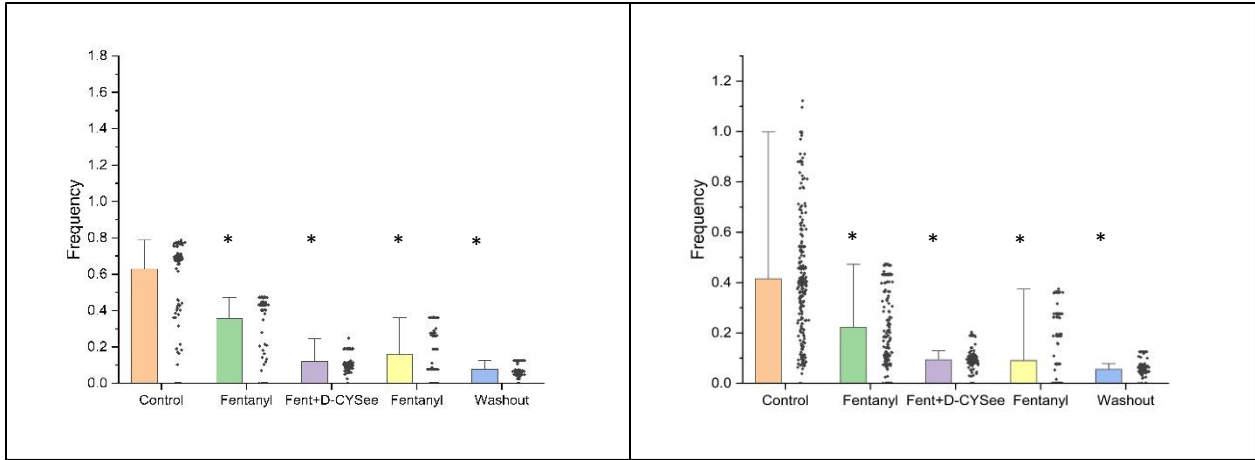


Figure 35. Summary graphs of SCG neurons and glia after application of 100uM D-CYSee. In presence of 100nM fentanyl. *Significantly different compared to control in phase 1 ($p < 0.01$).

Naloxone did not have any effect on the fentanyl mediated inhibition of intrinsic Ca²⁺ activity

Figure 36 show representative traces of the intrinsic Ca²⁺ activity observed in cells isolated from SCGs after application naloxone (100uM) in presence of fentanyl (100nM) in neurons (**Figure 36A**) and glia (**Figure 36B**). As is observed from the traces, 100nM fentanyl inhibited the activity in phase 2. After application of naloxone in phase 3 the activity was continually inhibited with similar effects seen after washout of naloxone in phase 4 with a partial return to control levels after washout of both drugs in phase 5.

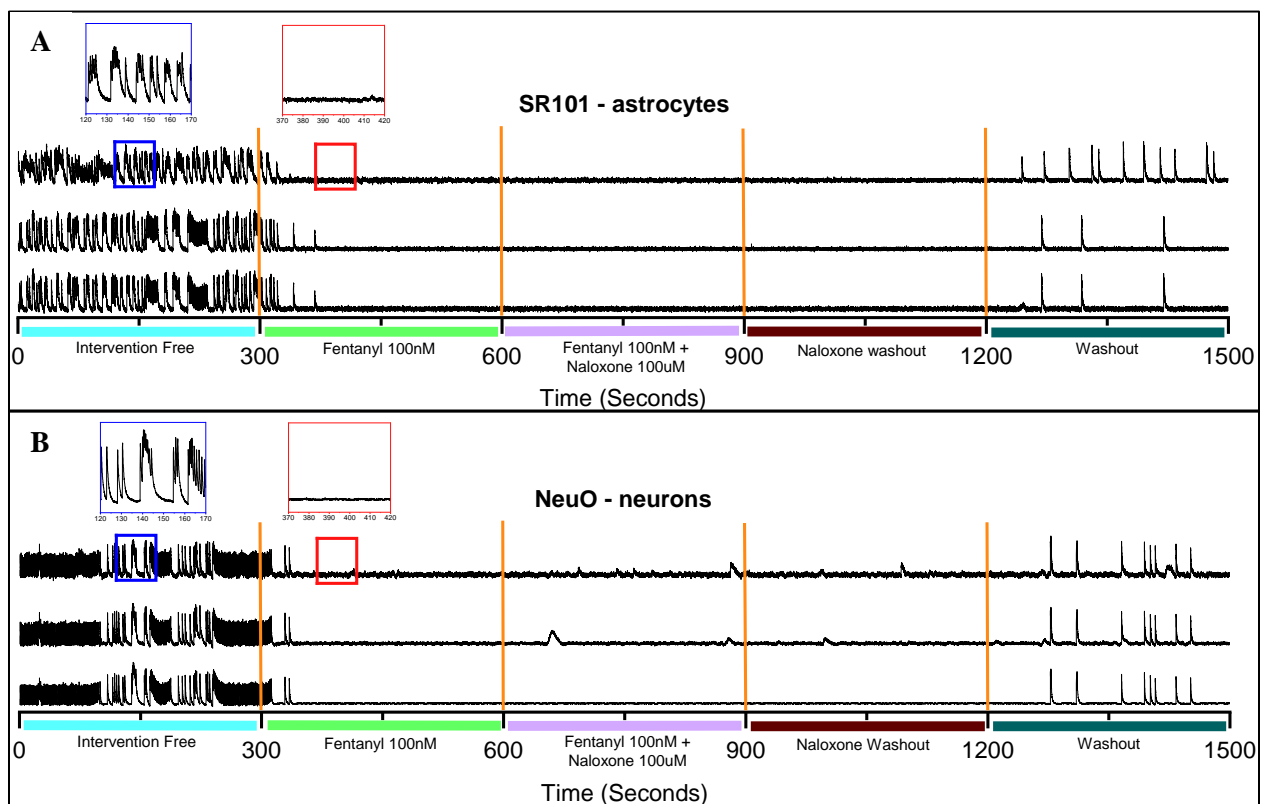


Figure 36: Effect of naloxone in presence of fentanyl. Typical traces depicting the effects of naloxone (100uM) in presence of fentanyl (100nM) in NeuO-labeled neurons and SR101 labeled astrocytes. Fentanyl displayed inhibition of activity in phase 2 which was not restored after addition of naloxone in presence of fentanyl in phase 3 with continued inhibition after washout

of naloxone only in phase 4 and a partial return to control level after complete washout of both drugs in phase 5.

NeuO Labeled Neurons: Naloxone in presence of fentanyl

Upon naloxone application in the presence of fentanyl, NeuO labeled neurons demonstrated distinct activity phenotypes. Initially, nearly all neurons were active (98.7%) in Phase 1 (drug free). By Phase 2 (fentanyl), a majority (85.2%) showed a decrease in activity, with smaller proportions showing no change or subthreshold activity. This decreasing trend persisted through Phases 3 (naloxone in presence of fentanyl) to 4 (naloxone washout), with most neurons exhibiting decreased activity. By Phase 5 (complete drug washout), majority of neurons (88.6%) started showing an increase in the activity and a small number of neurons (1.3% showed no change and decrease in activity. The number of subthreshold neurons (8.7%) also dropped by phase 5. Frequency analysis across phases (**Section 4a to 4c**) indicates significant reductions in activity frequencies, highlighting the modulatory impact of naloxone and fentanyl.

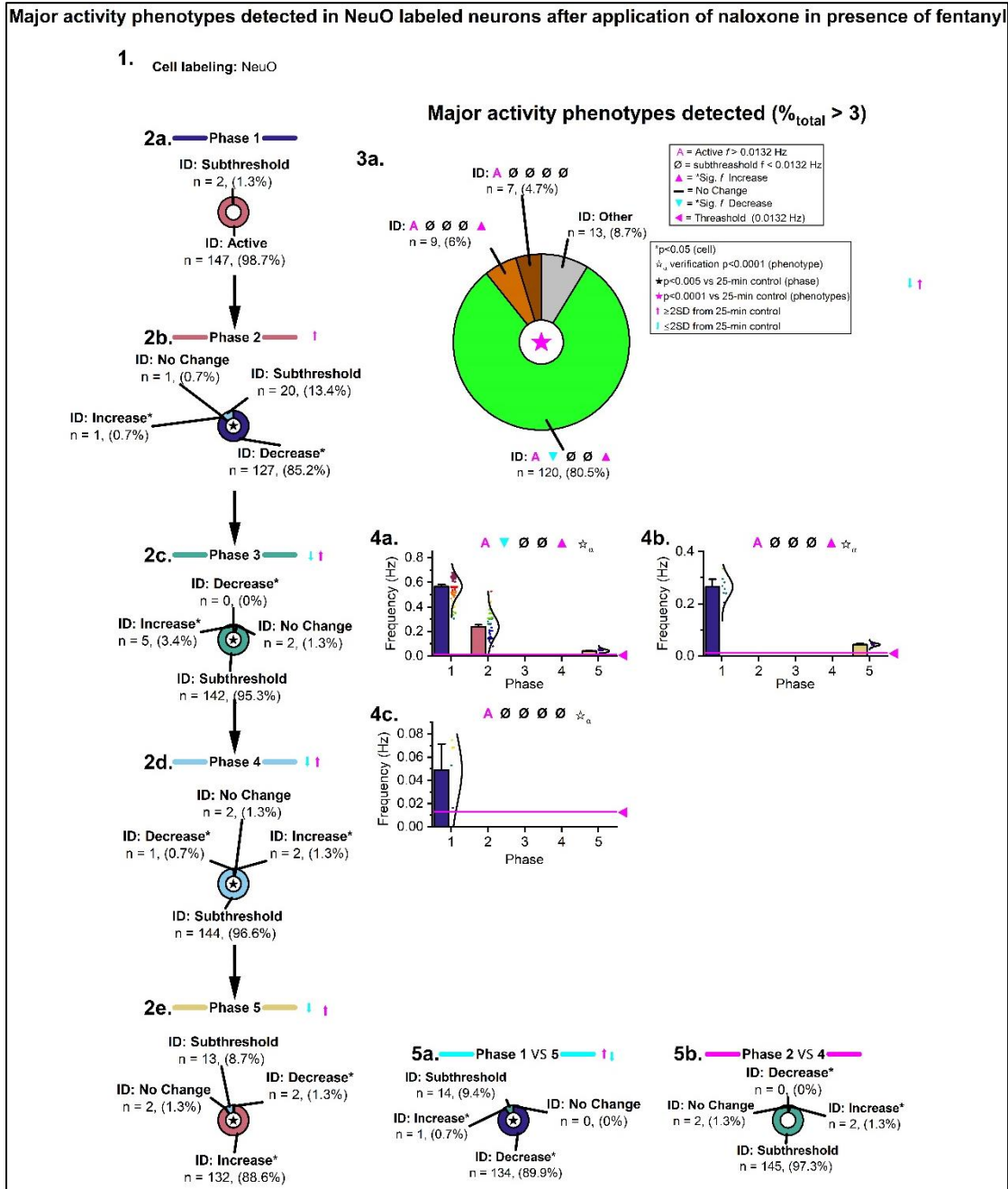
SR101 Labeled Glia: Naloxone in presence of fentanyl

In SR101 labeled glia, the application of naloxone in the presence of fentanyl resulted in a more pronounced decrease in activity (**Section 2a-2e**). In Phase 1, all glia were active. However, by Phase 2, a substantial portion (98.5%) showed decreased activity, with only a small fraction remaining active. This trend of decreased activity persisted through Phases 3 to 4. By Phase 5 (complete drug washout), majority of glia (98.5%) started showing an increase in the activity and no glia showed no change and decrease in activity. The number of subthreshold glia (1.5%) also dropped by phase 5. Minimal changes were observed in frequency analysis (**Section 4a**), indicating a significant inhibition of glial activity.

Conclusion

Naloxone, in the presence of fentanyl, induced substantial reductions in activity in both NeuO labeled neurons and SR101 labeled glia across multiple phases. The data suggest that while neurons exhibit a combination of increased and decreased activity, glial cells predominantly show decreased activity.

A



B

Major activity phenotypes detected in NeuO labeled neurons after application of naloxone in presence of fentanyl

1. Cell labeling: SR101

2a. Phase 1

ID: Subthreshold
n = 0, (0%)

ID: Active
n = 68, (100%)

2b. Phase 2

ID: Increase* n = 0, (0%) ID: No Change n = 0, (0%)

ID: Subthreshold n = 1, (1.5%) ID: Decrease* n = 67, (98.5%)

2c. Phase 3

ID: Increase* n = 0, (0%)

ID: Decrease* n = 0, (0%) ID: No Change n = 0, (0%)

ID: Subthreshold n = 68, (100%)

2d. Phase 4

ID: Increase* n = 0, (0%)

ID: No Change n = 0, (0%) ID: Decrease* n = 0, (0%)

ID: Subthreshold n = 68, (100%)

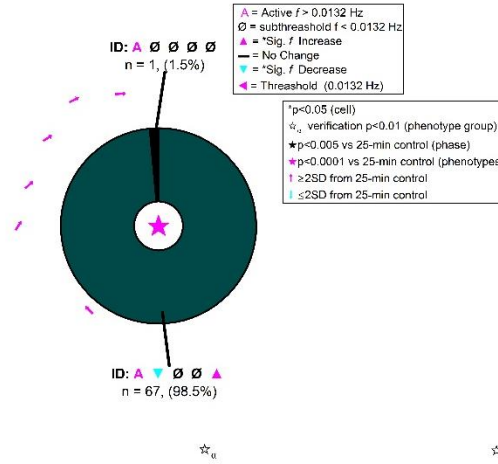
2e. Phase 5

ID: No Change n = 0, (0%) ID: Decrease* n = 0, (0%)

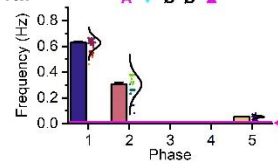
ID: Subthreshold n = 1, (1.5%) ID: Increase* n = 67, (98.5%)

3a.

Major activity phenotypes detected (%_{total} > 3)



4a.



5a. Phase 1 VS 5

ID: Increase* n = 0, (0%)

ID: No Change n = 0, (0%) ID: Subthreshold n = 2, (2.9%)

ID: Decrease* n = 66, (97.1%)

5b. Phase 2 VS 4

ID: Increase* n = 0, (0%)

ID: No Change n = 0, (0%) ID: Decrease* n = 0, (0%)

ID: Subthreshold n = 68, (100%)

Figure 37. Detailed analyses revealing the major activity phenotypes detected in neurons (A) and glia (B) after application of naloxone in presence of fentanyl. Section 2 (a-e) depicts the changing activity levels of the cells in all the Phases. The pie chart (3a) categorizes the major activity phenotypes and section 4 shows bar graphs of the most observed phenotypes detected. Section 5 shows a phase comparison in the changes in activity between Phases 1 and 5 and Phases 2 and 4

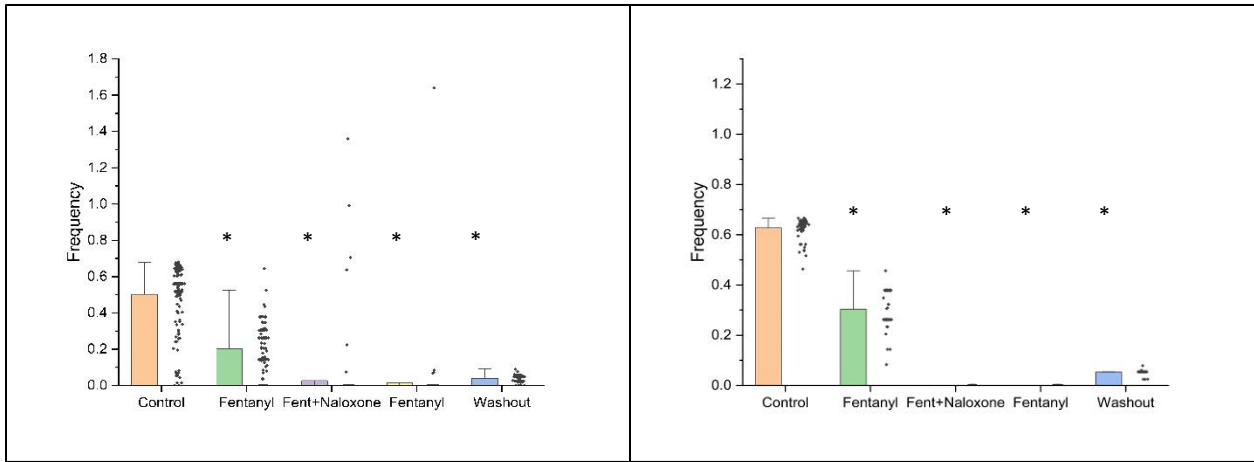


Figure 38. Summary graphs of superior cervical ganglion (SCG) neurons and glia after application of 100uM naloxone in presence of 100nM fentanyl. *Significantly different compared to control in phase 1 ($p < 0.01$).

CHAPTER IV — DISCUSSION

The main goal of my study was to investigate the main drivers of intrinsic Ca^{2+} activity and to determine whether D-CYSee had any effect on the fentanyl mediated inhibition of intrinsic Ca^{2+} activity in cells isolated from SCGs. My findings have indicated that LTCC and sodium channels appear to be the major drivers of the intrinsic Ca^{2+} activity. Findings regarding NTCC indicate partial involvement, since the Ca^{2+} activity resumed after a brief inhibition period. Although this can indicate involvement of intracellular stores of calcium, other important findings highlight the requirement of extracellular calcium to drive this activity. Findings from studies with fentanyl, naloxone, and D-CYSee demonstrated that fentanyl and naloxone had an inhibitory effect on the activity, whereas D-CYSee did not have a notable effect on the activity. The key findings from our studies showed that D-CYSee successfully reversed fentanyl-mediated inhibition of intrinsic Ca^{2+} activity, whereas naloxone had no effect on the fentanyl-mediated inhibition of intrinsic Ca^{2+} activity. Given that SCG has an indirect role in regulation of respiratory function, our data indicates that overdose of fentanyl may influence the SCG cells which in turn can contribute to OIRD. Our data with D-CYSee shows that it influences fentanyl-mediated inhibition on intrinsic Ca^{2+} activity in SCG cells, indicating the effectiveness of D-

CYSee in SCG cellular background. As these were collected from both neurons and glia, and we observed similar results from both cell types, this indicates involvement of glia in the network and in regulation of the cellular activity as well.

Role of superior cervical ganglion in breathing

The superior cervical ganglion (SCG) plays an indirect yet crucial role in regulating breathing by modulating the autonomic nervous system's influence on respiratory function³². The SCG is part of the sympathetic nervous system, which primarily prepares the body for 'fight or flight' responses. Although the SCG does not directly control respiratory muscles, it influences structures and functions that are vital to efficient breathing.

Firstly, the SCG affects the tone of the smooth muscles in the airways. Sympathetic stimulation from the SCG leads to the relaxation of bronchial smooth muscles, resulting in bronchodilation. This process enhances airflow and respiratory efficiency, particularly during physical activity or stress, when increased oxygen intake is necessary.⁷⁸ By regulating airway diameter, the SCG indirectly supports optimal respiratory function.

Secondly, the SCG has a role in regulating blood flow to the respiratory muscles and the lungs. Through its control over vasoconstriction and vasodilation of blood vessels, the SCG ensures that oxygen and nutrients are adequately delivered to the respiratory muscles. This regulation is crucial during heightened respiratory demand, such as during exercise or in response to stress, ensuring that the muscles involved in breathing receive sufficient blood supply to function effectively⁷⁹.

Additionally, the SCG influences the secretion of mucus in the respiratory tract. Sympathetic innervation from the SCG can modulate mucus production, which is important for keeping the airways clear of debris and pathogens. Proper mucus regulation ensures that the respiratory passages remain open and functional, facilitating unobstructed breathing^{80,81}.

Furthermore, the SCG impacts heart rate and cardiac output, which are intrinsically linked to respiratory function. During sympathetic activation, the SCG contributes to an increase in heart rate and cardiac output, enhancing the delivery of oxygenated blood to tissues, including those involved in respiration. This coordinated response ensures that the body's oxygen demands are met during periods of increased respiratory activity.⁸²

In summary, while the SCG does not directly control the respiratory muscles, it plays a significant role in supporting respiratory function through bronchodilation, regulation of blood flow to respiratory muscles, modulation of mucus secretion, and enhancement of cardiac output. These indirect influences are crucial for maintaining efficient and effective breathing, particularly during stress and physical exertion.

The involvement of the superior SCG in respiratory regulation makes it an ideal model for testing our drug, D-CYSee, particularly in the context of OIRD. Isolated SCG cells have proven invaluable for our research due to their homogeneity and the relative ease with which they can be cultured and maintained. They are a proven model for drug discovery which have been used previously in to deduce role of autonomic sensory ganglion in respiration.^{83,84}

Our data with fentanyl indicates an inhibitory effect on the SCG neurons. Fentanyl has been implicated as the major opioid responsible for overdose related respiratory depression. The effect of fentanyl on these neurons further cements its role in OIRD. Since neurons from the

SCGs are at least partly involved in regulating respiratory dynamics the data with fentanyl indicates that the effect of fentanyl leading to OIRD might not only be on the central nervous system but may also involve modulation of neuronal signaling in the peripheral nervous system as well.

Calcium and calcium channels in superior cervical ganglion

Calcium plays a crucial role in the function of the SCG, an essential component of the sympathetic nervous system. One of its primary roles is in neurotransmitter release. Calcium ions are necessary for the release of neurotransmitters at synapses. In the SCG, calcium influx into the presynaptic terminals triggers the release of neurotransmitters including norepinephrine, which is critical for the transmission of nerve signals to target organs⁸⁵. This process is fundamental for the sympathetic nervous system's function, influencing various physiological responses including heart rate, blood pressure, and glandular secretion⁸⁶

Calcium also acts as a second messenger in numerous intracellular signaling pathways. In neurons of the SCG, calcium signaling modulates numerous processes, including synaptic plasticity. Synaptic plasticity is vital for the adaptation and response to different stimuli, allowing the nervous system to adjust its responses based on experience and changing conditions⁸⁷. This role underscores the importance of calcium in maintaining the flexibility and responsiveness of the nervous system⁸⁶.

Furthermore, calcium ions contribute to the generation and propagation of action potentials in SCG neurons. Voltage-gated calcium channels open in response to membrane depolarization, allowing calcium influx that helps propagate the nerve impulse⁸⁶. This influx is

crucial for the continuation of the action potential along the neuron and the subsequent activation of downstream neurons or target tissues⁸⁶.

In addition to its role in action potential propagation, calcium is involved in the activation of various enzymes within SCG neurons. For instance, calcium/calmodulin-dependent protein kinase II (CaMKII) is activated by calcium and plays a significant role in synaptic function and plasticity^{88,89}. This enzyme modulates various aspects of neuronal function, including neurotransmitter release and receptor sensitivity, thus influencing overall neural activity^{88,89}.

Calcium signaling can also influence gene expression in SCG neurons by activating calcium-responsive transcription factors. These factors can lead to changes in the production of proteins that are important for neuronal function and survival^{90,91}. This regulatory mechanism ensures that neurons can adapt at a molecular level to long-term changes in their environment, supporting neuronal health and plasticity^{90,91}.

Finally, calcium ions affect the excitability of SCG neurons by modulating the activity of ion channels and receptors on the cell membrane. This regulation is essential for maintaining proper neuronal function and response to physiological stimuli⁹¹. By influencing ion channel activity, calcium helps set the threshold for neuronal activation and shapes the overall excitability of the neuron, ensuring appropriate responses to signals⁹¹.

L-type and N-type calcium channels play critical roles in the functioning of the SCG, each contributing uniquely to the regulation of neuronal activity and neurotransmitter release.

L-Type calcium channel. LTCCs are characterized by their long-lasting (L) activation and are primarily located in the cell bodies and dendrites of neurons. These channels play a crucial role in regulating the excitability of SCG neurons. When the neuronal membrane

depolarizes, LTCCs open, allowing the influx of Ca^{2+} ions into the cell. This influx of calcium triggers several important cellular responses. Firstly, it activates calcium-dependent enzymes such as calcium/calmodulin-dependent CaMKII, which is involved in synaptic plasticity and long-term potentiation⁸⁹. Secondly, calcium entry through LTCCs can lead to the activation of transcription factors like cAMP response element-binding protein, which regulate the expression of genes important for neuronal function and survival⁹². These processes are essential for the SCG's ability to adapt to prolonged stimuli and modulate sympathetic outflow accordingly.

N-Type calcium channels. NTCCs are predominantly located in the presynaptic terminals of SCG neurons. These channels are crucial for the rapid and precise release of neurotransmitters, particularly norepinephrine, which is essential for sympathetic signaling. When an action potential reaches the presynaptic terminal, depolarization triggers the opening of NTCCs, allowing Ca^{2+} ions to enter the terminal. This calcium influx leads to the fusion of synaptic vesicles containing neurotransmitters with the presynaptic membrane, facilitating neurotransmitter release into the synaptic cleft⁹³. The activation of NTCCs is tightly regulated and plays a key role in controlling the timing and efficiency of synaptic transmission in the SCG.

Functional importance. The functional importance of LTCCs and NTCCs in the SCG lies in their complementary roles in regulating neuronal excitability and neurotransmission. LTCCs regulate the overall excitability and synaptic plasticity of SCG neurons, influencing long-term changes in synaptic strength and neuronal adaptation. This regulation is crucial for maintaining homeostasis and responding to prolonged changes in the body's physiological state, such as during stress responses or changes in blood pressure⁹⁴. On the other hand, NTCCs ensure the rapid and precise release of neurotransmitters at synapses, facilitating fast and efficient sympathetic signaling required for responses to acute stimuli.

I investigated the role of LTCC and NTCC in driving the intrinsic Ca^{2+} activity using specific inhibitors, verapamil (LTCC) and conotoxin (NTCC). The data with LTCC (**Figure 18 and 19**) and NTCC (**Figure 15 and 16**) blockers was consistent with their functionality in the SCGs. Blocking both LTCC and NTCC invoked an inhibitory response to the intrinsic Ca^{2+} activity indicating their involvement in modulation of calcium dynamics, cellular excitability, and neurotransmission. Also, LTCC blocking initiated a more pronounced and prolonged response indicating stronger binding of verapamil to the LTCC and implicating LTCC involvement in LTP. Although NTCC inhibition also invoked an inhibitory response, there was resumption of activity after prolonged application of NTCC blocker indicating either the compensatory action of another calcium channel or involvement of intracellular calcium stores. Altogether, the SCG calcium activity was driven by LTCC and only partially by NTCC as shown in the figures 15,16,18 and 19

Sodium and sodium channels in superior cervical ganglion

The role of sodium and sodium channels in the SCG is fundamental to the excitability and function of sympathetic neurons within this autonomic ganglion⁹⁵.

Sodium channels in SCG. Sodium channels are integral membrane proteins that are responsible for the initiation and propagation of action potentials in neurons. In the SCG, like in other neurons, VGSCs play a critical role in the generation and propagation of electrical signals. VGSCs are activated upon membrane depolarization, allowing an influx of sodium ions (Na^+) into the cell, which rapidly depolarizes the membrane potential and triggers an action potential.

This process is crucial for the transmission of signals along sympathetic nerve fibers originating from the SCG to their target organs, including the heart, blood vessels, and glands⁹⁵.

Interaction with calcium channels. The activation of VGSCs and the subsequent depolarization of the neuronal membrane play a pivotal role in the modulation of calcium channels in the SCG. Specifically, sodium influx through VGSCs contributes to membrane depolarization, which is necessary to reach the threshold for VGCC activation. Once VGCCs are activated, calcium ions (Ca^{2+}) flow into the cell, initiating various calcium-dependent processes such as neurotransmitter release and intracellular signaling cascades⁹⁶.

Regulation of calcium dynamics. The interplay between sodium and calcium channels in the SCG is tightly regulated and essential for proper neuronal function. VGSCs ensure the rapid propagation of action potentials, which in turn regulate the timing and amplitude of calcium entry through VGCCs. This regulation is critical for controlling neurotransmitter release, particularly norepinephrine, which mediates sympathetic signaling from the SCG to target tissues⁹⁵.

Functionality and importance. The functionality of sodium channels in the SCG ensures the proper regulation of sympathetic nervous system activity. During sympathetic activation, neurons in the SCG receive excitatory signals that cause membrane depolarization. This depolarization opens VGSCs, leading to a rapid influx of sodium ions and the generation of action potentials. These action potentials propagate along the axons of sympathetic neurons, allowing for the fast and coordinated release of neurotransmitters such as norepinephrine at target tissues⁹⁵. This process underlies the SCG's role in regulating vital physiological functions, including heart rate, blood pressure, and the fight-or-flight response.

Regulation and adaptation. The regulation of sodium channels in the SCG is crucial for adapting to changes in physiological demands. Numerous factors including neurotransmitters, hormones, and local conditions can modulate the activity of sodium channels, thereby influencing sympathetic output. For example, neurotransmitters released within the SCG can bind to specific receptors on neurons and alter the excitability of these cells by modifying sodium channel activity⁹⁷. Such regulation allows the SCG to finely tune its responses to external stimuli and maintain homeostasis under varying conditions.

To answer the question of involvement of VGSCs in driving intrinsic Ca^{2+} activity, I exposed SCG cells to tetrodotoxin which is a VGSC blocker. Application of tetrodotoxin invoked a complete inhibitory effect on the intrinsic Ca^{2+} activity (**Figure 21 and 22**). This inhibition indicated the intricate crosstalk between VGSCs and VGCCs. Altogether, these data indicate that sodium channels can modulate intracellular calcium dynamics and have an inhibitory effect on the VGCCs.

Our studies highlighted the roles of extracellular Ca^{2+} , LTCC, NTCC, and VGSC as the major drivers of the intrinsic Ca^{2+} activity. Next, I moved to my major goal of deducing the effects of fentanyl, naloxone (mu opioid receptor antagonist), and D-CYSee on the intrinsic Ca^{2+} activity. I also wanted to determine whether D-CYSee reverses any fentanyl mediated effects on the activity. This data would give us insights into involvement of mu-opioid receptor in regulating intracellular changes in Ca^{2+} concentration.

Role of mu opioid receptor in calcium modulation in superior cervical ganglion

The involvement of MORs in calcium modulation within the SCG highlights their intricate role in regulating neurotransmission and neuronal function, particularly in the context of the sympathetic nervous system.

Distribution and function. MORs are widely distributed in the SCG, localized predominantly on presynaptic terminals of sympathetic neurons. Activation of MORs by endogenous opioids like β -endorphin or synthetic opioids such as morphine initiates a cascade of signaling events that impact calcium dynamics. MORs are coupled to G proteins, and their activation inhibits adenylyl cyclase activity, leading to a decrease in cyclic AMP (cAMP) levels and subsequent inhibition of VGCCs⁹⁸. This inhibition reduces calcium influx into the presynaptic terminals, thereby decreasing neurotransmitter release, including norepinephrine, which is crucial for sympathetic signaling in the SCG.

Mechanisms of calcium modulation. The modulation of calcium currents by MORs in the SCG occurs through multiple mechanisms. First, MOR activation leads to direct inhibition of VGCCs, specifically N-type calcium channels (NTCCs), which are critical for calcium-dependent neurotransmitter release. By reducing calcium influx through NTCCs, MORs effectively decrease the amount of neurotransmitter released into the synaptic cleft (Lacey et al., 1988). Second, MOR-mediated inhibition of adenylyl cyclase reduces cAMP levels, which in turn decreases the activity of other calcium channels, including L-type calcium channels (LTCCs), that contribute to calcium entry during sustained depolarization⁹⁸.

Physiological implications. The involvement of MORs in calcium modulation within the SCG has significant physiological implications. By regulating calcium influx and

neurotransmitter release, MORs contribute to the modulation of sympathetic tone and the regulation of cardiovascular function. Activation of MORs can lead to analgesia and sedation but may also impact cardiovascular stability due to their influence on sympathetic outflow from the SCG⁹⁹. Understanding these mechanisms is crucial for elucidating the physiological effects of opioid drugs and their potential therapeutic applications in pain management and cardiovascular disorders. With our collective data with fentanyl and D-CYSee we can say that, inhibition of the activity with fentanyl indicates presence of MORs in the SCG neurons. MOR inhibition by fentanyl as noted above has been implicated in OIRD. Our data related with these findings show that, after overdose of fentanyl, there is an inhibition of the SCG neurons along with other centers in the central nervous system which might collectively lead to OIRD. This fentanyl mediated inhibition can successfully be reversed by D-CYSee as demonstrated in our data; D-CYSee can become a crucial tool in fighting the opioid crisis.

Clinical relevance. The role of MORs in calcium modulation also has clinical relevance, particularly in the context of opioid pharmacotherapy. Opioid medications that target MORs can exert analgesic effects by reducing neurotransmitter release and modulating sympathetic activity. However, prolonged or excessive activation of MORs can lead to tolerance, dependence, and adverse effects such as respiratory depression⁹⁸. Therefore, understanding how MORs modulate calcium dynamics in the SCG is essential for developing safer and more effective opioid therapies.

Fentanyl and naloxone in our experiments both inhibited the intrinsic Ca^{2+} activity in a dose dependent manner, indicating the involvement of mu opioid receptor in normal functioning of the intrinsic Ca^{2+} activity (**Figure 24-29**). Our data showed us that fentanyl had a negative

effect on the intracellular calcium signaling. This reflects the role of fentanyl in OIRD. This also indicates the potential role of SCGs in OIRD and how fentanyl might influence the SCG.

Our data also indicated a negative (suppressive) effect of naloxone on intrinsic Ca^{2+} activity. This set of results surprised us the most since we expected the opposite, given the ability of naloxone to reverse respiratory suppression. The results after some deliberation also revealed a possible role of MORs in regulating the activity especially in SCGs. These data do not necessarily mean naloxone can be detrimental, but this does raise a concern regarding potential unidentified impacts of naloxone. Considering fentanyl and naloxone show similar on SCG neuronal activity results raises an alarm as to how is naloxone exactly functioning and whether high doses of naloxone might cause more harm than good. With naloxone primarily being a MOR antagonist, it can also have some off-target effects resulting in the effect that we have observed. The effect can also be attributed to effects of naloxone on calcium or sodium channels or other kinds of opioid receptors as well. All in all, our results do point out the need to do more studies with higher dose of naloxone since in most overdose cases with fentanyl more than one dose of naloxone needs to be administered to counter the effects.

After demonstrating that fentanyl and naloxone had an inhibitory effect in the SCG culture, I next sought to determine if these suppressive effects could be reversed. As shown in Figures 30 and 31, D-CYSee did not significantly alter intrinsic Ca^{2+} activity in SCG neurons when applied alone. Remarkably, D-CYSee also was able to reverse the fentanyl-mediated inhibition of intrinsic Ca^{2+} activity in the SCG cells (**Figure 33 and 34**) whereas naloxone had no effect on the fentanyl mediated suppression of intrinsic Ca^{2+} activity. This indicates potential of D-CYSee to emerge as a viable option in fighting against OIRD.

Recent findings in rats have shown the ability of D-CYSee against addiction as well. The key findings of the study were that fentanyl induced concentration and sex dependent reward seeking in these rats which was altered by treatment with D-CYSee, hence showing the potential of D-CYSee as a co-treatment with opioids. This could help in reducing opioid use disorder and in turn contribute towards reducing the addiction problem associated with these opioids as well^{100,101}.

Further examination of D-CYSee will probe the mechanisms of action and yield insights into how the drug is acting. The main questions to ask would be (1) what happens to D-CYSee once it gets inside the cells; (2) does it form a complex with any receptor; (3) does it interact with the mu-opioid receptor, and (4) whether D-CYSee interacts with voltage gated channels

REFERENCES

1. National Institute of Drug Abuse. Opioids. <https://nida.nih.gov/research-topics/opioids>.
2. Johns Hopkins Medicine. Opioids. <https://www.hopkinsmedicine.org/health/treatment-tests-and-therapies/opioids>.
3. Mayo clinic. What are opioids and why are they dangerous. <https://www.mayoclinic.org/diseases-conditions/prescription-drug-abuse/expert-answers/what-are-opioids/faq-20381270>.
4. Mohammadreza Azadfard; Martin R. Huecker; James M. Leaming. *Opioid Addiction.*; 2022.
5. Department of justice. Opioid Facts. <https://www.justice.gov/opioidawareness/opioid-facts>.
6. Centers for Disease Control and Prevention. Understanding the Opioid Overdose Epidemic. <https://www.cdc.gov/opioids/basics/epidemic.html>.
7. Gupta KPANMWJAL d; CFF a. Risk factors for opioid-induced respiratory depression and failure to rescue. *Current Issue in Anaesthesiology*. 2018;31(1):110-119.
8. Centers for Disease Control and Prevention (CDC). Synthetic opioid overdose data.
9. Kariisa M, et al. Illicitly Manufactured Fentanyl-Involved Overdose Deaths with Detected Xylazine. *MMWR Morb Mortal Wkly Rep*. 2022;71:1235-1242.
10. U.S. Department of Veteran Affairs. Fentanyl and car fentanyl.
11. National Institute on Drug Abuse (NIDA). Fentanyl and other synthetic opioids drug facts. Published online 2022.
12. Drug Enforcement Administration (DEA). DEA Issues Public Safety Alert on Sharp Increase in Fake Prescription Pills Containing Fentanyl and Meth.
13. Algera MH, Kamp J, van der Schrier R, et al. Opioid-induced respiratory depression in humans: a review of pharmacokinetic–pharmacodynamic modelling of reversal. *Br J Anaesth*. 2019;122(6):e168-e179. doi:10.1016/j.bja.2018.12.023
14. Baby SM, Gruber RB, Young AP, MacFarlane PM, Teppema LJ, Lewis SJ. Bilateral carotid sinus nerve transection exacerbates morphine-induced respiratory depression. *Eur J Pharmacol*. 2018;834:17-29. doi:10.1016/j.ejphar.2018.07.018
15. Henriksen G, Willoch F. Imaging of opioid receptors in the central nervous system. *Brain*. 2008;131(5):1171-1196. doi:10.1093/brain/awm255
16. U.S. Department of Health and Human Services (HHS). U.S. Surgeon General’s Advisory on Naloxone and Opioid Overdose. Published online 2021.
17. U.S. Food and Drug Administration (FDA). FDA Approves First Generic Naloxone Nasal Spray to Treat Opioid Overdose. Published online 2021.
18. National Institute on Drug Abuse (NIDA). Naloxone for Opioid Overdose: Life-Saving Science.

19. Centers for Disease Control and Prevention (CDC). Using Naloxone to Reverse Opioid Overdose in the Field.
20. Handel K A, Schaubel J L, Salamone F R. *Naloxone.*; 1983.
21. Kharasch ED. Opioid Half-lives and Hemlines: The Long and Short of Fashion. *Anesthesiology*. 2015;122(5):969-970. doi:10.1097/ALN.0000000000000634
22. Moss RB, Carlo DJ. Higher doses of naloxone are needed in the synthetic opioid era. *Subst Abuse Treat Prev Policy*. 2019;14(1). doi:10.1186/s13011-019-0195-4
23. Trescot AM, Datta S, Lee M, Hansen H. Opioid Pharmacology. *Pain Physician*. Published online 2008:133-153. www.painphysicianjournal.com
24. Berkovitz B. The relationship of pharmacokinetics to pharmacological activity: morphine, methadone and naloxone. *Clin Pharmacokinet*. 1976;1(3):219-230.
25. Walter Bouron, Boulapep Emile. *Medical Physiology: A Cellular and Molecular Approach.*; 2012.
26. F R Tang, C K Tan, E A Ling. A comparative study by retrograde neuronal tracing and substance P immunohistochemistry of sympathetic preganglionic neurons in spontaneously hypertensive rats and Wistar-Kyoto rats. *J Anat*. Published online 1995:197-206.
27. F R Tang CKTEAL. An ultrastructural study of the sympathetic preganglionic neurons that innervate the superior cervical ganglion in spontaneously hypertensive rats and Wistar-Kyoto rats. *J Hirnforsch*. 1995;36(3):411-420.
28. Llewellyn-Smith IJ, Arnolda LF, Pilowsky PM, Chalmers JP, Minson JB. *GABA-and Glutamate-Immunoreactive Synapses on Sympathetic Preganglionic Neurons Projecting to the Superior Cervical Ganglion*. Vol 71.; 1998.
29. Coffee G, Getsy P, Lewis S. Role of the ganglioglomerular nerve in response to hypoxia in juvenile rats. *FASEB*. 2019;33(S1):551.11-551.11.
30. Sankari A, Badr MS, Martin JL, Ayas NT, Berlowitz DJ. Impact of spinal cord injury on sleep: Current perspectives. *Nat Sci Sleep*. 2019;11:219-229. doi:10.2147/NSS.S197375
31. Getsy PM, Coffee GA, Hsieh YH, Lewis SJ. Loss of Cervical Sympathetic Chain Input to the Superior Cervical Ganglia Affects the Ventilatory Responses to Hypoxic Challenge in Freely-Moving C57BL6 Mice. *Front Physiol*. 2021;12. doi:10.3389/fphys.2021.619688
32. Coffee G, Getsy P, Lewis S. Role of the Superior Cervical Ganglion in Response to Hypoxia in Juvenile Rats. *FASEB*. 2018;32(S1):601.4-601.4.
33. Clapham DE. Calcium Signaling. *Cell*. 2007;131(6):1047-1058. doi:10.1016/j.cell.2007.11.028
34. Berridge MJ, Bootman MD, Roderick HL. Calcium signalling: dynamics, homeostasis and remodelling. *Nat Rev Mol Cell Biol*. 2003;4(7):517-529. doi:10.1038/nrm1155
35. Giorgi C, Marchi S, Pinton P. The machineries, regulation and cellular functions of mitochondrial calcium. *Nat Rev Mol Cell Biol*. 2018;19(11):713-730. doi:10.1038/s41580-018-0052-8

36. Neher E, Sakaba T. Multiple Roles of Calcium Ions in the Regulation of Neurotransmitter Release. *Neuron*. 2008;59(6):861-872. doi:10.1016/j.neuron.2008.08.019
37. Berridge MJ. Neuronal Calcium Signaling. *Neuron*. 1998;21(1):13-26. doi:10.1016/S0896-6273(00)80510-3
38. Hardingham GE, Arnold FJL, Bading H. Nuclear calcium signaling controls CREB-mediated gene expression triggered by synaptic activity. *Nat Neurosci*. 2001;4(3):261-267. doi:10.1038/85109
39. Bers DM. Cardiac excitation–contraction coupling. *Nature*. 2002;415(6868):198-205. doi:10.1038/415198a
40. Melzer W, Herrmann-Frank A, Lüttgau HC. The role of Ca²⁺ ions in excitation-contraction coupling of skeletal muscle fibres. *Biochim Biophys Acta*. 1995;1241(1):59-116. doi:10.1016/0304-4157(94)00014-5
41. Cheng H, Lederer WJ, Cannell MB. Calcium Sparks: Elementary Events Underlying Excitation-Contraction Coupling in Heart Muscle. *Science (1979)*. 1993;262(5134):740-744. doi:10.1126/science.8235594
42. Patergnani S, Danese A, Bouhamida E, et al. Various Aspects of Calcium Signaling in the Regulation of Apoptosis, Autophagy, Cell Proliferation, and Cancer. *Int J Mol Sci*. 2020;21(21):8323. doi:10.3390/ijms21218323
43. Orrenius S, Zhivotovsky B, Nicotera P. Regulation of cell death: the calcium–apoptosis link. *Nat Rev Mol Cell Biol*. 2003;4(7):552-565. doi:10.1038/nrm1150
44. Monteith GR, Prevarskaya N, Roberts-Thomson SJ. The calcium–cancer signalling nexus. *Nat Rev Cancer*. 2017;17(6):373-380. doi:10.1038/nrc.2017.18
45. Catterall WA, Perez-Reyes E, Snutch TP, Striessnig J. International Union of Pharmacology. XLVIII. Nomenclature and Structure-Function Relationships of Voltage-Gated Calcium Channels. *Pharmacol Rev*. 2005;57(4):411-425. doi:10.1124/pr.57.4.5
46. Söllner T, Whiteheart SW, Brunner M, et al. SNAP receptors implicated in vesicle targeting and fusion. *Nature*. 1993;362(6418):318-324. doi:10.1038/362318a0
47. Sheng ZH, Yokoyama CT, Catterall WA. Interaction of the synprint site of N-type Ca²⁺ channels with the C2B domain of synaptotagmin I. *Proceedings of the National Academy of Sciences*. 1997;94(10):5405-5410. doi:10.1073/pnas.94.10.5405
48. Zamponi GW. Targeting voltage-gated calcium channels in neurological and psychiatric diseases. *Nat Rev Drug Discov*. 2016;15(1):19-34. doi:10.1038/nrd.2015.5
49. Dolphin AC. Calcium channel auxiliary $\alpha\delta$ and β subunits: trafficking and one step beyond. *Nat Rev Neurosci*. 2012;13(8):542-555. doi:10.1038/nrn3311
50. Toth PT, BSS, & LRR. N-type calcium channels in the central and peripheral nervous system: localizing the target of clinical interest. *J Clin Pharmacol*. Published online 1998:425-49S.

51. Tseng CJ, SYC, & CJYH. N-type calcium channel blockade inhibits sympathetic transmission to the heart in spontaneously hypertensive rats. *Hypertension*. Published online 1994:705-710.
52. Kawai T, Watanabe M. Long-term potentiation of nicotinic synaptic transmission in the rat superior cervical ganglion. *Journal of Physiology*. Published online 2000:259-266.
53. Papke RL, Heinemann SF. The role of N-type calcium channels in synaptic transmission in the superior cervical ganglion. *Neuroscience*. Published online 1991:379-389.
54. Connor M, Christie MJ. Modulation of Ca²⁺ channel currents of acutely dissociated rat periaqueductal grey neurons. *J Physiol*. 1998;509 (Pt 1)(Pt 1):47-58. doi:10.1111/j.1469-7793.1998.047bo.x
55. Catterall WA. Voltage-gated calcium channels. *Cold Spring Harb Perspect Biol*. 2011;3(8):a003947. doi:10.1101/cshperspect.a003947
56. Law PY, Loh HH. Regulation of Opioid Receptor Activities. *Journal of Pharmacology and Experimental Therapeutics*. 1999;289(2):607. <http://jpet.aspetjournals.org/content/289/2/607.abstract>
57. Dang VC, Christie MJ. Mechanisms of rapid opioid receptor desensitization, resensitization and tolerance in brain neurons. *Br J Pharmacol*. 2012;165(6):1704-1716. doi:10.1111/j.1476-5381.2011.01482.x
58. Raehal KM, Schmid CL, Medvedev IO, Gainetdinov RR, Premont RT, Bohn LM. Morphine-induced physiological and behavioral responses in mice lacking G protein-coupled receptor kinase 6. *Drug Alcohol Depend*. 2009;104(3):187-196. doi:https://doi.org/10.1016/j.drugalcdep.2009.04.011
59. Bohn LM, Gainetdinov RR, Lin FT, Lefkowitz RJ, Caron MG. μ -Opioid receptor desensitization by β -arrestin-2 determines morphine tolerance but not dependence. *Nature*. 2000;408(6813):720-723. doi:10.1038/35047086
60. Reeves KC, Shah N, Muñoz B, Atwood BK. Opioid Receptor-Mediated Regulation of Neurotransmission in the Brain. *Front Mol Neurosci*. 2022;15:919773. doi:10.3389/fnmol.2022.919773
61. Christie MJ. Cellular neuroadaptations to chronic opioids: tolerance, withdrawal and addiction. *Br J Pharmacol*. 2008;154(2):384-396. doi:10.1038/bjp.2008.100
62. Trescot AM. Opioid Pharmacology. *Pain Physician*. 2008;2s;11(3;2s):S133-S153. doi:10.36076/ppj.2008/11/S133
63. Nestler EJ. Molecular basis of long-term plasticity underlying addiction. *Nat Rev Neurosci*. 2001;2(2):119-128. doi:10.1038/35053570
64. Ueda H. Molecular mechanisms of neuropathic pain—phenotypic switch and initiation mechanisms. *Pharmacol Ther*. 2006;109(1):57-77. doi:https://doi.org/10.1016/j.pharmthera.2005.06.003

65. Williams JT, Christie MJ, Manzoni O. Cellular and Synaptic Adaptations Mediating Opioid Dependence. *Physiol Rev.* 2001;81(1):299-343. doi:10.1152/physrev.2001.81.1.299
66. Cox BM, Christie MJ, Devi L, Toll L, Traynor JR. Challenges for opioid receptor nomenclature: IUPHAR Review 9. *Br J Pharmacol.* 2015;172(2):317-323. doi:10.1111/bph.12612
67. Seward E, Hammond C, Henderson G. *μ-Opioid-Receptor-mediated Inhibition of the N-Type Calcium-Channel Current.* <https://royalsocietypublishing.org/>
68. Caminski ES, Antunes FTT, Souza IA, Dallegrave E, Zamponi GW. Regulation of N-type calcium channels by nociceptin receptors and its possible role in neurological disorders. *Mol Brain.* 2022;15(1). doi:10.1186/s13041-022-00982-z
69. Al-Hasani R, Bruchas MR. Molecular mechanisms of opioid receptor-dependent signaling and behavior. *Anesthesiology.* 2011;115(6):1363-1381. doi:10.1097/ALN.0b013e318238bba6
70. Seseña E, Vega R, Soto E. Activation of μ -opioid receptors inhibits calcium-currents in the vestibular afferent neurons of the rat through a camp dependent mechanism. *Front Cell Neurosci.* 2014;8(MAR). doi:10.3389/fncel.2014.00090
71. Harlan Laboratories. Sprague Dawley Outbred Rat. Published online 2010.
72. Mouseion at the JAXlibrary. Sprague Dawley Rats. *The Jackson Laboratory.* Published online 2017.
73. Charles River Laboratories. Sprague Dawley Rats: The Gold Standard for Research. *Charles River.* Published online 2020.
74. Sengupta P. The Laboratory Rat: Relating Its Age With Human's. *Int J Prev Med.* 2013;4(6):624-630.
75. Baker HJ, Lindsey JR, Weisbroth SH. The Laboratory Rat, Volume I: Biology and Diseases. *Academic Press.*
76. Hedrich HJ. *Guide for the Care and Use of Laboratory Animals.* National Academies Press; 2011. doi:10.17226/12910
77. Reeb-Whitaker CK, Paigen B, Beamer WG, et al. The impact of reduced frequency of cage changes on the health of mice housed in ventilated cages. *Lab Anim.* 2001;35(1):58-73. doi:10.1258/0023677011911381
78. van der Velden VHJ, Hulsmann AR. Autonomic Innervation of Human Airways: Structure, Function, and Pathophysiology in Asthma. *Neuroimmunomodulation.* 1999;6(3):145-159. doi:10.1159/000026376
79. Joyner MJ, Casey DP. Regulation of increased blood flow (hyperemia) to muscles during exercise: a hierarchy of competing physiological needs. *Physiol Rev.* 2015;95(2):549-601. doi:10.1152/physrev.00035.2013
80. Rogers DF. Motor control of airway goblet cells and glands. *Respir Physiol.* 2001;125(1-2):129-144. doi:10.1016/S0034-5687(00)00209-7

81. Rogers DF. Physiology of airway mucus secretion and pathophysiology of hypersecretion. *Respir Care*. 2007;52(9):1134-1146; discussion 1146-9.
82. Narkiewicz K, van de Borne P, Montano N, Hering D, Kara T, Somers VK. Sympathetic Neural Outflow and Chemoreflex Sensitivity Are Related to Spontaneous Breathing Rate in Normal Men. *Hypertension*. 2006;47(1):51-55. doi:10.1161/01.HYP.0000197613.47649.02
83. Adeoye OO, Silpanisong J, Williams JM, Pearce WJ. Role of the sympathetic autonomic nervous system in hypoxic remodeling of the fetal cerebral vasculature. *J Cardiovasc Pharmacol*. 2015;65(4):308-316. doi:10.1097/FJC.000000000000192
84. Takahashi H, Yoshika M, Komiyama Y, Nishimura M. The central mechanism underlying hypertension: a review of the roles of sodium ions, epithelial sodium channels, the renin-angiotensin-aldosterone system, oxidative stress and endogenous digitalis in the brain. *Hypertens Res*. 2011;34(11):1147-1160. doi:10.1038/hr.2011.105
85. Brini M, Cali T, Ottolini D, Carafoli E. Neuronal calcium signaling: function and dysfunction. *Cellular and Molecular Life Sciences*. 2014;71(15):2787-2814. doi:10.1007/s00018-013-1550-7
86. Hille B. *Ion Channels of Excitable Membranes (3rd Ed.)*; 2001.
87. Berridge MJ. Neuronal Calcium Signaling. *Neuron*. 1998;21(1):13-26. doi:https://doi.org/10.1016/S0896-6273(00)80510-3
88. Yamauchi T. Neuronal Ca²⁺/Calmodulin-Dependent Protein Kinase II-Discovery, Progress in a Quarter of a Century, and Perspective: Implication for Learning and Memory. *Biol Pharm Bull*. 2005;28(8):1342-1354. doi:10.1248/bpb.28.1342
89. Hanson PI, Schulman H. NEURONAL Ca²⁺/CALMODULIN-DEPENDENT PROTEIN KINASES. *Annu Rev Biochem*. 1992;61(1):559-601. doi:10.1146/annurev.bi.61.070192.003015
90. Dolmetsch RE, Lewis RS. Signaling between intracellular Ca²⁺ stores and depletion-activated Ca²⁺ channels generates [Ca²⁺]_i oscillations in T lymphocytes. *J Gen Physiol*. 1994;103(3):365-388. doi:10.1085/jgp.103.3.365
91. Catterall WA. Structure and Regulation of Voltage-Gated Ca²⁺ Channels. *Annu Rev Cell Dev Biol*. 2000;16(1):521-555. doi:10.1146/annurev.cellbio.16.1.521
92. Wheeler DG, Barrett CF, Groth RD, Safa P, Tsien RW. CaMKII locally encodes L-type channel activity to signal to nuclear CREB in excitation–transcription coupling. *J Cell Biol*. 2008;183(5):849-863. doi:10.1083/jcb.200805048
93. Dunlap K, Luebke JI, Turner TJ. Exocytotic Ca²⁺ channels in mammalian central neurons. *Trends Neurosci*. 1995;18(2):89-98.
94. Catterall WA, Perez-Reyes E, Snutch TP, Striessnig J. International Union of Pharmacology. XLVIII. Nomenclature and Structure-Function Relationships of Voltage-Gated Calcium Channels. *Pharmacol Rev*. 2005;57(4):411-425. doi:10.1124/pr.57.4.5

95. Marban E, Yamagishi T, Tomaselli GF. Structure and function of voltage-gated sodium channels. *J Physiol*. 1998;508 (Pt 3)(Pt 3):647-657. doi:10.1111/j.1469-7793.1998.647bp.x
96. de Lera Ruiz M, Kraus RL. Voltage-Gated Sodium Channels: Structure, Function, Pharmacology, and Clinical Indications. *J Med Chem*. 2015;58(18):7093-7118. doi:10.1021/jm501981g
97. Katz B, Miledi R. The role of calcium in neuromuscular facilitation. *J Physiol*. 1968;195(2):481-492. doi:10.1113/jphysiol.1968.sp008469
98. Law PY, Wong YH, Loh HH. Molecular Mechanisms and Regulation of Opioid Receptor Signaling. *Annu Rev Pharmacol Toxicol*. 2000;40(1):389-430. doi:10.1146/annurev.pharmtox.40.1.389
99. North RA, Williams JT. On the potassium conductance increased by opioids in rat locus coeruleus neurones. *J Physiol*. 1985;364:265-280. doi:10.1113/jphysiol.1985.sp015743
100. Knauss ZT, Hearn CJ, Hendryx NC, et al. Fentanyl-induced reward seeking is sex and dose dependent and is prevented by D-cysteine ethylester. *Front Pharmacol*. 2023;14:1241578. doi:10.3389/fphar.2023.1241578
101. Knauss ZT. FENTANYL-INDUCED REWARD SEEKING IS SEX AND DOSE DEPENDENT AND IS PREVENTED BY D-CYSTEINE ETHYLESTER WHICH SELECTIVELY ALTERS FENTANYL CA²⁺ SIGNALING DYNAMICS IN THE PREFRONTAL CORTEX. Published online 2024. Accessed November 11, 2024. http://rave.ohiolink.edu/etdc/view?acc_num=kent1721223495953922